ENERGY DEPENDENCE OF TRANSITION PROBABILITIES AND LEVEL DENSITIES DETERMINED FROM THE (n,γ) REACTION

ENERGY DEPENDENCE OF TRANSITION PROBABILITIES AND LEVEL DENSITIES DETERMINED FROM THE (n,γ) REACTION

by

LEONARD BLAND HUGHES, B.Sc.

A Thesis

Submitted to the Faculty of Graduate Studies

in Partial Fulfilment of the Requirements

for the Degree

Doctor of Philosophy

McMaster University

May, 1967

DOCTOR OF PHILOSOPHY (1967)
(Physics)

McMASTER UNIVERSITY
Hamilton, Ontario

TITLE: Energy Dependence of Transition Probabilities and Level Densities Determined from the (n,γ) Reaction

AUTHOR: Leonard Bland Hughes, B.Sc. (McMaster University)

SUPERVISOR: Dr. T.J.Kennett

NUMBER OF PAGES: viii, 152

SCOPE AND CONTENTS:

High resolution lithium-drifted Germanium detectors have been used to study the γ radiation emitted after thermal neutron capture in ten odd-proton even-neutron nuclei in the mass range $56 \leq A \leq 204$. From the energies and intensities of these radiations, the energy dependence of the partial radiative widths to bound states with excitation energies in the region 0 to 2.5 MeV have been deduced. The energy dependence for the average spacing between the levels populated in this reaction have also been deduced over the same region of excitation energies.

The energy dependence of the partial radiative widths are in agreement with the single particle estimate for dipole radiation and the energy dependence of the average level spacing favours the constant temperature model.

ACKNOWLEDGEMENTS

I would like to express my sincere thanks to the members of my Supervisory Committee, Dr. T. J. Kennett, Dr. M. W. Johns and Dr. R. H. Tomlinson for the guidance given during the course of this study. I am greatly indebted to my Research Director, Dr. T. J. Kennett, whose invaluable advice and assistance throughout the course of this work, made its completion possible. It was during the many stimulating discussions with him and Dr. W. V. Prestwich, that the problems as well as the techniques used in their solution, were generated.

I would also like to express my gratitude to the many people involved in handling the vast amount of data that was used in this work. The assistance of Dr. N. P. Archer, Mr. L. V. Johnson and Mr. H. Lycklama, in this regard, is greatly appreciated.

This research would not have been possible without the use of solid state detectors. The fabrication of detectors of sufficient quality was made possible through the efforts of Dr. H. J. Fiedler and Mr. B. J. Wall. For this determined effort I would like to express my thanks.

I would like to thank Mrs. Helen Kennelly, whose fast and accurate typing of this manuscript is greatly appreciated. I am also indebted to Mr. A. H. Colenbrander for the many hours spent in preparing the illustrations for reproduction.

Finally, I would like to thank my wife, Phyllis, for her moral support during the course of this study. Her assistance in the preparation of this manuscript is also greatly appreciated.

TABLE OF CONTENTS

LIST OF TABLES

LIST OF ILLUSTRATIONS

CHAPTER I

INTRODUCTION

1.1 General Survey

When neutrons are incident on a target consisting of nuclei of mass number A, there is a finite probability that they will be absorbed. The system so formed has a mass number A + 1 and will be referred to as the compound system. This compound system is created with an excitation energy

$$E_x = S_n + T$$

where T is the relative kinetic energy between the neutron and the target nucleus before the interaction. The neutron separation energy, S_n, is the energy required to remove a neutron from the ground state of the compound system. Reported separation energies range from 2.225 MeV for the deuteron to 11.5 MeV for B^{11} with most values being of the order of 8 MeV.

The excitation energy is released through the emission of particles or photons. For this discussion we will assume that the incident neutron energy is low (<10 keV) so that the only open channels for the decay other than the entrance channel are, in general, those associated with photon emission. We will further assume that only s-wave neutrons interact, an assumption that is quite reliable for low incident neutron energies.

The study of the (n,γ) reaction supplies information in two broad areas. It can be used to study the properties of the nuclear levels that are populated, or it can be used to study the reaction mechanism itself. Since this work relies on, and hopefully contributes to information in both areas, a brief discussion of the previous work in these areas was felt to be necessary.

Under the above assumption that only photon emission and elastic neutron scattering are important, the only states populated in the reaction are those of the previously defined compound system.† The properties of this system above the neutron separation energy can be obtained by measuring the cross section as a function of the incident neutron energy, T. The observation of resonances in the cross section with widths of the order of 10 eV indicates discrete energy levels with lifetimes of the order of 10^{-16} sec. In some cases the partial widths[1,2], total angular momentum[3,4], and parity of these states can be determined.

The study of the bound levels of the compound system requires the use of high resolution γ-ray spectrometers. These are necessary because of the complexity of the spectra that results from the large number of levels that are populated. Since these spectrometers have, in general, very low sensitivities they can not be used with the low fluxes and poor duty cycles that are inherent with the neutron time-of-flight experiments. As a result, the properties of the bound states have been studied using the very much higher thermal neutron fluxes ($T \sim 0.03$ eV).

---

† In this discussion the β-decay of the ground state or any isomers has been neglected. In practice the γ-rays following these decays can be recognized and subtracted from the observed spectrum.

As for the quasi-bound levels, the branching ratios, total widths or lifetimes, total angular momenta and parities of these bound levels can be obtained in favourable cases[5].

It is possible, then, to obtain information about the level structure of this compound system over a wide energy range ($\sim$ 8 MeV). The study of this reaction is then ideally suited for determining the energy variation of parameters associated with these levels. In particular, the level spacing can be measured over a wide energy range. Since this is pertinent to this work, a more detailed discussion of the literature in this area will be presented later.

The study of the reaction mechanism itself has received much less attention, due, in part, to the difficulty of obtaining precise information. The most extensive treatment of radiative capture is that of Lane[6] and Lane and Lynn[7,8,9]. In their analysis, the two extreme cases were discussed; the direct-reaction and the compound-reaction mechanisms. The lifetime of the compound state that is formed determines which mechanism is important. For a direct reaction the lifetime of the compound state is less than the time taken by an average bound nucleon to cross the nucleus ($\sim 10^{-22}$ sec) and the resulting width is therefore of the order of 10 MeV. The initial state from which the transition occurs consists of an s-wave neutron coupled to a core consisting of the ground state of the target nucleus. It therefore would seem likely that the transitions will be most intense to bound states that have a strong single-particle character. On the other hand the compound-reaction mechanism describes reactions that proceed through a compound state whose lifetime is much greater than

the nucleon period. During this period the excitation energy is shared among many nucleons resulting in the excitation of many degrees of freedom. The transition to bound levels then proceeds from this complex state, the so-called compound nucleus. Lane and Lynn[8] show that enhanced transitions to bound states with a strong single-particle character can also occur in resonance capture. These transitions correspond to an initial compound elastic scattering followed by the direct capture of the scattered neutron. This process will then be most important when the neutron width, Γ_n, is large. Because of this process, the observation of enhanced transitions to good single-particle states does not rule out the possibility of compound-nucleus formation.

The variation of transition probabilities over a wide range of energies can be studied with this reaction. In particular, the theoretical predictions of Blatt and Weisskopf[10] and Axel[11] may be tested over a large energy range. Since one of the objectives of this work is to test these predictions, further discussions in this area are postponed until later.

Before leaving this general introduction, it should be mentioned that the development of Ge(Li) counters, will permit new and better experiments in this field. At the present stage of development the resolution obtainable above 2.5 MeV is better than any other γ-ray spectrometer presently available. The relatively high sensitivity of these detectors also permits coincidence measurements to be made with good energy resolution. This will allow much more detailed information to be obtained from coincidence measurements than has been possible before.

1.2 Radiative-Transition Probabilities

The theory of radiative-transition probabilities has been treated in detail by several authors[10-14]. In this discussion we will be content to summarize these results, since rigorously developed theories can be found in the references above.

The partial width, $\Gamma(i,f)$, for transitions from state i to state f is given by first-order time-dependent perturbation theory as

$$\Gamma(i,f) = 2\pi |\langle f|O|i\rangle|^2 \rho_f$$

where ρ_f is the density of final states of the system. Since the final nuclear states are discrete, the density of final states in this case, is that associated with the emitted photon.

Because the initial and final nuclear states have definite angular momenta and parities, it is desirable to expand the operator associated with the interaction in terms of operators that have special properties under coordinate rotations and inversion. Spherical tensors, T_L^M, which transform under rotations like the spherical harmonics $Y_L^M(\Omega)$, have the desired rotational properties. The expansion of the operator associated with the interaction in terms of a set of operators T_L^M leads to a finite number of terms in the resulting series for the radiative width. In fact, using the Wigner-Ekhart theorem which applies to operators of this type, it can be shown that the only non-zero matrix elements are those associated with a value of L in the range

$$|J_i - J_f| \leq L \quad J_i + J_f$$

This is also a statement of the conservation of angular momentum where L is the angular momentum associated with the photon field.

It should also be mentioned that L is not the orbital angular momentum of the photon field , but the total angular momentum which is the sum of the intrinsic angular momentum and the orbital angular momentum. Since the electromagnetic field is a vector field, that is it has three internal degrees of freedom, the internal angular momentum of the photon is 1. This implies that electric monopole emission (L=0) is not possible.

We are now left to consider the properties of the operators T^M_L under coordinate inversion. In general we can write

$$T^L_M = Q_{LM} + M_{LM}$$

where Q_{LM} and M_{LM} have opposite parities. Since the initial and final nuclear states have definite parities, π_i and π_f, either $\langle f|Q_{LM}|i\rangle = 0$ or $\langle f|M_{LM}|i\rangle = 0$. If we choose the parity of Q_{LM} to be $(-1)^L$ we have the result

$$\langle f|T^L_M|i\rangle = \langle f|Q_{LM}|i\rangle \text{ if } (-1)^L \pi_f\pi_i = 1$$

$$= \langle f|M_{LM}|i\rangle \text{ if } (-1)^L \pi_f\pi_i = -1$$

The following simple arguments make plausible the connection of the operator Q_{LM} with electric 2^L-pole (EL) radiation and M_{LM} with magnetic 2^L-pole (ML) radiation. We first note that the electric field associated with a static electric dipole has positive parity as does the magnetic field associated with a static magnetic dipole. For radiating systems these fields oscillate in phase so that the parities of the oscillating fields are the same as for the static system. We also note that for a radiating system, the direction of the energy flow is

radially out from the source and is given by $\underline{E} \times \underline{H}$. By choosing $\underline{E}$ or $\underline{H}$ to describe the radiating field, it follows that the field associated with E1 radiation has opposite parity from that associated with M1 radiation. It can also be shown (see for example ref. 14 p. 152) that the normal statement of parity conservation holds if the parity associated with the radiating field is that of the magnetic field $\underline{H}$. We then conclude that Q_{LM} is the operator associated with EL transitions and M_{LM} the operator associated with ML transitions.

The radiative width for the emission of 2^L-pole radiation can be found by calculating the density of final states of the photon and using explicit expressions for the operators associated with the interaction. The result is

$$\Gamma(L) = 8\pi\frac{e^2}{c}\frac{(L+1)}{L\left[(2L+1)!!\right]^2}\left(\frac{E_\gamma}{hc}\right)^{2L+1} B(L)$$

where

$$B(L) = \frac{c}{e^2}\sum_{M,M_i} \langle f|Q_{LM}|i\rangle \text{ if } (-1)^L\pi_i\pi_f = 1$$

$$= \frac{c}{e^2}\sum_{M,M_i} \langle f|M_{LM}|i\rangle \text{ if } (-1)^L\pi_i\pi_f = -1$$

The explicit expressions for Q_{LM} and M_{LM} are,

$$Q_{LM} = \sum_j e_j r_j^L Y_L^{M*}(\Omega_j) - ik\mu_o g_{sj}(L+1)^{-1} 2\underline{S}j \times \underline{r}_j \cdot \nabla r_j^L Y_L^{M*}(\Omega_j)$$

$$M_{LM} = \mu_o \sum_j (g_{sj}\underline{S}_j + 2(L+1)^{-1} g_{Lj}\underline{\ell}_j) \cdot \nabla r_j^L Y_L^{M*}(\Omega_j))$$

In order to proceed further the matrix elements must be calculated. This implies a knowledge of the nuclear wave functions and hence the result depends on the nuclear model that is assumed to apply. Order-

of-magnitude calculations have been performed by Blatt and Weisskopf[10] for a simple independent-particle model. The results suggest that the matrix elements are independent of energy, and lead to the following estimates;

$$\Gamma_W(E1) = 2.0 \times 10^{-1} A^{2/3} E_\gamma^3$$

$$\Gamma_W(M1) = 6.3 \times 10^{-2} E_\gamma^3$$

$$\Gamma_W(E2) = 2.7 \times 10^{-7} A^{4/3} E_\gamma^5$$

$$\Gamma_W(M2) = 7.5 \times 10^{-8} A^{2/3} E_\gamma^5$$

Since the level density at excitation energies of several MeV is much larger than that obtainable with an independent particle model, the radiative widths, Γ_W, are obviously not correct at these energies. In order to extend the estimates to these energies Blatt and Weisskopf[10] use the following approximation. The level density obtained using an independent-particle picture can be greatly increased by splitting up the highly degenerate levels through the introduction of some correlations between the particles. If this is done the "strength" of the single-particle transition is shared among many levels. The radiative width associated with a single level is then, on the average

$$\Gamma = \Gamma_W D/D_o$$

where D_o is the level spacing obtained from the independent-particle model and D is the observed spacing. The single-particle estimate for E1 radiation becomes

$$\Gamma(E1) = 2.0 \times 10^{-1} A^{2/3} E_\gamma^3 D(E)/D_o$$

with $D_o \sim 0.5$ MeV.

The estimate of Axel[11] for the transition probability for El radiation arises from the observation that the cross section for the inverse process (photon absorption) contains the same matrix elements. For the absorption of El radiation it can be shown that

$$\langle \sigma_a \rangle = C\, E_\gamma \left| \langle f | Q_{1,1} | i \rangle \right|^2 / D(E_\gamma)$$

where $D(E_\gamma)$ is the spacing of the levels that can be reached by photon absorption. As has been indicated above, the single-particle estimate assumes that $\left| \langle f | Q_{1,1} | i \rangle \right|^2$ is independent of energy. This would suggest that the cross section for the absorption of El radiation varies with energy as $E_\gamma / D(E_\gamma) \sim E_\gamma \exp(E_\gamma)$. This is in contrast to the measured cross section which shows a broad resonance, the so-called giant dipole resonance, at an excitation energy of $\sim$15 MeV. By assuming a Lorentz shape for the absorption cross section, with a full width at half maximum of 5 MeV and a peak energy $E_r = 80\, A^{-\frac{1}{2}}$, Axel[11] finds that for an excitation energy of $\sim$7 MeV

$$\langle \sigma_a \rangle = 5.2 \times 10^{-3} \left(\frac{E_\gamma}{7\ \text{MeV}} \right)^3 \left(\frac{A}{100} \right)^{8/3}$$

This can then be used to estimate the radiative width to the ground state which is given by

$$\Gamma(\text{El}) = 2.2 \times 10^{-5} \left(\frac{A}{100} \right)^{8/3} \left(\frac{E_\gamma}{7\ \text{MeV}} \right)^5 / D(E)$$

In order for this estimate to be applicable for transitions to states other than the ground state, one has to assume that the low energy state in question has an associated dipole resonance. Further, this resonance must have the same shape and be at the same relative excitation energy as the ground state giant dipole resonance. The observation of such resonances is, of course, impossible using (γ,n) or

(γ,p) reactions. Recently Singh et al[15] have observed a giant resonance structure associated with the first excited state of ^{28}Si by looking at the $^{27}Al(p,\gamma)^{28}Si$ reaction. This resonance was displaced from the ground state resonance by about the same energy as the energy of the first excited state. This result suggests that Axel's[11] prediction for El ground state transitions might also apply to transitions to excited states.

An extensive survey of the neutron capture results to obtain transition probabilities for known El and Ml transitions, has been published by Bartholomew[5]. He finds reasonable agreement with the single-particle estimates using a value of D_o of 15 MeV. Carpenter[2] has measured ground state radiative widths in the mass region $143 \leqslant A \leqslant 201$ to try to test Axel's[11] predictions. These experiments were performed using resonance capture and averaging over up to fifteen resonances in order to reduce Porter-Thomas[16] fluctuations. The data did not allow any distinction between the single-particle estimates and Axel's[11] prediction.

1.3 Nuclear Level Densities

The theoretical description of nuclear level densities depends, to some extent, on the nuclear model that is assumed to hold. The earliest descriptions, that is those of Bethe[17,18] and of Lang and Le Couteur[19], considered non-interacting Fermions confined to the nuclear volume. The calculations were extended by Block[20], Cameron[21], and Newton[22] to include shell model effects by considering the Fermions to be moving in a shell model potential with no residual interactions.

The difference in binding energy for odd A systems compared to even A systems has been included in the calculations of Ericson[23], and Lang and Le Couteur[24]. More recently the analogue between nuclear matter and a superconducting metal suggested by Bohr et al[25] and extended in detail by Belyaev[26], has been used by Ericson[23], by Lang[27] and by Vonach et al[28] to calculate level densities.

The theoretical approach to the problem is essentially that of statistical mechanics. Starting with the energy levels available to a single particle of the system, one can construct the possible energies for a system of N such particles. To do this one can distribute the N particles among the possible states, subject to the constraints imposed by the constants of motion that apply to the system. By calculating the total energy associated with each of the possible configurations and ordering them in increasing size, the level density can be found. Hence the problem is a combinatorial one whose solution can be approximated by the usual methods of statistical mechanics.

Starting from the grand partition function

$$Z(\alpha,\beta) = \sum_{ij} \exp\,(\alpha N_j - \beta E_i)$$

and the required level density of the form

$$\rho(E,N) = \sum_{ij} \delta(E-E_i)\delta(N-N_j)$$

the partition function can be rewritten

$$Z(\alpha,\beta) = \int\rho(E,N)\,\exp(\alpha N - \beta E)\,dN\,dE$$

Here the N_j's are the eigenvalues associated with some constant of motion of the system.†

---

† For simplicity we have here considered only such constant of motion. The extension to any number is obvious .

The level density is then the Laplace transform of the partition function

$$\rho(E,N) = \frac{1}{(2\pi i)^2} \int_{-i\infty}^{i\infty}\int_{-i\infty}^{i\infty} Z(\alpha,\beta)\, \exp\,(\beta E-\alpha N)\,d\alpha d\beta$$

This integral can be approximated by the method of steepest descent to give

$$\rho(E,N) = \frac{\exp\left[\ln Z(\alpha_o,\beta_o)-\alpha_o N+\beta_o E\right]}{2\pi(-\det A)^{\frac{1}{2}}}$$

where α_o and β_o are determined by the equations for the saddle point of

$$f(\alpha,\beta) = \ln Z(\alpha,\beta) - \alpha N + \beta E$$

that is $\left(\frac{\partial f}{\partial \alpha}\right)_{\alpha_o} = 0$ and $\left(\frac{\partial f}{\partial \beta}\right)_{\beta_o} = 0$. The determinant of A is given by

$$\det A = \begin{vmatrix} \frac{\partial^2 \ln Z}{\partial \beta_o^{\,2}} & \frac{\partial^2 \ln Z}{\partial \beta_o \partial \alpha_o} \\ \frac{\partial^2 \ln Z}{\partial \beta_o \partial \alpha_o} & \frac{\partial^2 \ln Z}{\partial \alpha_o^{\,2}} \end{vmatrix}.$$

Hence the determination of the partition function leads directly to the level density.

The entropy S of the system can be identified with

$$S = \ln Z + \beta E - \alpha N$$

and neglecting the energy dependence in det A we get

$$\rho(E,N) \approx \exp(S)$$

For an isolated system

$$TdS = dE$$

and for a Fermi gas

$$C_V = \left(\frac{\partial E}{\partial T}\right)_V \sim T.$$

Hence $E \sim T^2$ and $dS \sim dE/\sqrt{E}$ so that

$$\rho(E) \sim \exp \sqrt{E}$$

A more detailed calculation[29] shows that $(-\det A)^{\frac{1}{2}} \sim E^{5/4}$ and gives the form of the level density as

$$(E) = \frac{\sqrt{\pi}}{12} \frac{\exp (2\sqrt{aE})}{a^{1/4} E^{5/4}}$$

This expression can be expected to hold at high excitations where the effects of residual interactions are expected to be small.

At low excitation energies the residual interactions lead to differences between the observed energy spectrum and that of a Fermi gas. In lowest order this residual interaction gives rise to a pairing effect between pairs of particles in degenerate orbits. In an electron gas these pairing interactions lead to the existence of an energy gap in the spectrum and are responsible for the superconducting properties of such a system. The existence of a gap between the ground state and the first intrinsic excitation in even-even nuclei implies that such an interaction is also present in nuclear systems[25]. Ericson[23] has suggested that the existence of such correlations should lead to a second order phase transition. This transition is caused by the breaking up of the correlated pairs which result in a decrease in the gap with increasing excitation energy. The region of excitation energies over which this phase transition occurs is expected to be extensive because of the rather small number of particles in the system.

Again using thermodynamical arguments, the temperature is expected to be constant during this phase transition so that $S \sim E/T$ and

$$\rho(E) \sim \exp(E/T)$$

More elegant methods have been used by Ericson[23], by Lang[27] and by Vonach et al[28] to include the effects of the superconducting model in the calculation of the level density. These results, although not expressible in a simple analytical form, suggest that the temperature is almost constant for excitation energies below the transition from the superconducting state. The energy at which this transition occurs has been estimated at between 15 and 18 MeV[28].

The parameters associated with the level density obtained from different experiments in general will be different. This occurs because of the preferential population of certain classes of states. For example, the resonant capture of s-wave neutrons leads to the selective population of states characterized by a total angular momentum $|J_T - \frac{1}{2}| \leq J \leq J_T + \frac{1}{2}$ and parity $\pi = \pi_T$ where J_T and π_T are the total angular momentum and parity of the target nucleus. Hence the level density measured in this case is much less than the true level density which consists of levels of both parities and all angular momenta.

It is therefore necessary to know the probability of finding a level with angular momentum J as a function of excitation energy E. Following the arguments of Bethe[17,18] it is assumed that the distribution in the Z projection of the angular momentum, M, is given by

$$P(M) = (2\pi\sigma^2)^{\frac{1}{2}} \exp(-M^2/2\sigma^2)$$

Here $\sigma^2 = g\langle M^2 \rangle T$ where g is the sum of the neutron and proton single-particle level spacings, T is the thermodynamic temperature of the

nucleus and $\langle M^2 \rangle$ is the mean square magnetic quantum number for the single-particle states. From this, one obtains immediately the distribution in J, that is

$$\rho(J) = (2\pi\sigma^2)^{-\frac{1}{2}} \left[\exp(-J^2/2\sigma^2) - \exp(-(J+1)^2/2\sigma^2)\right]$$

$$\approx \frac{(2J+1)}{\sqrt{\pi}2\sigma^3} \exp(-J(J+1)/2\sigma^2) \qquad (1\text{-}1)$$

With the assumption that σ^2 is independent of energy

$$\rho(E,J) = \rho(E) \frac{(2J+1)}{2\sigma^2} \exp(-J(J+1)/2\sigma^2)$$

where

$$\rho(E) = \frac{\sqrt{\pi}}{12} \frac{\exp(2\sqrt{aE})}{a^{1/4} E^{5/4}} \qquad \text{(Fermi gas)}$$

or

$$\rho(E) = \rho_o \exp(E/T) \qquad \text{(constant T)}$$

1.4 The Statistical Model

The measurement of some physical quantity is, in effect, a sampling from a distribution associated with the "true value" of the quantity. The distribution from which the sample is obtained is, in general, the convolution of two distributions. One of these is related to the precision of the experiment while the second is the inherent distribution in the quantity itself. An example of the limiting case, where the inherent distribution is a delta function, is the measurement of the mass of a stable nucleus since this quantity has no inherent statistical properties. For such quantities it is usually assumed that the distribution from which the sample was obtained is

normal. Hence the well-developed statistical analysis for such variates can be used. The number of counts per second from a radioactive source is a familiar example of the other extreme, where provided the number of counts obtained is not too large, the fluctuations are the result of the inherent statistical nature of the quantity being measured. The statistical analysis of such quantities must take into account this inherent distribution.

The quantities of concern here, that is the primary γ-ray intensities, I, and the spacing between adjacent energy levels, S, according to the statistical model, have inherent distributions. The object of this section, then, is to discuss the theoretical predictions and experimental confirmation of this model, particularly in relation to the inherent distributions of these variates.

The theoretical description of the energy levels of a nucleus must be obtained by diagonalizing a Hermitian matrix; the so-called Hamiltonian matrix. The eigenvalues correspond to the energies of the levels and the eigenvectors give the wave functions of the levels in the basis in which the Hamiltonian was described. If there are no degeneracies, that is if no two eigenvalues are the same, the size of the Hermitian matrix to be diagonalized would be N x N where N is the number of energy levels. Clearly such a program for all but the simplest systems would be prohibitive.

There are symmetries associated with the physical system that reduce the problem. For example, the conservation of total angular momentum and parity introduce certain symmetries into the Hamiltonian. If a representation is chosen that is diagonal in the total angular

momentum, J, and parity π, that is, if the basis vectors are eigenvectors of the operators associated with J and π, the Hamiltonian matrix divides into submatrices, all of which are zero except for those on the diagonal. The Hamiltonian matrix can then be diagonalized by independently diagonalizing each submatrix. Since each submatrix corresponds to a definite value of J and π, the size of the submatrix is of the order of the number of levels of the system with a particular J, and π. Hence, except for very large J where the number of levels is expected to be small the problem is still prohibitive.

It is natural, then, to try to develop a statistical treatment. Such a treatment has been suggested by Wigner[30,31] and modified by Dyson[32]. The ensemble suggested by Wigner is unique in that he considers the ensemble of Hamiltonians of all nuclei rather than the ensemble of all possible states of a given nucleus, as would be done in classical statistical mechanics. The Hamiltonian of a given system (for instance ^{235}U) is then a sample from this ensemble. Dyson's treatment differs from that of Wigner only in the distribution function associated with this ensemble.

Most theoretical work has been done using the Gaussian ensemble[33,34] which is defined as follows. Consider the real (time-reversal invariant) symmetric Hamiltonian submatrix associated with a given J and π. When expressed in terms of some simple basis, for example the single-particle wave functions, each of the N(N+1)/2 different matrix elements is sampled from a Gaussian distribution. The off-diagonal elements are assumed to have zero mean and the diagonal elements the

same mean. Under the assumption that the matrix elements are statistically independent and their distribution is independent of the representation, Porter and Rosenzwieg[33] have shown that the variance of the diagonal elements is twice that of the off-diagonal ones. The distribution function associated with the Gaussian ensemble is then

$$P(H) = A \exp(-\sum_i H_{ii}^2 + 2 \sum_{i \neq j} H_{ij}^2)/4a^2$$

An analysis by Porter and Rosenzwieg[33] of the distribution of the matrix elements calculated by Kurath[35] shows rather striking agreement with the above distribution.

Proceeding from the above distribution, one would like to calculate the distribution in the nearest neighbour spacings between the eigenvalues and the distribution of the eigenvector components. The calculation of the latter distribution has proved to be relatively simple compared to calculation of the former.

As pointed out by Porter and Rosenzwieg[33], the assumption of the independence of the Hamiltonian to the representation implies that the component distribution is that obtained from a randomly oriented vector. Hence the distribution function of the components, c, is

$$P(c) = (N/2\pi)^{\frac{1}{2}} \exp(-c^2/(2/N))$$

where N, the dimension of the representation, is assumed large. Since the partial width of a level is proportional to the transition probability into that channel and the transition probability is proportional to c^2, it follows that the distribution of single channel widths is a χ^2 distribution with one degree of freedom, that is

$$P(\Gamma) = (2\pi\Gamma/\bar{\Gamma})^{-\frac{1}{2}} \exp(-\Gamma/2\bar{\Gamma})$$

where $\bar{\Gamma}$ is the mean width. The very precise statistical treatment by Porter and Thomas[16] on the neutron width data is in agreement with this distribution. Fluctuations in partial γ-ray widths[36,37] indicate that they also have a broad distribution consistent with a χ^2 distribution of one degree of freedom.

The calculation of the spacing distribution of the eigenvalues of a random matrix presents a much more difficult problem. By noting a repulsion effect between eigenvalues of a 2 x 2 matrix, Wigner[32] surmised a spacing distribution of the form

$$P(S) = (\pi/2)\ X \exp\ (-(\pi/4)\ X)$$

where $X = S/\bar{S}$. Monte-Carlo calculations have been performed by many authors[33,38,39,40] and compared with Wigner's surmise. No discrepancies were found for random matrices up to a dimension of 20 x 20. Metha[34], by calculating analytically an upper and lower bound for the spacing distribution, has shown that although Wigner's surmise is not exact for large random matrices, the difference between it and the true distribution is negligible. The nearest neighbour spacing distribution for observed neutron resonances with the same J seems also to be in agreement with this distribution[33].

CHAPTER II

INSTRUMENTATION

2.1 Through Tube Facility

There are in general two possible geometries that can be used in the study of gamma rays emitted in thermal neutron capture. The sample of the isotope to be studied can be located outside the reactor shielding in a beam of neutrons extracted from the core or the sample can be located in the vicinity of the core and a beam of the emitted gamma rays extracted. Each has distinct advantages dependent upon the spectrometer to be used, the nuclide to be studied and the information desired.

In general external irradiation offers ease in changing samples and the possibility of coincidence as well as single spectrum measurements. Internal irradiation on the other hand, offers lower backgrounds, higher efficiencies and a well collimated gamma ray beam that is necessary for many spectrometers.

A through tube, that is a beam tube which passes through the core, offers an irradiation facility that can be used in both geometries; graphite or heavy water being used as a scatterer when a neutron beam is desired. In addition, relatively low backgrounds are possible by removing direct radiations from the core through proper collimation.

A schematic drawing of the tube is shown in Figure 2-1. Constructed from 65 ST aluminum pipe, the tube occupies a position

FIG 2-1

SCHEMATIC OF BEAM TUBE

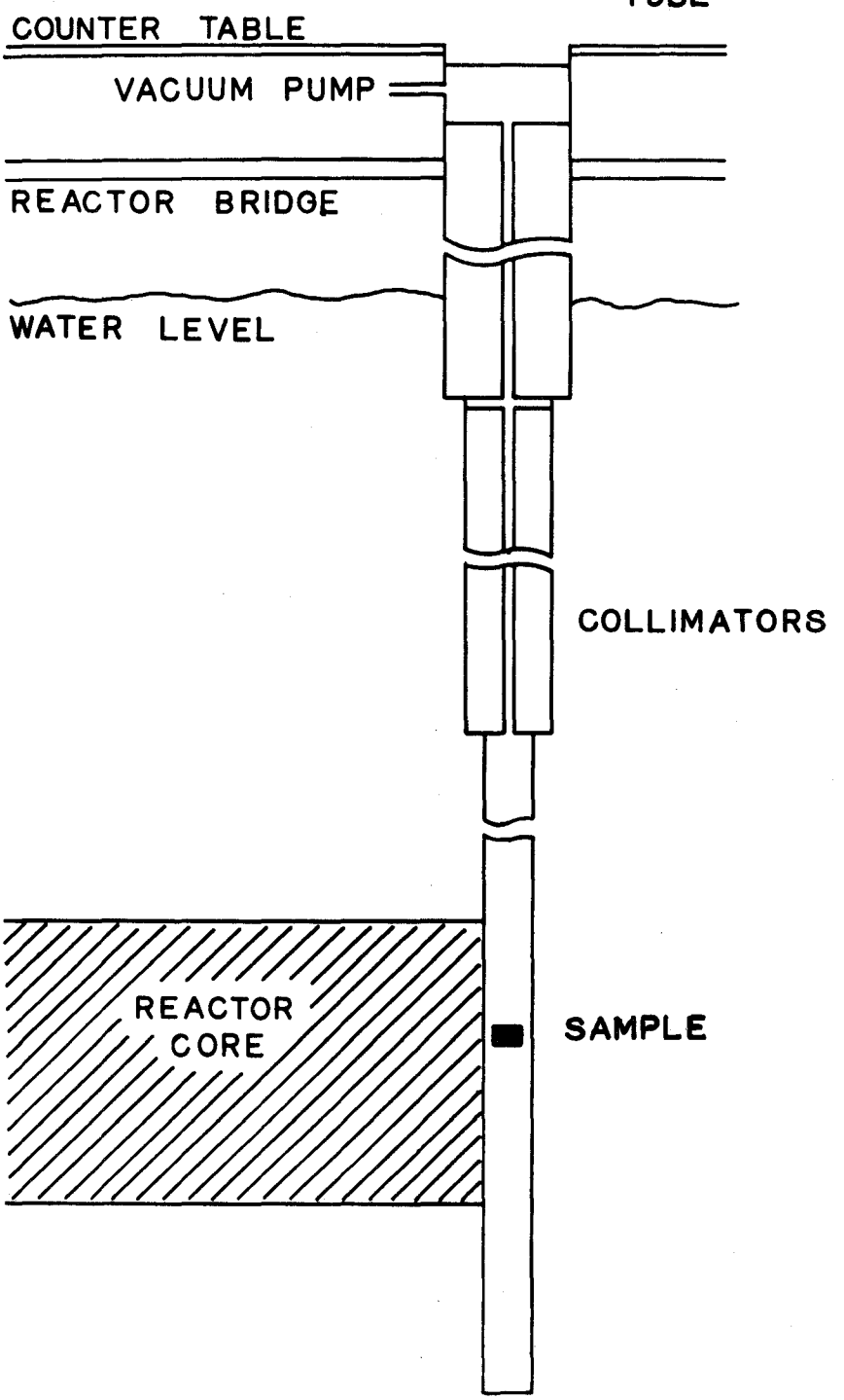

normally taken by a fuel rod, extending approximately 60 cm below the grid plate. Collimation is provided by two removable tanks as shown. The steps prevent the streaming of neutrons and gamma rays along the walls as well as providing seats for the tanks. Collimators whose inside diameters are less than 2.5 cm insure that only radiation from the end of the tube 60 cm below the grid plate can pass through. Since at this position the neutron flux is lower than the peak flux by a factor of 200 , the background due to neutron capture in the bottom of the tube is small. These collimators also only transmit γ-rays from the core that are scattered through 180°. Since these have energies of less than 250 keV, which can easily be scattered out of the beam, the background is minimal. To stop the scattering of unwanted radiations into and the wanted radiations out of the beam, provision was made for evacuating the tube.

Because of the availability of large samples of the nuclides studied in this work, the more flexible external irradiation made was used exclusively.

A schematic drawing of the tube being used in this manner is shown in Figure 2-2. With three 17 cm sections of graphite placed in the bottom of the tube, the flux at the sample position was of the order of 10^7 neutrons/cm^2 sec. A cadmium ratio of 134, measured with a 1/V detector, when compared with the ratio that is obtained in the lattice of graphite or deuterium pile (which is $\sim$33) indicates a small fast neutron contribution. For smaller cross section materials, fluxes as high as 10^8 neutrons/cm^2 have been used.

FIG. 2-2
IRRADIATION FACILITY

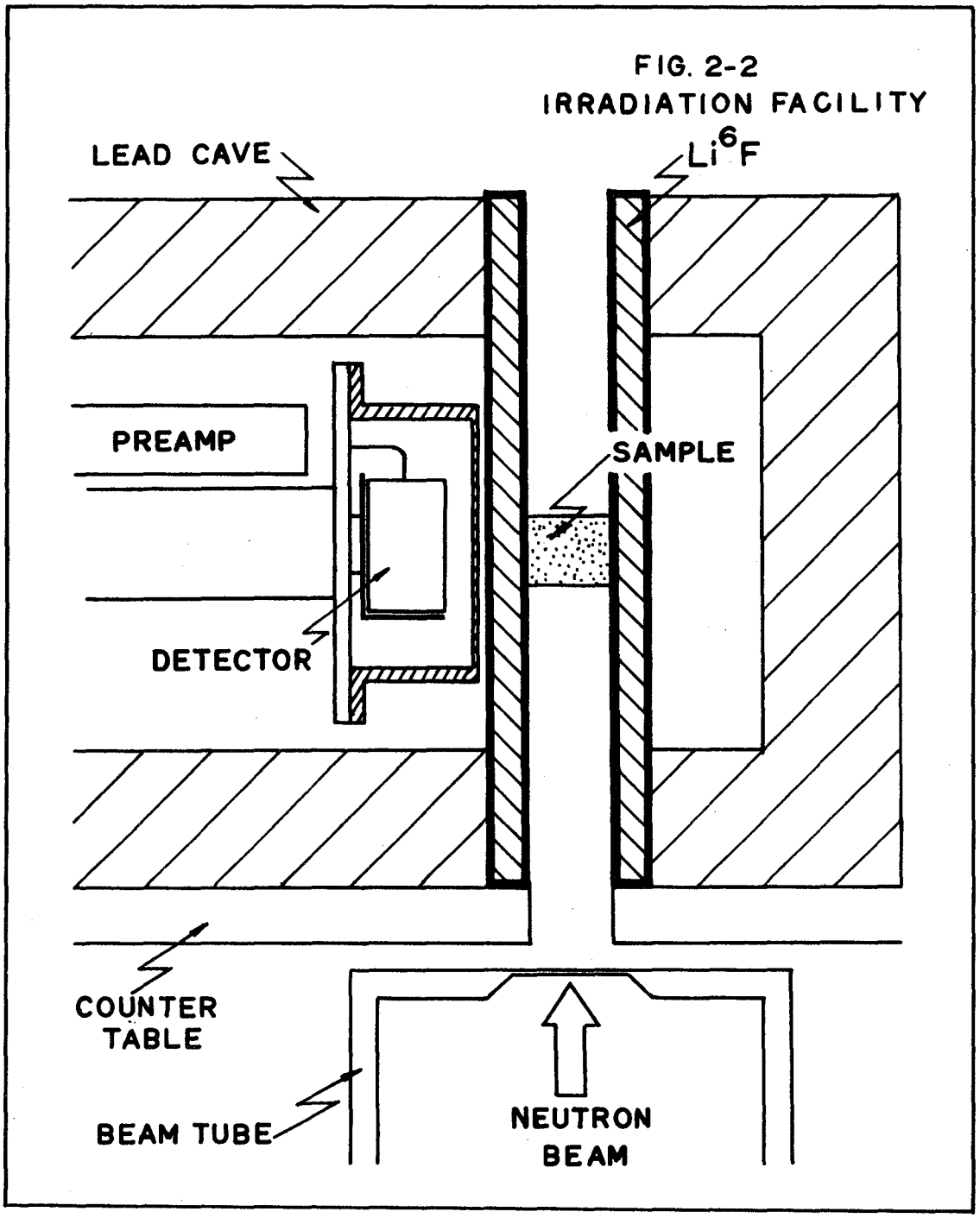

Protection for the counters from scattered neutrons is provided by a 3 mm thick annulus of LiF enriched to 98% in ^{6}Li. The large (n,α) cross section of ^{6}Li (950 barns) provides good thermal neutron absorption with no gamma ray emission. Because of the low number of electrons/atom, this thickness of material causes negligible absorption of the gamma rays of interest, and hence little perturbation of the spectra under study.

2.2 Solid State Counters for γ-Ray Detection

The interaction of a γ ray with a semiconductor occurs through three primary processes resulting in so-called photoelectric, Compton and pair production events. These processes give rise to energetic electrons or in the case of pair production, electrons and positrons. The charged particles so produced are then thermalized in the material, creating by collision, phonons and electron-hole pairs. Schematic drawings of the energy distributions of the primary electrons for these processes are shown in Figure 2-3 for a γ-ray energy E = 2.7 MeV. The sum of these three distributions, weighted according to their relative cross sections, is the probability of a primary electron being produced between E' and E' + dE' when a γ ray of energy E interacts with the material.

The energy deposited in the semiconductor, E_d, deviates from the above because of two effects that depend on the size of the material. The first effect results from the further interaction of a Compton scattered γ ray. These multiple events lead to an enhancement of the peaks relative to the continuum which increases with the size of

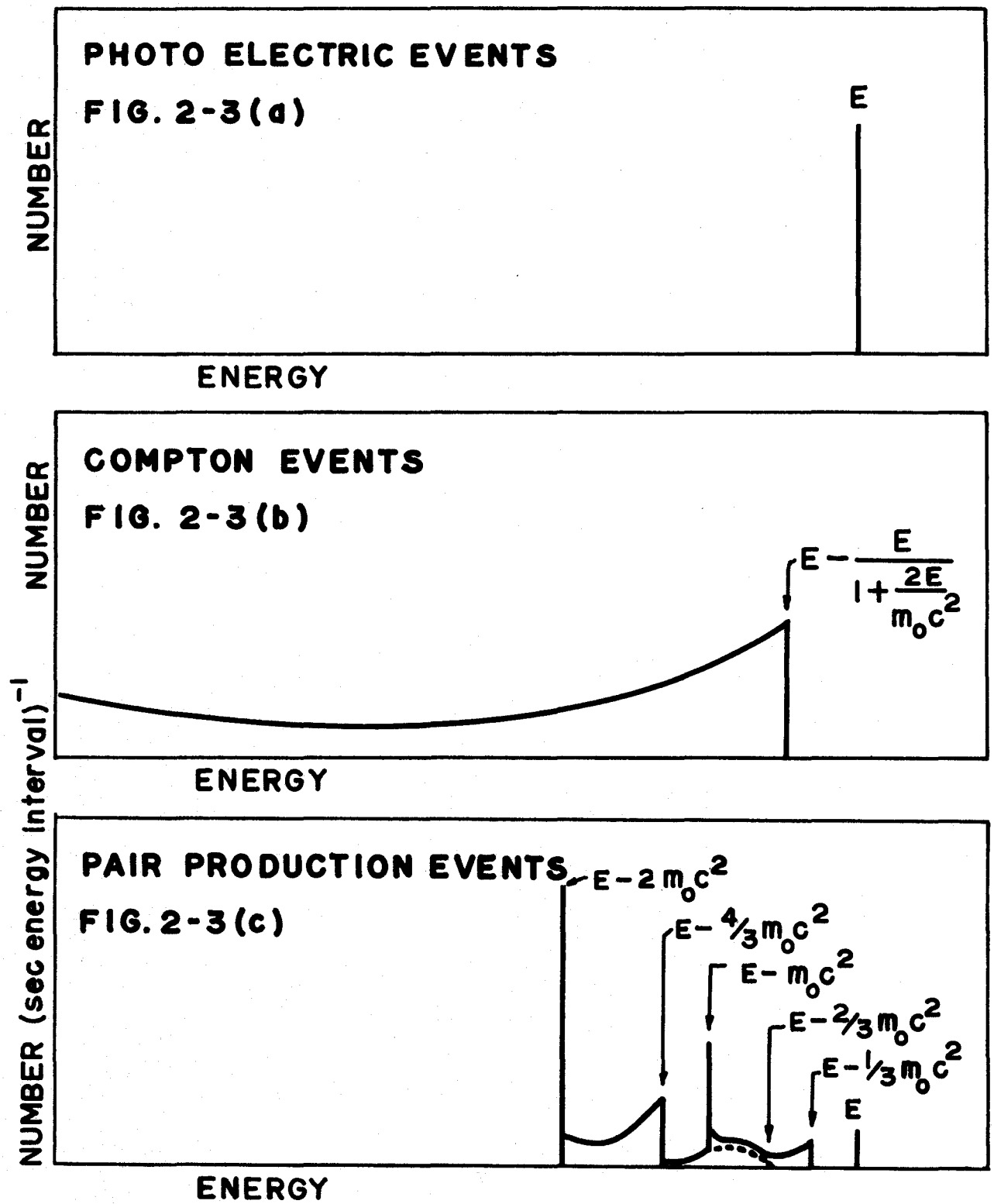
PHOTO ELECTRIC EVENTS
FIG. 2-3(a)
NUMBER
E
ENERGY
COMPTON EVENTS
FIG. 2-3(b)
NUMBER
$E-\frac{E}{1+\frac{2E}{m_0c^2}}$
ENERGY
PAIR PRODUCTION EVENTS
FIG. 2-3(c)
NUMBER (sec energy interval)$^{-1}$
$E-2m_0c^2$
$E-4/3m_0c^2$
$E-m_0c^2$
$E-2/3m_0c^2$
$E-1/3m_0c^2$
E
ENERGY

the semiconductor. The second effect arises from the loss of energetic electrons or positrons from the material. Such partial energy transfer removes events from the peaks into a continuum. Here again the peaks are enhanced over the continuum as the volume increases. The frequency function for the distribution in energy deposited, E_d, can be written

$$P_1(E_d,E) = \sum_{i=0}^{2} p_1^i(E_d,E) + p_1^c(E_d,E)$$

where

$$p_1^i(E_d,E) = p_i(E)\,\delta(E_d - E + iE_a) \quad .$$

Here E_a is the energy of the two γ rays emitted in the annihilation of the positron and $p_i(E)$, i = 0 to 2, are the probabilities of the three precise energy transfers indicated. The distribution $p_1^c(E_d,E)$ is a continuous one over the range $0 \leq E_d \leq E$ caused by partial energy transfer events due to Compton interactions and electron or positron escape as mentioned above.

This energy deposited in the semiconductor produces n to n + dn electron-hole pairs with probability $P_2(n,E_d)dn$. The frequency function for n electron-hole pairs being produced by a γ ray of energy E is then

$$P_3(n,E) = \int P_2(n,E_d)\,P_1(E_d,E)\,dE_d$$

The three δ-function energy transfers lead to peaks in $P_3(n,E)$ whose mean positions are given by

$$n_i = \int n\,P_2(n,E - iE_a)dn$$

and variances by

$$\sigma_i^2 = \int n^2\,P_2(n,E - iE_a)dn$$

Since n_i depends on E the counting of the number of electron-hole pairs produced leads to a measure of E. The usefulness of the spectrometer so produced depends on the energy resolution, $R_i = \sigma_i'/n_i$, and on the peak-to-total ratio, $p_i(E)$.

The properties of the spectrometer depend, then, on $P_2(n,E_d)$, the frequency function for the number of electron-hole pairs produced when an energy E_d is deposited in the detector. It is usually assumed that $P_2(n,E_d)$ is Poisson with a mean and variance of $\bar{n} = E_d/\bar{\omega}$ where $\bar{\omega}$ is the average energy required to create an ion pair. As pointed out by Fano[41] this assumes that the number of interactions required to transfer the energy to the crystal is fixed whereas, in fact, the total energy lost is fixed. The effect of this correlation between interactions is to reduce the variance as given by the Poisson distribution by the so-called Fano factor, F. For large $\bar{n}$, $P_2(n,E_d)$ then becomes approximately Gaussian with a mean of $\bar{n}$ and a variance of $F\bar{n}$, that is

$$P_2(n,E_d) = G\left(\left\{\bar{n}\middle|F\bar{n}\right\} n\right)$$

We have introduced the notation

$$G\left(\left\{\bar{x}\middle|\sigma^2\right\} x\right) = (2\pi\sigma^2)^{-\frac{1}{2}} \exp\left(-(x-\bar{x})^2/2\sigma^2\right)$$

The mean energy required to create an ion pair, $\bar{\omega}$, is to high order independent of E_d and for germanium is 2.8 eV. Mann[42] has found the Fano factor for germanium to be independent of E_d also, but dependent on the detector bias. Extrapolating to infinite field he finds $0.05 \leqslant F \leqslant 0.10$. Using $F = 0.075$ the intrinsic energy resolution of the total absorption peak, R_o, is approximately 0.05% for a 1 MeV γ-ray.

As we have seen, in order to measure energies, the number of

current carriers produced by the γ ray must be measured. In order to make use of the inherently good energy resolution this measurement must be done with high efficiency as can be seen from the following. If f is the fraction of ion pairs counted, the frequency function for the number counted, n', is binominal with mean $\bar{x}$ = fn and variance σ^2 = fn(1-f) where n is the total number of ion pairs produced. Since n is large, this frequency function becomes approximately Gaussian

$$P_4(n',n) \quad G(\{fn|fn(1-f)\}\ n')$$

For the total absorption peak the frequency function for the number of ion pairs detected is given by the convolution of $P_4(n',n)$ into $P_2^o(n,E)$

$$P_5^o(n',E) = \int P_4(n',n)\ P_2^o(n,E)dn$$

Provided the variance of $P_4(n',n)$ doesn't change appreciably in the region where $P_2^o(n,E)$ is large, $P_4(n,n')$ can be replaced by $G(\{fn|f\bar{n}\ (1-f)\}\ n')$ and $P_5^o(n,E)$ becomes

$$P_5^o\ (n',E) = G(\{f\bar{n}|f\bar{n}(1 - f + fF)\}\ n')$$

In this approximation, and noting that $\bar{n} = E/\bar{\omega}$ for the total absorption peak, the detector response for this peak is

$$R_d^o(q,E) = G(\{2efE/\bar{\omega}\ |\ (4e^2fE/\bar{\omega})(1 - f + fF)\}\ q)$$

$$= G(\{\bar{q}\ |\ \sigma_q^2\}\ q)$$

where the charge collected is q = 2en', e being the charge of the elect tron. The associated energy resolution is $\sigma_q/\bar{q} = R_o(1 + (1-f)/fF)^{\frac{1}{2}}$ where R_o is the intrinsic resolution defined previously. We see then, a collection efficiency of 93% would increase the resolution by 10%

assuming a Fano factor of 0.075.

The need for a high collection efficiency seriously limits the semiconductor materials that can be used. Immediately after being formed the number of hole-electron pairs decreases, the decrease being exponential with a mean life τ_o that depends on the semiconductor material. If detection is achieved by collecting the current carriers at two parallel electrodes a distance d apart by means of a D.C. field, ε, the maximum collection time is given by

$$\tau_c = d/\mu\varepsilon$$

where μ is the mobility of the hole or electron whichever is the smallest. Complete charge collection then implies that

$$\tau_o > \tau_c$$

or that the carriers must have long lifetimes and high mobilities in the semiconductor used. Dislocations and impurities reduce the carrier lifetimes and mobilities, and hence should be avoided.

In practice, the only materials presently available that have sufficiently long carrier lifetimes and high carrier mobilities are germanium and silicon. To achieve complete collection in these materials requires fields of 300 volts/cm. Such fields are obtainable in back bias diodes.

The sensitive region for such devices is the depleted region. The square of the depth of the depleted region, d, is proportional to the resistivity of the material, ρ, and the applied voltage, V, that is

$$d = k(\rho V)^{\frac{1}{2}}$$

The value of k depends on the dielectric constant of the crystal and on the mobility of the majority carriers. Depths of the order of 0.5 mm are obtainable with diodes made from $10^4 \Omega$ cm silicon back biased with 100 volts.

In order to detect γ rays efficiently, depths of the order of 3 mm must be depleted. Depleted depths of this size have been successfully made by compensating p-type silicon or germanium with lithium as first suggested by Pell[43]. The method used consists of diffusing lithium into p-type material to give a concentration profile as shown in Figure 2-4(a). A junction is formed at d_j where the lithium concentration equals the doping concentration of the base material. When this diode is back-biased at room temperature, Li^+, being highly mobile, travels into the crystal under the influence of the field and pairs up in the proximity of the acceptor sites to produce intrinsic material. This new concentration profile is shown in Figure 2-4(b). The active region of the counter is now this compensated region. Depths as large as 1 cm can be produced by this method.

The absorption coefficients for photoelectric, Compton and pair production interactions for silicon and germanium as a function of the γ-ray energy are shown in Figure 2-5. The higher photoelectric and pair production absorption coefficients make germanium the obvious choice for γ-ray spectroscopy. Partial energy transfer caused by the escape of positrons or electrons from the sensitive volume of the counter with energies greater than $\bar{\omega}$ reduce the obtainable efficiencies below that expected from the absorption coefficients. For a given vol-

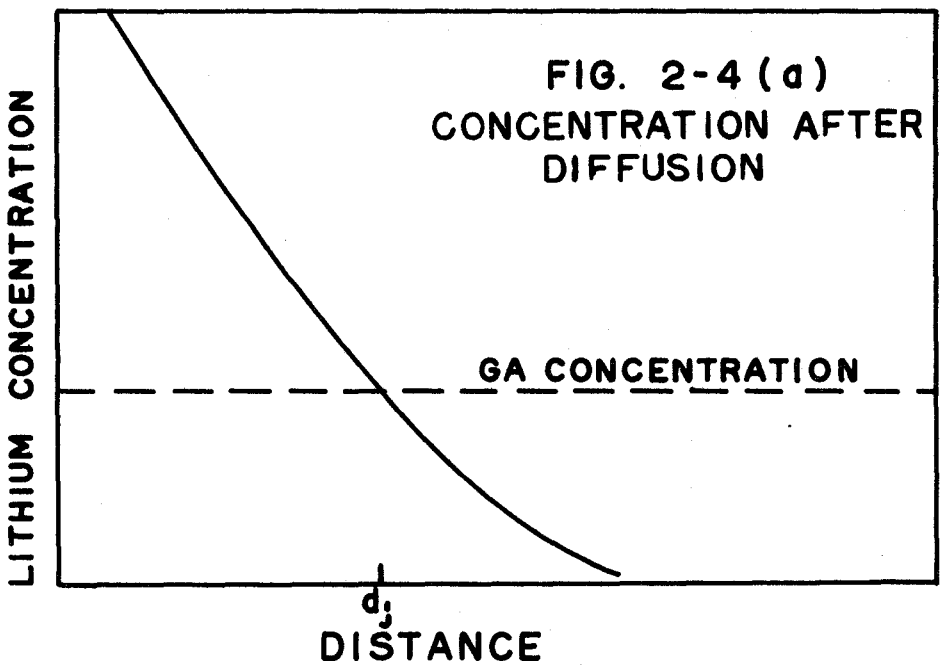

FIG. 2-4 (a)
CONCENTRATION AFTER
DIFFUSION

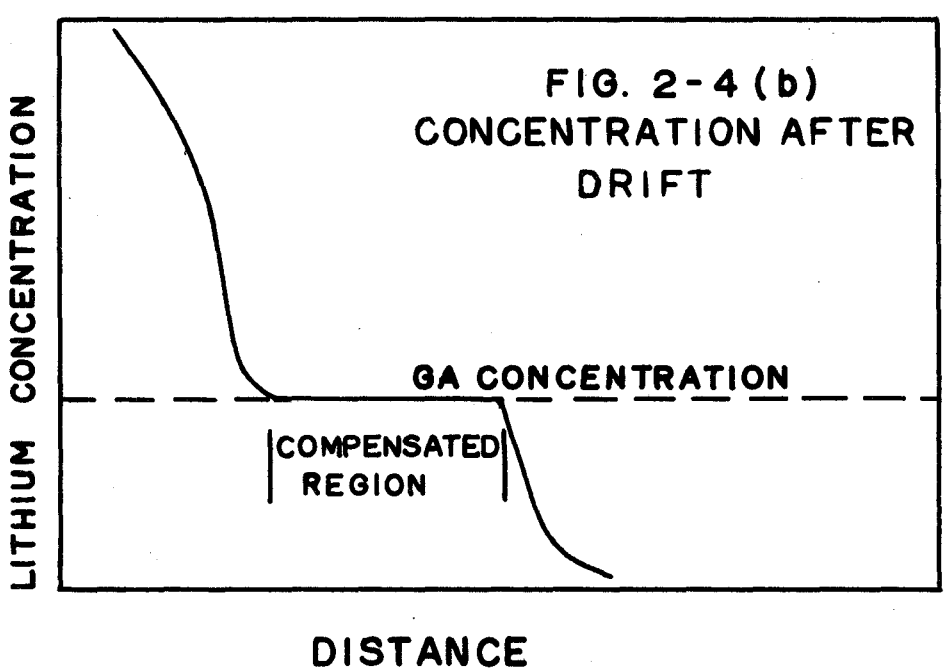

FIG. 2-4 (b)
CONCENTRATION AFTER
DRIFT

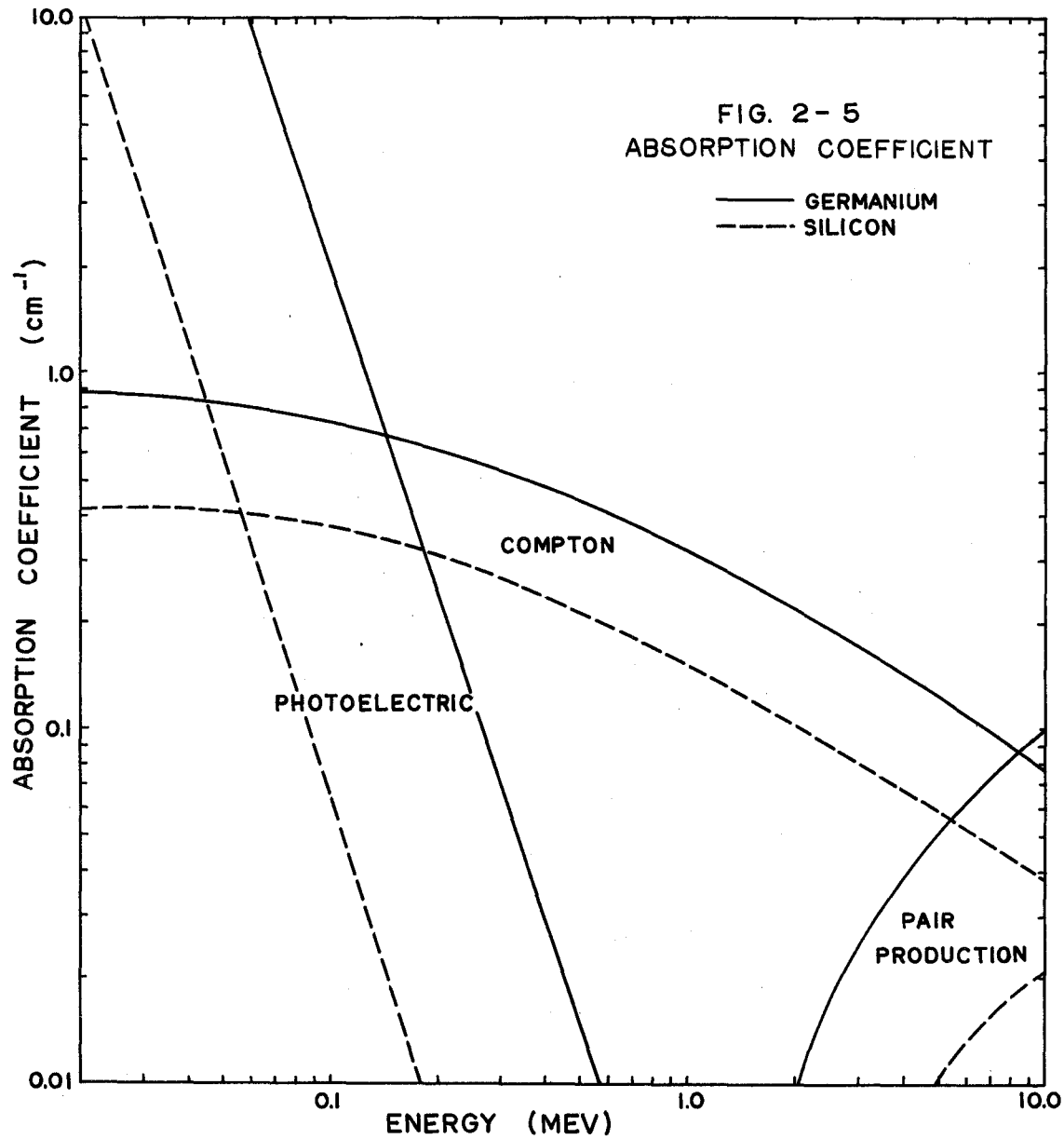
FIG. 2-5
ABSORPTION COEFFICIENT
GERMANIUM
SILICON
ABSORPTION COEFFICIENT (cm⁻¹)
10.0
1.0
0.1
0.01
COMPTON
PHOTOELECTRIC
PAIR
PRODUCTION
0.1
1.0
10.0
ENERGY (MEV)

ume the higher density of germanium, with the corresponding reduction in the range, reduces these partial energy transfer events.

The need for large counters for high-energy gamma-ray spectroscopy is obvious. Unfortunately, there are at present serious restrictions on the depth of the material that can be compensated. Under the influence of the field, ε, the lithium ions have an average velocity in the direction of the field given by

$$V = \mu\varepsilon$$

For a planar device

$$\varepsilon = V/d$$

where V is the applied voltage and d is the depleted depth. Provided the drift occurs at constant voltage and temperature it can be shown that

$$d^2 = 2\mu Vt$$

For a coaxial device

$$\varepsilon = \frac{V}{\ell n(b/a)} \frac{1}{r}$$

where a and b are the inner and outer radii respectively. Again provided that drift occurs at constant voltage and temperature

$$2\mu Vt = b^2 \ell n(b) - \frac{b^2}{2} - a^2 \ell n(a) + \frac{a^2}{2}$$

The percentage of the volume compensated as a function of time for a planar and coaxial configuration is shown in Figure 2-6. The crystal size used for both calculations was 1 cm thick with a 1 cm radius. It is obvious that much greater volumes can be depleted in a given time by the coaxial configuration, as has been suggested by Miller et al[44].

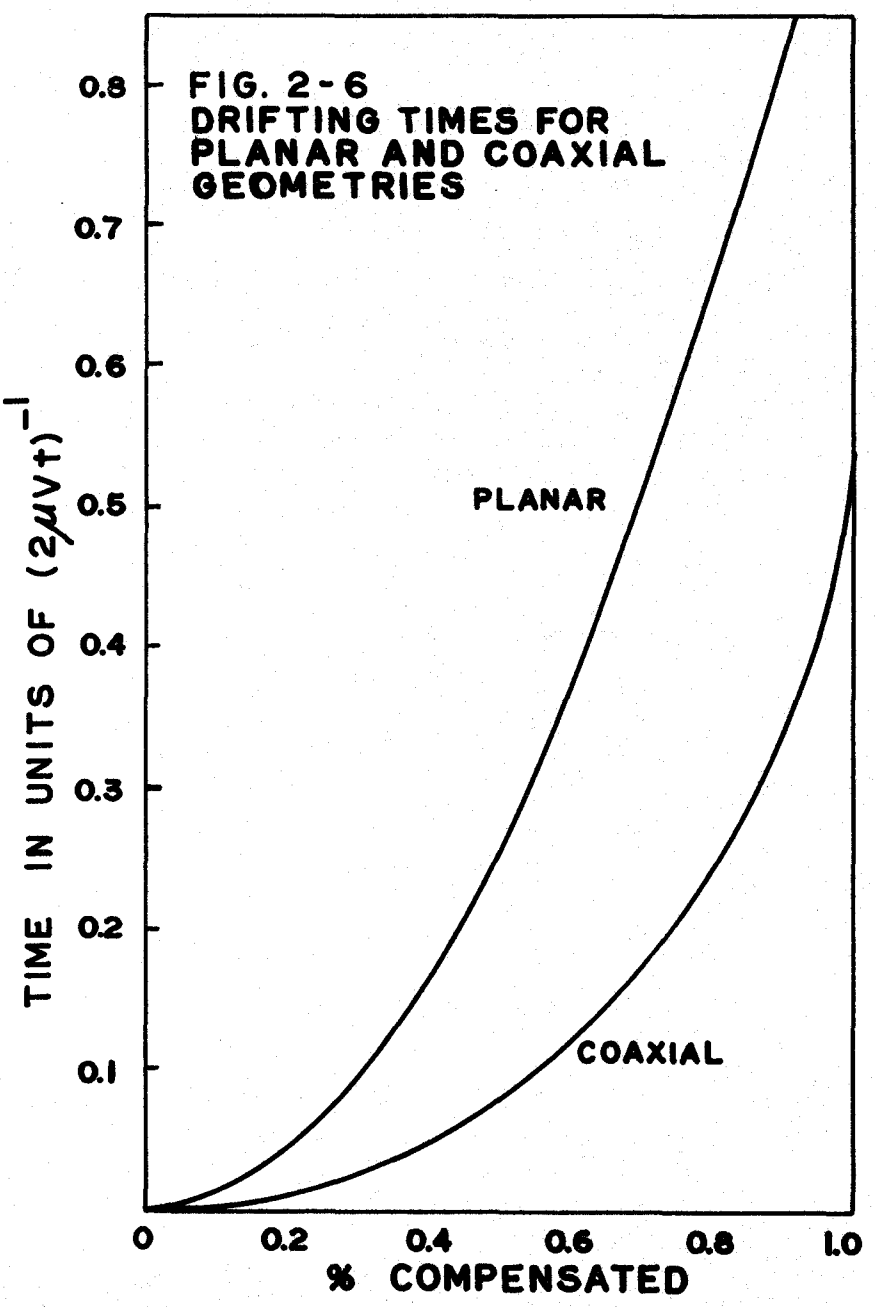
FIG. 2-6
DRIFTING TIMES FOR
PLANAR AND COAXIAL
GEOMETRIES
TIME IN UNITS OF $(2\mu Vt)^{-1}$
0.8
0.7
0.6
0.5
0.4
0.3
0.2
0.1
PLANAR
COAXIAL
0
0.2
0.4
0.6
0.8
1.0
% COMPENSATED

With a "wrap-around" configuration[45,46] where the drift proceeds from all but one face even shorter times may be expected. This also has the advantage that the area of the junction exposed is smaller than the other two configurations, minimizing surface effects.

The drifting time becomes important when one realizes that the devices are not stable at the drifting temperature. Reiss et al[47] have measured the solubility of lithium in germanium as a function of gallium concentration. For the gallium concentration of interest here ($\sim 4 \times 10^{16}$ atom/cm^3) the lithium solubility at room temperature is of the order of the gallium concentration. To form a junction at room temperature a supersaturated solution of lithium in germanium must be formed. The time taken for this solution to reach equilibrium depends on the number of precipitation centres in the crystal and the mobility of the lithium. In practice, good diodes last about one week at the drifting temperature ($\sim 50^{\circ}$C). During this time the drifted region can be extended from 0 to about 5 mm. To make larger compensated regions it is necessary to realloy the device and continue. During the heating cycle the compensated region is disturbed and the first half-day drifting is used to recompensate this region. Because of these considerations the maximum depth that is practical with present technology is about one cm.

2.3 Detector Fabrication

The fabrication of the detectors used in this work is described in detail by Fiedler et al[46]. The detector used for the majority of this work consisted of a 6 cc active volume counter constructed in the

wrap-around configuration. The initial resolution was approximately 9 keV at 8 MeV but due to radiation damage from the fast-neutron background deteriorated during the course of these experiments. Another counter of the same design with 7 cc active volume was then used with a resolution of approximately 12 keV at 8 MeV.

The starting material consisted of float-zoned, size No. 4, germanium ingots obtained from Sylvania Electric. This loaf-shaped ingot was gallium doped to between 5 and 10 Ωcm resistivity with a carrier lifetime of greater than 115 μsec. and a dislocation density of less than 2,000 pits/cm^3. After cutting to the required length with a high speed diamond saw the surfaces were lapped to remove saw damage. The ingot was then cleaned and dried in preparation for lithium diffusion.

Lithium was diffused into all but one cut face by electroplating Li^+ onto the desired surfaces from a molten solution of LiCl and KCl. The amount of KCl is chosen to lower the melting point of the solution below that required for optimum lithium diffusion which is around 420°C. A solution of 50% LiCl-50% KCl giving a melting point around 400°C was used. The electroplating apparatus shown in Figure 2-7 was carefully designed to give a uniform deposition of lithium and to resist the corrosive effect of nascent chlorine produced at the anode. Since a build-up of lithium on the surfaces causes pitting, the current was limited to avoid excessive deposition. This usually resulted in currents of the order of 0.02 amps per cm^2 of cathode surface.

After alloying, the device was removed from the bath and cooled. In order to avoid cracking, thermal shocks must be minimized and all ex-

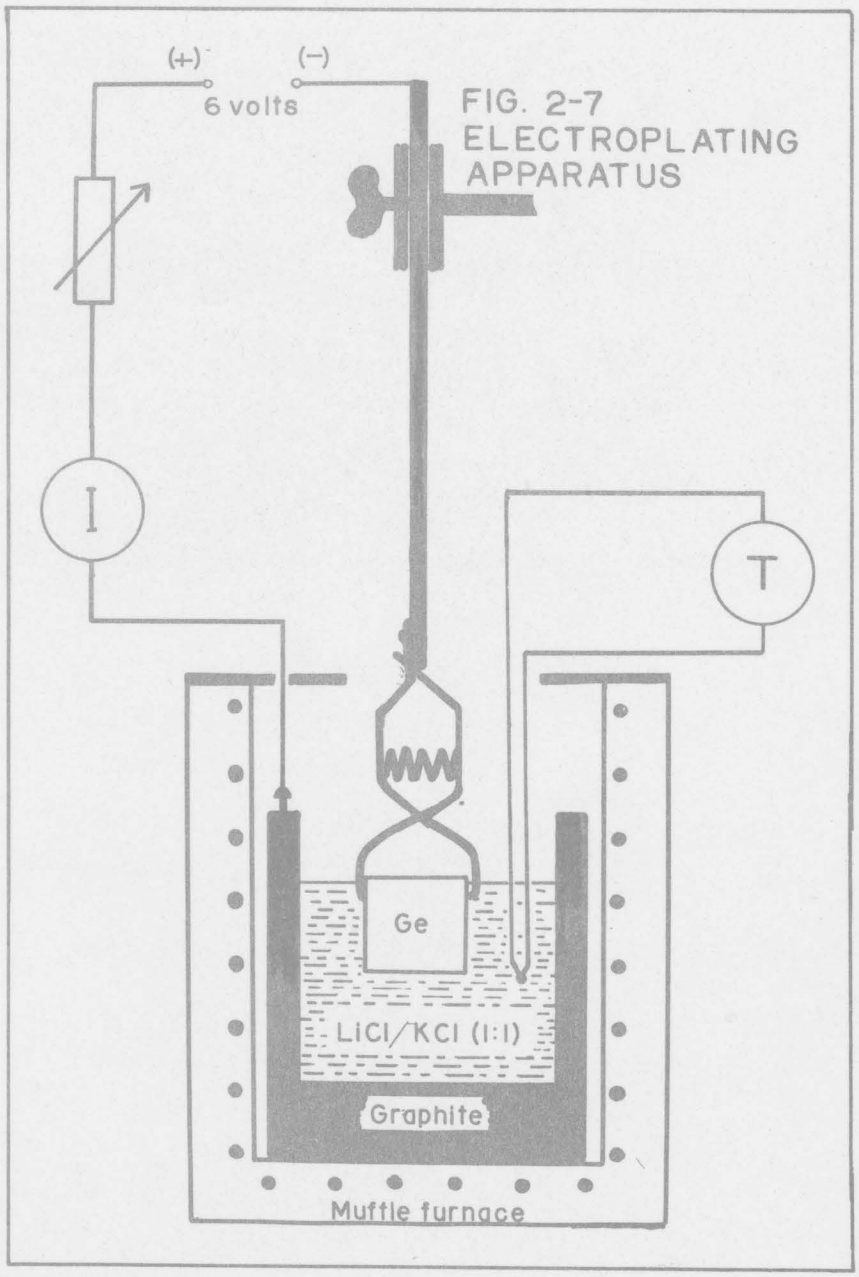

FIG. 2-7
ELECTROPLATING
APPARATUS

cess lithium is removed and the junction revealed on the unalloyed face by a standard copper-plating technique. This surface is then lapped until copper plating reveals the junction to be parallel to the sides of the device. Typical junction depths are 2 mm with a surface resistivity of approximately 0.01 $\Omega/\square$ for a 30 min alloying time. The diode is then prepared for drifting by etching the surface with the exposed junction until it is scratch-free. The etch, consisting of HF/HNO_3 (1:5 vol) activated with red fuming nitric acid (1:1 vol), was washed from the surface using distilled water.

The lithium is then drifted into the device using a D.C. voltage. In order to remove the power most efficiently and therefore drift most effectively, the device is immersed in a vapour-phase coolant with a boiling point at the temperature required for drifting. Freon TF solvent (B.P. 47.6°C) obtained from DuPont was almost exclusively used for the coolant. The current was limited by inserting 200-watt light bulbs in series with the detector. Typical diodes stabilized at 1 amp and 200 volts after a day of conditioning at lower power. Such a device could be depleted 5 mm in a week. Continual checking of the surface resistivity is necessary because of lithium precipitation. Above about 1 $\Omega/\square$ drifting virtually ceases and the diode characteristics must be reclaimed by heating or realloying.

When the device of the desired volume has been realized the exposed junction must be carefully prepared prior to packaging the detector in a dry, inert atmosphere and cooling to liquid nitrogen temperatures. The best counter characteristics seem to be obtained

when the device is etched and the acid washed from the surface with methanol. Two baths of electronic grade methanol were used. The majority of the acid on the surface was removed in the first and the counter quickly transferred to the second where it was immersed for about 5 min. The counter was then dried in an inert atmosphere and quickly transferred into the vacuum jacket of a specially designed liquid nitrogen Dewar. This surface treatment is that suggested by the results of Armantrout[48].

The liquid nitrogen Dewar, the design of which closely follows that of the Lawrence Radiation Laboratory[49], is shown in Figure 2-8. The construction is entirely from stainless steel except for the thin aluminum cap that provides an entrance window for the γ radiation. All gaskets are of Viton A which permits high vacuums with the convenience of reusable seals. The detector is secured to the liquid nitrogen finger using Dow Corning 200 silicon grease and electrical contact made through gold-plated pressure contacts. Connection is made to the preamplifier through a glass feed-through in the other wall as shown. A pressure of approximately 10^{-5} mm of Hg is maintained by a 1 litre per second vacion pump.

2.4 Data Acquisition for Single Counter Experiments

The experiments under consideration here, in general, are used to obtain energies and intensities of the emitted γ rays. If $S(E)dE$ is the probability of the sample emitting a γ ray of energy E to E + dE, we require a data acquisition system that can collect a statistically significant sampling of

$$M(q)dq = \int \varepsilon(E,\omega)\, R_d(q,E)\, S(E)dEdq$$

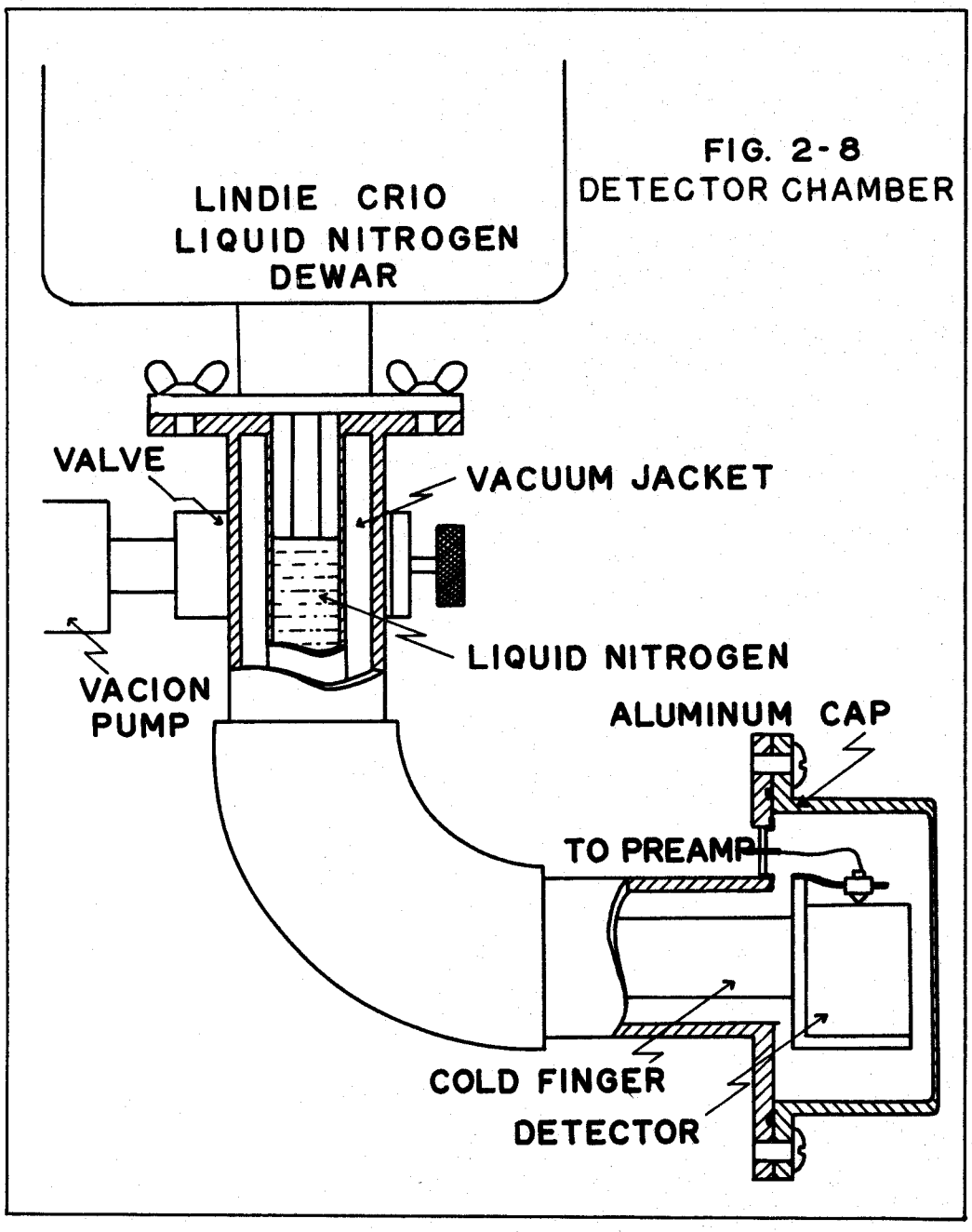

FIG. 2-8
DETECTOR CHAMBER

where $\varepsilon(E,\omega)$ is the detector efficiency when the counter subtends a solid angle ω from the source, and $R_d(q,E)$ is the previously mentioned detector response. Provided some information about $R_d(q,E)$ and $\varepsilon(E,\omega)$ is available, an estimate $S^*(E)$ can be obtained which approaches the required function, $S(E)$, in the limit of infinite sample size and zero detector resolution. Background radiation and γ rays following β decay of the ground state or any isomers of the system composed of the target nucleus and a neutron, if they exist, have been ignored in the above discussion. In practice the energies and effective intensities of these unwanted γ rays can be obtained and subtracted from $S^*(E)$ which, after renormalization, gives the required frequency function.

We require, then, a system that counts the number of charge pulses between q and q + dq for all possible values of q. In order to do this the charge pulse is converted to a voltage pulse and amplified to a workable pulse height h. If $R_a(h,q)$ is the frequency function for this process the response of the detector-amplifier system to a γ ray of energy E is

$$R(h,E) = \int R_a(h,q)\, R_d(q,E)dq$$

The required distribution

$$M(h)dh = \int \varepsilon(E,\omega)R(h,E)S(E)dEdh$$

can be obtained by counting the number of pulses with heights between h + dh. Since the spectrum contains discrete energies we can write $S(E) = \sum_i I_i\, \delta(E-E_i)$ and

$$M(h)dh = \sum_i I_i\, \varepsilon(E_i,\omega)R(h,E_i)dh$$

The normalization of the intensities I_i implied here, that is $\Sigma I_i = 1$, is arbitrary. It is customary to quote the intensities in number of γ rays per 100 captured neutrons.

The transfer function $R_a(h,q)$ is, of course, a function of the amplifier design. It is desirable that it contributes negligibly to the resolution of the spectrometer. This implies that the energy resolution is the smallest possible for a given detector since in this case the resolution is determined solely by the detector. In conflict with this requirement is the ability to handle high counting rates. This ability is desirable in order to reduce the time needed to collect the desired sample size of the pulse-height distribution. This compromise between energy resolution and collection time is most noticeable when the system is to be used with solid state counters because of their extremely good inherent energy resolution. In a well designed system the balance between high counting rates and good energy resolution should be adjustable to suit the requirements of the particular experiment.

The effects of the amplifier on the energy resolution can be seen by writing

$$R_a(q,h) = P_6(a,b)\ \delta\ (h-a-bq)$$

where $P_6(a,b)$ is the frequency function for the intercept, a, and the slope, b, of the assumed linear conversion of the charge to pulse height. The effects of electronic noise on the energy resolution can easily be seen using this notation. Since the signal is a minimum at the first stage of amplification we will consider only that noise introduced here. This noise is the result of random processes such as ther-

mally generated currents in parallel and series resistances, fluctuations in the current through the input electrode and fluctuations in the current controlled by the input electrode that are uncorrelated with the input electrode potential. When averaged over the finite time of the pulse duration these fluctuations cause, in effect, an amount of charge q_o to be added to the input signal. The probability distribution function of q_o is $G(\{0|\sigma^2_{q_o}\}\ q_o)$ where σ_{q_o} is the rms equivalent noise charge. Assuming negligible fluctuations in gain

$$R_a(q,h) = G(\{0|b^2\sigma^2_{q_o}\}\ a)\ \delta(h-a-bq)$$

where $a = bq_o$.

The noise contributions mentioned above have white spectra generated across either the input capacitance or the first stage load resistor. The former, which includes the bulk leakage current of the detector, gives rise to a mean-square voltage proportional to ω^{-2}, the latter to a mean-square voltage that is consistant. Since these are uncorrelated, the total mean-square voltage due to these contributions is

$$V^2 = c + d/\omega^2$$

Because this frequency distribution is, in general, different from the frequency spectrum of the signal the averaging process can be chosen for maximum signal-to-noise ratio, S/N[50,51].

The most common filters used in low-noise amplifiers to date are simple RC networks. Although with these filters, S/N is up to 40% larger than for the ideal filter[52] their simplicity makes possible a variable band pass so that S/N can be maximized for a given detector.

With these filters the low frequency cut-off is defined by a RC differentiator while one or more RC integrators defines the high frequency cutt-off. For maximum noise reduction these should be located near the output to filter out the noise introduced throughout the amplifier. Analysis of a single RC differentiator and integrator network indicates maximum S/N for equal integrating and differentiating time constants[53].

The overlap in time of pulses whose relative heights are random also causes fluctuations in the a and b associated with the transformation of the second event. Since the relative occurrence of these events depends on the counting rate and the time duration of a single pulse, the latter should be short. With the RC filters discussed above, the time duration is restricted by the differentiator which, to reduce the overlap of pulses in the early stages of amplification, must be located near the input. This compromise, with the resulting decrease in S/N, is necessary to keep the amplifier in its linear range. A further reduction in the time duration of a pulse can be obtained by adding a second differentiator. This decreases the S/N by $\sim 5\%$ in the case of RC filters with all three time constants the same, but may result in enhanced energy resolution if the counting rates are sufficiently high.

The conversion of charge to voltage presents unique problems. With a voltage sensitive preamplifier, the input charge, q, is integrated on the input capacitance and linearly amplified, producing an output voltage proportional to q/C_{in}. The output voltage fluctuates, then, with changes in C_{in}. In the above context these fluctuations appear as fluctuations in the gain, b, of the system. Hence knowing the probability density function of C_{in} one could calculate

the resulting amplifier response $R_a(q,h)$. In practice the effect is made negligible by using a so-called "charge-sensitive" preamplifier. This consists of an operational amplifier with capacitive feedback so that the peak output voltage is given by q/C_f where C_f is the feedback capacitance. Since this capacitance is passive, consisting solely of a condenser, the resulting output is extremely stable.

The distribution in pulse heights from the amplifier must now be measured. This measurement is performed by a pulse-height analyser which, analogous to the previous discussion, can be represented mathematically by an integral transformation of the pulse height h to what will be called the channel number x. The response of the spectrometer which includes the detector, amplifying system, and pulse-height analyser is then

$$R_s(x,E) = \int R_c(x,h)\, R(h,E)dh$$

where $R_c(x,h)$ is the kernel of the above mentioned transformation. The pulse-height analyser then collects a sampling of

$$M(x) = \sum_i I_i\, \varepsilon(E_i,\omega)\, R_s(x,E_i)$$

for a finite number of values of x from which an estimate

$$S^*(E) = I_i^*\, \delta(E-E^*)_i$$

can be obtained.

The simplest pulse-height analyser is the so-called single channel analyser which consists of two pulse-height discriminators connected in anticoincidence to a scaler. The scaler then counts the number of pulses with heights in the interval defined by the two triggering levels of the discriminators. Dividing the output of the

scalar by the pulse-height interval and the total number of γ rays emitted during the sampling period gives an estimate $M^*(x)$. If we define x to be the lower of the two triggering levels, the response function of this pulse-height analyser is

$$R_{sc}(x,h) = 1/\Delta \text{ for } x \leqslant h \leqslant x + \Delta$$
$$= 0 \text{ otherwise}$$

The spectrometer response becomes

$$R_s(x,E) = \frac{1}{\Delta} \int_x^{x+\Delta} R(h,E)dh$$

The efficiency of the spectrometer can be increased by a factor of n using n such single channel analysers simultaneously. If each estimate $M^*(x_i)$, i = 1 to n, is to be statistically independent of the values for different i, the intervals can not overlap. The most efficient arrangement is to have $x_i = (i - 1/2)\Delta$ and n and Δ sufficiently large so that nΔ is equal to the maximum pulse height of interest.

The maximum pulse-height interval or channel width, Δ, that can be used is limited by the detector resolution. If, for example, the channel width, Δ, is equal to one-third the FWHM of an assumed Gaussian peak in the detector response function, the energy resolution is increased by approximately 2.5% by the pulse-height analyser. If one will accept increase in resolution of this order and one has a detector with a 9 keV FWHM then 2,700 channels are required to cover the range 0 to 8 MeV. It is, of course, impossible to obtain this many channels by extending the single-channel analyser as suggested above. An analogue-to-digital converter (ADC) of the Wilkinson type is used in all commerc-

ially available pulse-height analysers. In this case the pulse height is converted to a proportional time interval by discharging a condenser with a constant current from an initial voltage that is equal to the pulse height. The time interval is then measured by scaling a high frequency oscillator during this discharge. The response of this pulse-height analyser is, to a good approximation,

$$R_c(x,h) = (R_{sc}(x,h)\delta(x-x_1)R_{sc}(x,h)\delta(x-x_2), \ldots, R_{sc}(x,h)\delta(x-x_n)$$

where $R_{sc}(x,h)$ is the previously mentioned single channel analyser response and $x_i = (i-1)\Delta$. A plot of the channel profile for the analyser used in this work is shown in Figure 2-9.

2.5 Two Counter Time Correlations

In order to fit γ rays of known energy into a decay scheme it is extremely useful to know their time correlations. If a_{ij} is the probability that the γ rays with energies E_i and E_j are both emitted within some small time 2τ the object of the coincidence experiment is to estimate the matrix A where

$$A = (a_{ij})$$

In order to do this two detection systems are required. From each detector we require the energy and the time for each interaction. The energy information is, as we have seen, present in the pulse height. For these experiments a phase point in the wave form is also required that occurs at some fixed time, t, after the detection of the γ ray. This phase point is then electrically sensed and a timing marker generated for the interaction. Two commonly used pulse shapes and the

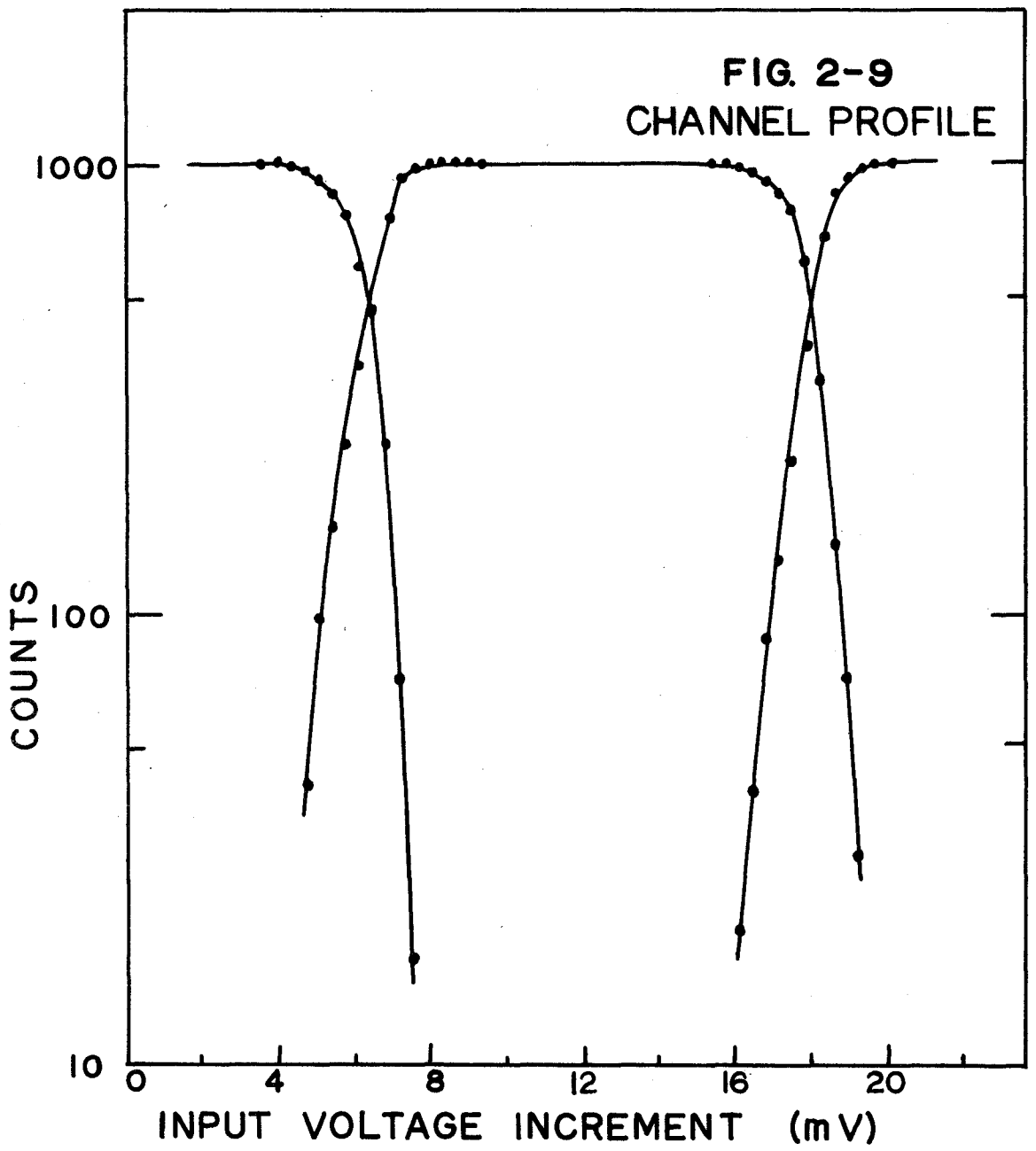
FIG. 2-9
CHANNEL PROFILE
1000
100
10
COUNTS
0
4
8
12
16
20
INPUT VOLTAGE INCREMENT (mV)

method of generating the time markers at their appropriate phase points, are shown in Figure 2-10. If the timing marker has a pulse width τ, a logic AND circuit can be used to determine when a pulse produced in counter 1 occurs within time 2τ of a pulse produced in counter 2. It is then necessary to analyse the pulse heights from counter 1 and counter 2 in order to determine the energies of the coincident γ rays. Using the notation previously introduced, the surface so obtained approaches in the limit of infinite sample size

$$M(x,y) = N \sum_{ij} a_{ij}\, \varepsilon_1 (E_i, \omega_i) R_{s1}(x,E_i)$$

$$\varepsilon_2(E_j, \omega_j)\, R_{s2}(x,E_j)$$

where N is the total counting time divided by T, the time during which 100 neutrons are captured. The probability a_{ij} can be written

$$a_{ij} = a_{ij}^t + a_{ij}^c$$

where a_{ij}^t is the number of times per 100 captured neutrons that the i^{th}-j^{th} pair is emitted from the same nucleus and a_{ij}^c is the number of times per 100 captured neutrons that the members of this pair are emitted from different nuclei within the time interval 2τ. The former gives, then, the number of true events and the latter the number of chance events. The number of chance events per 100 neutron captures for the i^{th}-j^{th} pair is given by

$$a_{ij}^c = \frac{2\tau}{T}\, I_i\, I_j$$

where T is the time required to capture 100 neutrons. For ease of notation the coincidence surface will be written as

FIG. 2-10

DOUBLY DIFFERENTIATED PULSES - THE ENERGY INFORMATION IS CARRIED BY THE PULSE HEIGHT

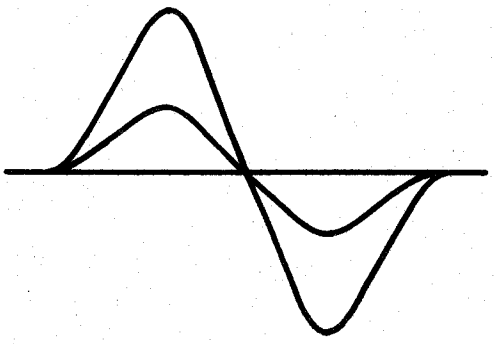

TIME INFORMATION GENERATED AT THE CROSS OVER

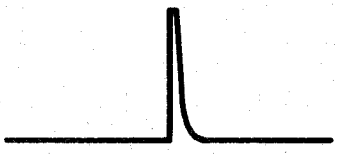

SINGLY DIFFERENTIATED PULSES - THE ENERGY INFORMATION IS CARRIED BY THE PULSE HEIGHT

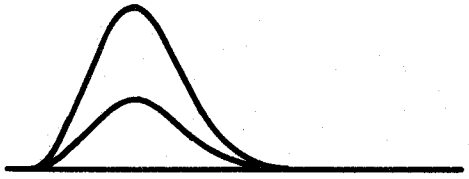

TIME INFORMATION GENERATED AT THE LEADING EDGE

$$M(x,y) = N \sum_{ij} \alpha_{ij} R_{s1}(x,i) R_{s2}(y,j)$$

where

$$\alpha_{ij} = a_{ij} \varepsilon_1(E_i, \omega_i) \varepsilon_2(E_j, \omega_j) \text{ , } R_{s1}(x,i) = R_{s1}(x,E_i) \text{ and}$$

$$R_{s2}(y,j) = R_{s2}(y,E_j)$$

It is, of course, necessary for τ to be small in order to reduce the number of times that the coincidence circuit is triggered because of a chance overlap of the timing markers. There is, however, a minimum value of τ that can be used which is determined by fluctuations in t, the time between the detection of the γ ray and the generation of the timing marker by the discriminator circuit. With both pulse heights fixed, t fluctuates around some mean value, $\bar{t}$. This timing marker jitter is caused by statistical fluctuations in the processes that determine the phase point at which the timing-marker discriminator is triggered. The mean time $\bar{t}$ may also be a function of the two pulse heights. This so-called timing-marker walk should be small in order that the coincidence efficiency be independent of the two pulse heights. This is extremely important when one analyses concurrently all possible coincident pairs, independent of the two pulse heights, as is possible with present two parameter analysers.

In order to minimize τ it is necessary to reduce the fluctuations in t. This in general requires a pulse shape that is incompatable with that needed for good energy definition. It is necessary in this case, to divide the signal before the pulse-shaping networks into a time channel and an energy channel. The energy channel is analogous to the slow channel in the common fast-slow coincidence circuit, while the time

channel is analogous to the fast side. A schematic drawing of this arrangement is shown in Figure 2-11. The time channel has a pulse shaping network designed to minimize τ while the energy channel has shaping networks designed for optimum energy resolution. The energy channel requires an amplifier identical to that used in a one parameter measurement. For the time channel a double differentiated pulse can be used. As pointed out by Fairstein[54], the cross-over phase point for such a pulse is, to high order, independent of the pulse height. This point can then be used for the time definition of the event by using a discriminator that senses this cross-over point, a so-called cross-over pick-off gate. The most commonly used pulse shaping networks for this time channel are shorted delay lines. Using double delay-line clipping with no integration to limit the pulse rise-time, resolving times $2\tau \sim 40$ nanoseconds can be used with 100% coincidence efficiency over 90% of the range of the amplifier. This permits source strengths of the order of 35 microcuries to be used with a 10% chance contribution.

The two parameter analyser requires two separate ADC's. The outputs from each of the two amplifiers in the energy channel are then coupled through linear gates to these ADC's. Analyses of the pulses for the energy information is inhibited unless they are accompanied by a gating pulse from the time channel.

The storage capacity required is very large. Since two orthogonal vectors of size n_1 and n_2 map one-to-one onto the vector of size

FIG 2-11
COINCIDENCE SYSTEM

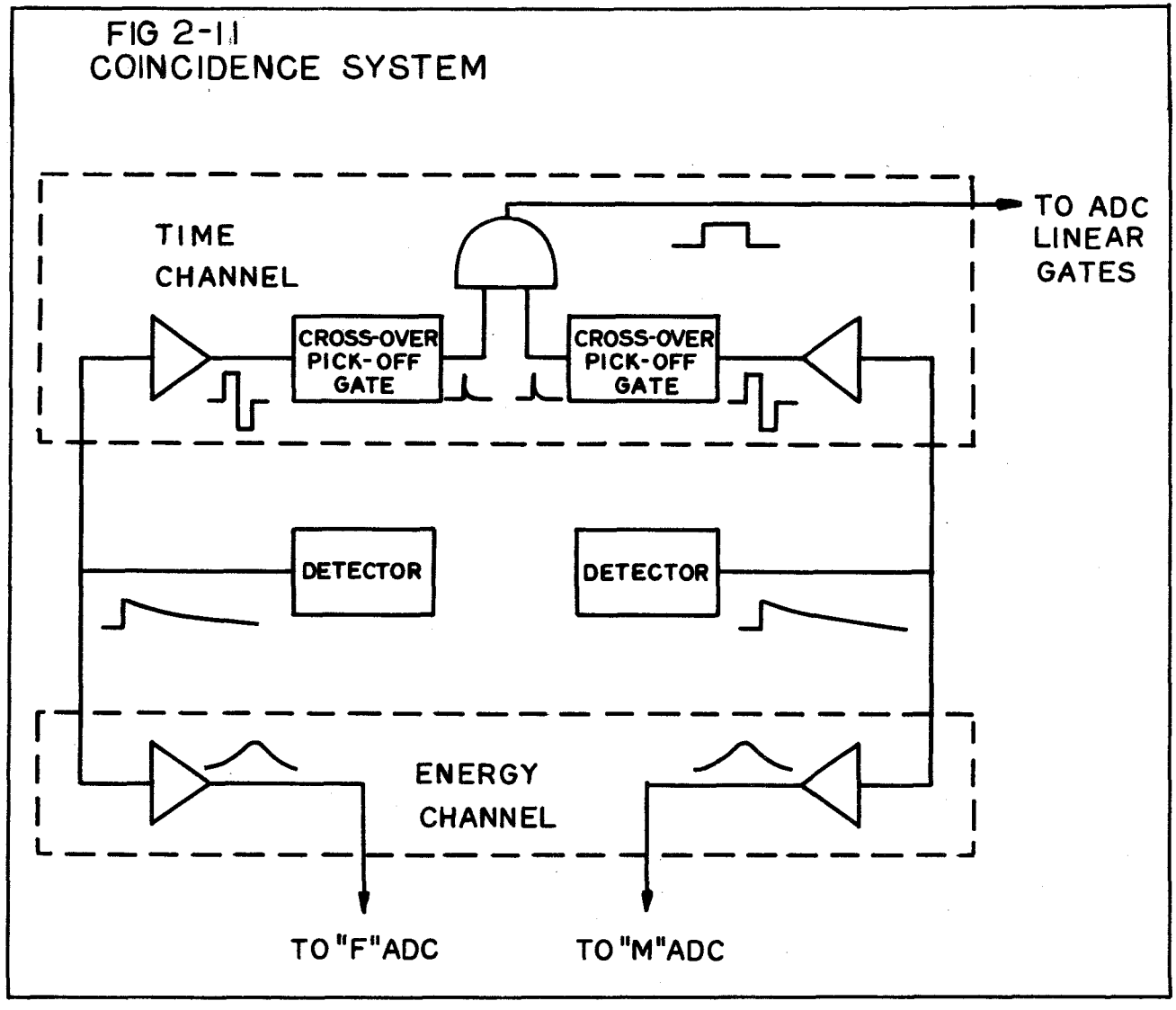

$n = n_1 \times n_2$, the 1000 channel digital conversion of the pulses from each counter requires 10^6 memory locations for storage. This mesh would be adequate for a Ge(Li)-Ge(Li) coincidence experiment covering a γ-ray energy from 0 to 8 MeV. The scaling down of each ADC from that required for optimum energy resolution which, as we have seen, is approximately 3,000 channels, is permissible since energy resolution is no longer the sole consideration.

At the present time such experiments do not seem feasible because of the low detection efficiency of such counters. In order to obtain data at a more profitable rate Ge(Li)-NaI(Tl) coincidence experiments are suggested. For these experiments the ADC used with the NaI detector can be further scaled down to 250 channels without any significant loss in detail. This still requires 2.5×10^5 memory locations which is well above the size of presently available random-access memories. It should also be mentioned that with the lower resolution of NaI(Tl) detectors, the pulse shape used in the time channel is also sufficient for the energy definition, hence allowing a common amplifier to be used for both.

Data fields of the size mentioned above can be obtained by what is commonly referred to as delayed-time analysis. This consists of storing the encoded pairs of addresses in a serial fashion. Later, after the required sample size has been accumulated, the number of times a particular address-pair occurs is tallied for all possible pairs, giving the required sampling from which the matrix A may be

estimated. Using this technique, a much larger memory is required for storing the events but it no longer needs to be of the random access type. As a result less costly types of storage can be used. Magnetic tape is almost exclusively used in this application. Its advantages are relatively low cost, high packing density, high read-write speed, reliability and compatability with large computers.

The input to the analyser is, because of the nature of the processes being considered, random in time. To take full advantage of the inherent properties of magnetic tape the input must be periodic. Because of this, it is usual to buffer the output of the ADC's before writing on the tape. The buffer must be capable of accepting information at random times and out-putting it at fixed time intervals.

Physically, the buffer consists of a small memory similar to the random-access memory used in real-time analysers. Address-pairs from the ADC's are stored sequentially, the addresses occupying the same position that the number of counts would occupy in a real-time analyser. A "book-keeping" register counts the number of events processed and initiates the sequence for writing these addresses on the tape when the buffer memory is full. The write cycle so initiated consists of starting the tape drive, allowing sufficient time for the tape to reach the required speed, transforming each buffered address to the form required for storing on magnetic tape and writing this information sequentially at fixed time intervals. After the contents of the buffer have been transferred onto the tape, the tape is stopped until the next write cycle. The analysis of events is, of course, interrupted during the dumping of the buffer.

The main objection to such a system is the uncertainty in the quality of the data being handled because of the time required to convert the data to an understandable form. To overcome this disadvantage a monitoring device is necessary which converts and collects the data in a comprehensible form. Such a device should have a fast readout for quickly displaying the progress of the experiment. The obvious system is a random-access memory with an oscilloscope readout. Such a memory will, of course, be too small to collect the data in the mesh in which it is being recorded. It should, however, be large enough to record at least the full mesh from each ADC separately in order to facilitate the setting up of the experiment. It is also desirable to be able to monitor the experiment in different ways. This feature can be obtained by appropriately mapping the two ADC outputs into the address register of the monitor.

2.6 The Data Handling System

The data handling system used here is well suited for use with the Ge(Li) counters presently available. For single counter experiments a Tennelec 100C preamplifier and a TC200 amplifier was used. This preamplifier is of the charge-sensitive type having a noise level of 3 keV FWHM, when using a 20 pf detector and 0.8 sec main amplifier RC differentiating and integrating time constants. The main amplifier uses RC differentiating and integrating filters, separately variable in a binary sequence from 0.05 to 12.8 sec. A second differentiater can also be switched in which is variable over the same range.

The pulse-height analyser used was a Nuclear Data ND-160 system consisting of two independent 10-bit ADC's (ND-160F), referred to as

$(ADC)_F$ and $(ADC)_M$, and a random-access memory (ND-160M) with 4096 locations and an 18-bit word length. The storage position in the memory of the events encoded by the ADC can be chosen by the experimenter. An analogue readout is available which is suitable for use with a CRT or pen recorder. Digital readout on punched paper tape or IBM-compatible magnetic tape is also possible.

In order to obtain at least 3 keV/channel digital resolution with only 1024 channels available, an Ortec 201 biased amplifier was used initially. For these experiments three runs were usually required to cover the energy range of interest. Recently a 12-bit ADC was obtained which now permits the recording of the entire range with a digital resolution of approximately 2 keV/channel.

For two parameter measurements, transistorized DD2 amplifiers, cross-over pick-off gates, and coincidence circuits designed by Chase[55] were used for timing definition. The output pulses from the DD2 amplifier were also analysed for the energy information when used with a NaI(Tl) detector, while the energy information from the Ge(Li) detector was handled by the Tennelec amplifier. With this system a resolving time, 2τ, of 50 nanoseconds gave a coincidence efficiency of 100% over the desired range of pulse heights.

For storage the two 10-bit ADC's of the ND-160F unit can be mapped into the 12-bit memory register allowing meshes ranging from 64 x 64 to 4 x 1024 to be used for real-time analysis. For delayed-time analysis the Nuclear Data ND-160BT buffer tape control unit,

ND-160R/S read/search unit, and Potter M910-1 magnetic tape transport system was available. With these, two parameter measurements can be recorded in digital meshes of 512 x 512 or 256 x 1024.

For delayed time analysis, one half of the ND-160M memory (2048 18 bit words) is available for monitoring, and the other half can be used for buffer (2044 18-bit words) and for programming (4 18-bit words). The sorting of addresses written on the tape can also be accomplished in the so-called monitor-search mode. In this mode only the monitor memory is available for storage, allowing up to 2048 different addresses to be sorted in one pass of the tape. The address to be sorted can be selected by the operator. Because of the slow counting rate per channel it has been found necessary to program the monitor to look at a coarser mesh than that recorded. Since the main information desired from the monitor is whether there has been a gain shift in one of the dimensions, it was found most convenient to monitor the projections of the coincidence surface along each axis. Since this requires only 1024 + 256 or 1280 channels, these can be stored simultaneously in the monitor memory. The procedure followed was to store one such projection while the information was being collected. The other projection was obtained by reading the tape after it was filled using the monitor-search mode.

The tape format is compatible with that of IBM. Each 18-bit address is written as three 6-bit data words and each data word has a lateral parity check. The data from $(ADC)_M$ is written first followed by that from $(ADC)_F$. Each buffer dump contains 2048 18-bit words, the

first two words being identical 18-bit identification words that are set by the use of 18 binary switches. After the 2044 18-bit addresses, two more 18-bit words are written which satisfy the Longitudinal Redundancy Character check used in the IBM format.

Each dump is recorded on a density of 200 bits per inch with a 0.75 inch Inter Record gap between them. This allows about 1.5×10^6 events to be stored on one 2500 ft reel of tape. A dumping time of about 600 milliseconds was negligible compared to the time taken to fill the buffer so that the dead time of this system was unimportant.

Sorting of the recorded address-pairs was accomplished on an IBM 7040 computer with a 36-bit word memory having 32K locations. In order to reduce the number of passes of the tape needed to sort the full array, the 36-bit computer word was split into four 9-bit words, allowing a maximum of 512 counts in any channel per reel of tape. For the configuration used (256 x 1024) digital windows, with a width of 4 channels, can be set in the 1024 channel dimension. Four passes were required to sort the entire array. Sorting a 2,500-ft reel of tape requires about one half hour of computer time.

CHAPTER III

SPECTROMETER CALIBRATION

3.1 The Problem

Because of the high-energy resolution possible using Ge(Li) detectors, the determination of γ-ray energies with high precision is possible. For example, if the peak response is Gaussian with a FWHM of 7 keV, least-squares estimates of the positions of peaks containing more than 10,000 counts can be determined with a standard deviation of less than 30 eV. For a 9-MeV γ ray this implies a precision of 3 parts per million.

In order to achieve the above energy precision, the transformation from channel number to energy must be accomplished with negligible error. For the ideal system this transformation would be linear, that is

$$E = a + bx$$

where E is the energy peak, x the channel position of the peak, a the energy of the zeroth channel, and b the gain of the system. In practice, deviations from this ideal case are slight and can be accounted for by a quadratic term so that

$$E = a + bx + cx^2$$

The determination of a, b and c are the main contributors to the final accuracy that can be obtained.

The most useful method of determining a, b and c is to measure the peak positions of γ rays whose energies are accurately known.

The constants can then be determined using least-squares techniques. Provided one can insure that these constants are the same when the unknown spectrum was obtained, they can be used to calculate the unknown energies. The method of mixed sources, where one obtains concurrently the spectrum of the standard and the unknown, insures that the constants determining the channel-to-energy transformation are the same for both spectra. In this way, the energies of the dominant peaks can be determined. The energy of the weaker lines can then be measured relative to these internal standards by observing the γ-ray spectrum of the unknown alone.

It is necessary then, to have a large number of γ-ray standards whose energies are known to approximately $\pm$ 30 eV. These γ rays should have energies throughout the range of interest in order to avoid large extrapolations. Table 3-1 lists some precise γ-ray energies available, along with the spectrometer used to measure them. Above 3 MeV, the only measurements available are those of Carter and Motz[58]. These were determined by a one-point calibration using the γ ray of 2754 keV emitted following the β decay of ^{24}Na. The sum of the energies of stop-over γ rays, when checked against the crossover energies, showed deviations of as much as 2.2 keV because of nonlinearities in the system. Since the errors present in these measurements are comparable with those that could be obtained with a Ge(Li) detector, it was felt profitable to try to calibrate our spectrometer using the accurately known γ-ray standards below 3 MeV.

TABLE 3-1

Precise γ-ray Energy Standards

Energy	Reaction	Spectrometer	Reference
511.006^{5}	Calculated from the least-squares adjusted value of the 1963 fundamental constants		56
411.795^{9}	β-decay of ^{198}Au	iron-free π 2 β-ray spectrometer	
1173.226^{40} 1332.483^{46}	β-decay of ^{60}Co		
1368.526^{44} 2753.92^{12}	β-decay of ^{24}Na		
583.139^{23} 2614.47^{10}	β-decay of ^{208}Tl		
2223.18^{20}	$^{1}H(n,\gamma)^{2}H$	double flat-crystal spectrometer	57
1262.3^{5} 3684.3^{3} 4946.6^{6}	$^{12}C(n,\gamma)^{13}C$	Compton π 2 magnetic spectrometer	58*
3533.2^{5} 5268.8^{3} 5297.8^{4} 5533.8^{4} 5562.6^{5} 7300.1^{6} 10833.2^{7}	$^{14}N(n,\gamma)^{15}N$		

* The errors quoted by the authors are least squares statistical errors. The largest difference between the sum of the energies of the stopover γ-rays and the energy of the crossover γ ray is 2.2 keV.

Since the $^{35}Cl(n,\gamma)^{36}Cl$ reaction has very intense γ rays, well-spaced through the region from 5.0 to 8.5 MeV, and it has a large neutron capture cross section, it provides an ideal calibration spectrum. The problem was then to determine, as accurately as possible, the energies of the γ radiation associated with this reaction.

In order to safely extrapolate from 3 MeV to 8 MeV, it would be desirable to have two γ rays of approximately 4 MeV whose energies, when corrected for recoil losses, add up to another γ ray in the spectrum, the so-called crossover transition. The second escape peaks of these two γ rays could then be measured relative to the γ rays following the β decay of ^{24}Na or ^{208}Tl and the crossover γ-ray energy at 8 MeV calculated.

Cascades of this type are not observable in the $^{35}Cl(n,\gamma)^{36}Cl$ decay because of the complexity of the spectrum in the region of 3 MeV. Fortunately the $^{28}Si(n,\gamma)^{29}Si$ reaction provides a very intense cascade of this type. For this reason, this reaction was studied in detail and the high energy Cl capture γ-ray transitions calibrated using the results of this study.

The energies quoted here resulted from a series of experiments. These experiments were carried out initially using a 1024 channel ADC. The accuracy of the energies so obtained was limited by the relatively large channel width. When a 4096 channel ADC became available, the calibration was repeated. The results of these final experiments are those reported here.

The errors quoted are estimates only and may be interpreted

as 60% confidence limits. These estimates are obtained from internal consistency checks and from the consistency of the energies obtained from different runs.

3.2 The $^{28}Si(n,\gamma)^{29}Si$ γ-Ray Energies

The γ-ray spectrum associated with thermal neutron capture in naturally occurring Silicon is shown in Figure 3-1. This spectrum was accumulated in approximately 12 h using a target consisting of 2 g of silicon. In order to achieve the best possible resolution, the amplifier was used in the single-differentiation mode and the counting rate was limited to less than 1,000 counts/sec. Electronic instabilities resulted in a resolution of about 12 keV FWHM for runs of this length.

Naturally occurring silicon contains 92.3% ^{28}Si, 4.7% ^{29}Si and 3.0% ^{30}Si. The contributions of these isotopes to the thermal neutron capture cross section are 82%, 14% and 4% respectively. Thirteen of the twenty transitions seen by Adyasevich et al[59] have been assigned to the $^{28}Si(n,\gamma)^{29}Si$ reaction. Only the γ rays in this group of thirteen will be discussed here.

The $^{28}Si(n,\gamma)^{29}Si$ γ-ray spectrum is characterized by two strong lines of 3539 keV and 4934 keV. Since this pair make up a cascade to the ground state[60] their sum, when corrected for recoil, gives the energy of the ground-state transition. Furthermore, the 4934-keV γ ray can be determined relative to the 3539-keV γ ray by extrapolating from the photopeak of the latter to the 2nd escape of the former. This requires an extrapolation of only 373 keV and hence should be relatively free from systematic errors.

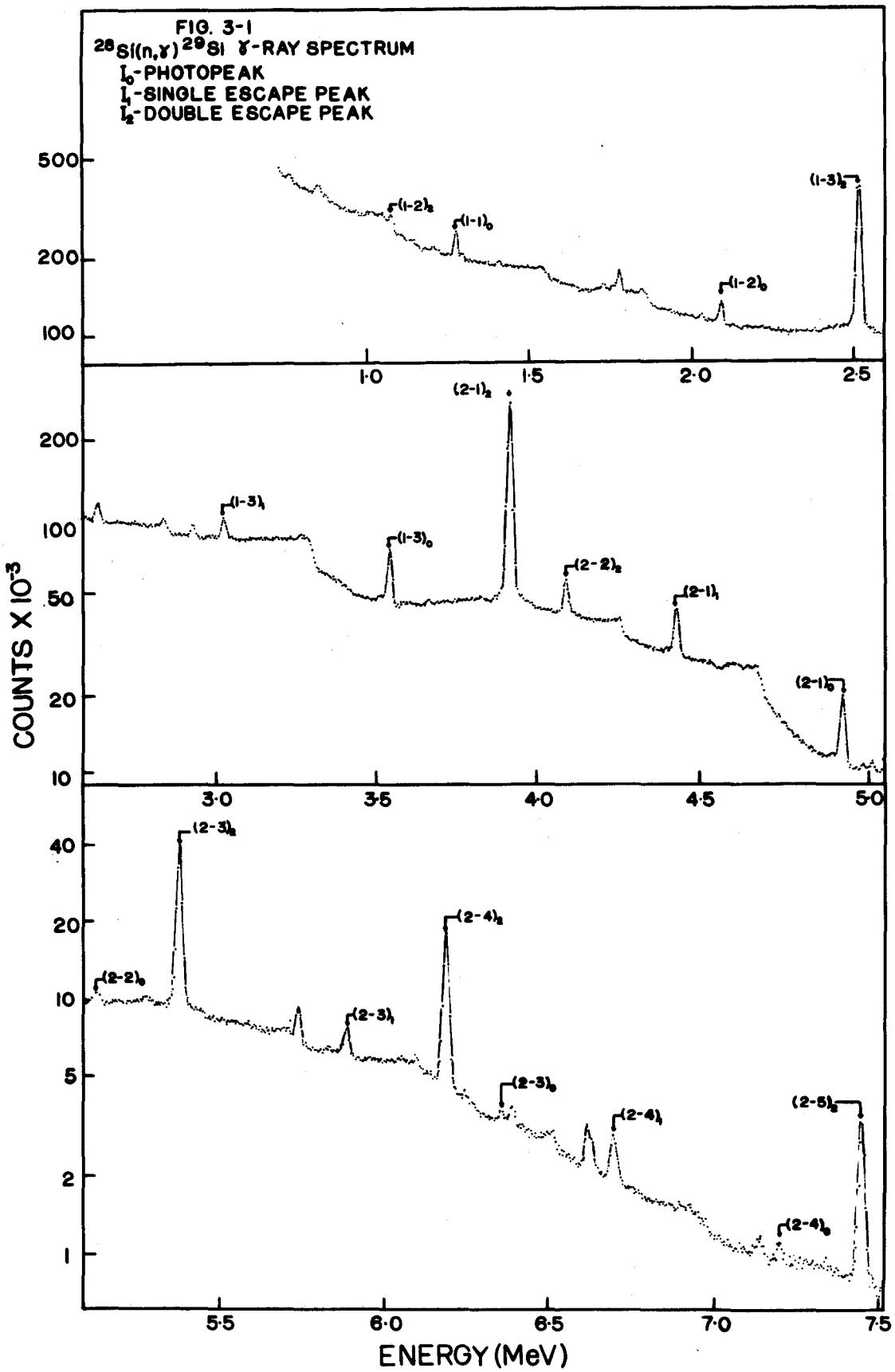
FIG. 3-1
$^{28}Si(n,\gamma)^{29}Si$ γ-RAY SPECTRUM
I_0-PHOTOPEAK
I_1-SINGLE ESCAPE PEAK
I_2-DOUBLE ESCAPE PEAK
COUNTS X 10^{-3}
ENERGY (MeV)
$(1-2)_2$
$(1-1)_0$
$(1-3)_2$
$(1-2)_0$
$(2-1)_2$
$(1-3)_1$
$(1-3)_0$
$(2-2)_2$
$(2-1)_1$
$(2-1)_0$
$(2-3)_2$
$(2-2)_0$
$(2-4)_2$
$(2-3)_1$
$(2-3)_0$
$(2-4)_1$
$(2-5)_2$
$(2-4)_0$

The energy of the 3539-keV transition has been measured relative to the photopeak of the 2754-keV γ ray emitted in the β decay of ^{24}Na and the photopeak of the 2614 keV γ ray emitted in the decay of Thorium. The precise energies of Murray et al[56] were used for the calibration energies.

The results of Adyasevich et al[59], along with the coincidence measurements of Manning and Bartholomew[60] suggest the presence of other cascades that can be used to determine the Q-value. In particular, the cascades involving the 1273- and 7200-keV γ rays and the 2092- and 6381-keV γ rays can also be used. These, of course, lead to less accurate determinations of the Q-value since they entail extrapolations over large energy ranges. They do, however, provide a means of internally checking the consistency of the results.

The accurate extrapolation from below 3 MeV to 8 MeV requires a precise measurement of the gain of the system. Assuming a channel dependence that is quadratic, the gain of the system is given by

$$\frac{dE}{dx} = g(x) = b + 2cx$$

Two peaks separated by a known energy give estimates of g(x), where x is the mean of the positions of the two peaks in question, that is

$$g(\bar{x}) = b + 2c(x_2 + x_1)/2$$

$$= \frac{bx_2 + cx_2^2 - bx_1 - cx_1^2}{x_2 - x_1}$$

$$= \frac{\Delta E}{\Delta x}$$

Three different methods are available for estimating the gain. The recognition of photopeaks and first and second escape peaks corresponding to the same γ ray gives such estimates since these are known to be separated by 511 or 1022 keV. Such peaks are easily seen in simple spectra above approximately 2 MeV. A cascade and its cross-over transition also gives an estimate of the gain, provided that one member of the cascade is observable in the low energy region. This estimate can be obtained by measuring the low energy γ ray involved against the accurate low energy standards. This energy, when corrected for recoil losses, is equal to the energy difference between the two high energy transitions. At the bottom end of the spectrum where the γ-ray energies can be accurately measured, energy differences are known and give estimates of the gain in this region.

Using all the available information of this type, the gain of the system as a function of channel number of a $^{28}Si(n,\gamma)^{29}Si$ spectrum was obtained. To better determine gain in the low energy region, the γ rays following the β decay of ^{60}Co and ^{208}Tl were mixed with the $^{28}Si(n,\gamma)^{29}Si$ radiation and included the analysis.

A mixed spectrum of the radiations from thermal neutron capture in Si and Cl was also analysed in this way. Since both data were obtained using the same system with slightly different values of a and b, it was felt that the quadratic term, c, should be the same for both. Hence, the following procedure was used. Consider the two experiments (labelled 1 and 2). For experiment No. 1, there is a set of estimates of the gain g for different channel numbers, (g_{1i}, x_{1i}). The same is

true for the second experiment. The model equations are

$$g_{1i} = b_1 + 2cx_{1i}$$

$$g_{2j} = b_2 + 2cx_{2i}$$

Note that c is the same for experiments 1 and 2.

Using standard least-square techniques, one seeks the maximum of the likelihood function $L(b_1,b_2,c)$ or the minimum in

$$R^2 = \sum_{i=1}^{n_1} W_{1i}(g_{1i}-b_1-2cx_{1i})^2$$

$$+ \sum_{j=1}^{n_2} W_{2j} \quad (g_{2j}-b_2-2cx_{2j})^2$$

This can be written

$$R^2 = \sum_{i,k} W_{ki} \ (g_{ki}-b_k-2cx_{ki})^2 \quad k = 1,2$$

where $W_{ki} = 0$ if $i \quad n_k$. The solution of the resulting normal equation is

$$Y = A^{-1} X$$

where

$$Y = \begin{pmatrix} b_1 \\ b_1 \\ 2c \end{pmatrix}$$

$$X = \begin{pmatrix} \sum_i W_{1i} \ g_{1i} \\ \sum_i W_{2i} \ g_{2i} \\ \sum_{ik} W_{ki} \ g_{ki} \ x_{ki} \end{pmatrix}$$

$$\begin{pmatrix} \Sigma W_{1i} & 0 & \Sigma W_{1i} x_{1i} \\ 0 & \Sigma W_{2i} & \Sigma W_{2i} x_{2i} \\ \Sigma W_{1i} x_{1i} & \Sigma W_{2i} x_{2i} & \Sigma W_{ki} x_{ki}^2 \end{pmatrix}$$

This procedure assumes that the estimates of g_{ki} are independent. This is true if a given peak is used only once to estimate the gain. The following problem then arises. Suppose we have three peaks associated with the same γ-ray energy (corresponding to the photopeak, the first escape peak and the second escape peak). Let us assume that the estimate of the position of the first escape peak is higher than the true value. The gain calculated from the photopeak and the first escape peak is then too large. Similarly, the gain obtained from the first and second escape peaks is too small. Hence, if we include both estimates, their errors tend to cancel. The inclusion of all estimates, even though statistically incorrect, tends to reduce the errors. For this reason, all estimates of the gain were included in the analysis.

Having obtained b and c for the Si capture γ-ray spectrum, the energies of the γ rays following the β decay of ^{60}Co and ^{208}Tl were used to find a. The energies of the $^{28}Si(n,\gamma)^{29}Si$ radiations, so obtained, showed systematic deviations of approximately 2 keV when cascades were checked with the crossover γ-ray energies.

Since the energies of the standards were reproduced to less than $\pm$ 0.5 keV, the γ-ray energies obtained in the low energy region were felt to be reasonably good. These values are quoted in Table 3-2

TABLE 3-2

$^{28}Si(n,\gamma)^{29}Si$ γ-ray Energies

Line No.	Energy	Calibration	Relative Intensity
1-1	1273.0	β-decay of ^{60}Cs	20
1-2	2092.0	$^{1}H(n,\gamma)^{2}H$	20
1-3	3539.7	β-decay of ^{24}Na and ^{208}Tl	64
2-1	4933.9	Calibrated using	61
2-2	5018.3	constraints	4.5
2-3	6380.9		14.5
2-4	7199.8		10
2-5	8471.8		2.7

TABLE 3-3

Estimates of the $^{28}Si(n,\gamma)^{29}Si$ Q-value

E_2 (keV)	R_2 (keV)	E_1 (keV)	R_1 (keV)	Q (keV)	Deviation (keV)
8471.8	1.3			8473.1	- 0.5
7199.8	1.0	1273.0	0.1	8473.9	+ 0.3
6380.9	0.7	2092.0	0.1	8473.7	+ 0.1
5108.3	0.5	1273.0	0.1		
		2092.0	0.1	8474.0	+ 0.4
4933.9	0.4	3539.0	0.2	8473.5	- 0.1
			Q =	8473.6 $\pm$ 0.4	

with an assigned error of $\pm$ 0.5 keV. The 2092-keV transition could not be determined from this run since it was masked by the single-escape peak of the 2614-keV standard. The value for this transition given in Table 3-2 was obtained from a mixture of Si and H_2O. The value of the deuteron binding energy used for this calibration was that reported by Knowles[57] and by Prestwich et al[61].

The high-energy results presented in Table 3-2 were calculated by updating the results obtained by the differential method used above. To do this, the positions of the prominent peaks in the $^{28}Si(n,\gamma)^{29}Si$ spectrum shown in Figure 3-1 were estimated. These were divided into two groups. Group No. 1 consisted of the peaks associated with the low-energy internal standards while group No. 2 contained the peaks associated with the high-energy member of the known ground-state cascades. The absolute energies are known for the members of group No. 1.

The energies of the members of group No. 2 can be obtained from an initial estimate of the neutron separation energy, Q. They are given by

$$E_{2i} = Q - R_{2i} - \sum_j (E_{1j} + R_{1j})$$

where the sum over j includes all the other members of the cascade to the ground state. The recoil energies, R_{1j} and R_{2i}, are necessary to convert γ-ray energies to level energy differences. Since the energies E_{1j} are the energies of the internal standards and since R_{2i} is at most only a few keV, the relative energies, $E_{2i} - E_{2j}$, are accurately known although the absolute energies are not. The problem of including both groups as standards is just an extension of the

problem encountered in determining the gain of the system. In the present case we have two sets of data with the same gain but with different intercepts on the energy axis.

The model functions are then

$$E_1 = a_1 + bx_1 + cx_1^2$$

$$E_2 = a_2 + bx_2 + cx_2^2$$

and the solution of the normal equations is

$$Y = A^{-1} X$$

where

$$Y = \begin{pmatrix} a_1 \\ a_2 \\ b \\ c \end{pmatrix}$$

$$X = \begin{pmatrix} \Sigma W_{1i} & E_{1i} & & \\ \Sigma W_{2i} & E_{2i} & & \\ \Sigma W_{ki} & E_{ki} & X_{ki} & \\ \Sigma W_{ki} & E_{ki} & X_{ki}^2 & \end{pmatrix}$$

and

$$\begin{pmatrix} \Sigma W_{1i} & 0 & \Sigma W_{1i} X_{1i} & \Sigma W_{1i} X_{1i}^2 \\ 0 & \Sigma W_{2i} & \Sigma W_{2i} X_{2i} & \Sigma W_{2i} X_{2i}^2 \\ \Sigma W_{1i} X_{1i} & \Sigma W_{2i} X_{2i} & \Sigma W_{ki} X_{ki}^2 & \Sigma W_{ki} X_{ki}^3 \\ \Sigma W_{1i} X_{1i}^2 & \Sigma W_{2i} X_{2i}^2 & \Sigma W_{ki} X_{ki}^3 & \Sigma W_{ki} X_{ki}^4 \end{pmatrix}$$

The least-squares estimates for the γ-ray energies obtained by this procedure are given by

$$E = a_1 + bx + cx^2$$

For convenience the solution to this problem was found graphically. The energies, E_{2i}, were initially calculated using an estimate of the Q-value obtained from the differential analysis discussed previously. Both the high- and low-energy groups were then used to find least-squares estimates for a, b and c. Using these estimates, the residual, R^2, was calculated. The Q-value was then changed until the value, Q_f, that minimized $R^2(Q)$ was found. A plot of the residual as a function of Q, as found in this analysis, is shown in Figure 3-2.

The energies presented in Table 3-2 as being internally calibrated were calculated using the estimates of a, b and c that were obtained with $Q = Q_f$. In the case where more than one peak was seen for a given γ-ray energy, the energy quoted is the weighted average of the different estimates. The errors associated with these high-energy transitions are approximately ± 1 keV.

The cascades used in this analysis are shown in Figure 3-3. Using these cascades, the internal consistency of the calibration can be checked. The results of such a study are shown in Table 3-3. The average Q-value for the $^{28}Si(n,\gamma)^{29}Si$ reaction of 8473.8 with a standard deviation of 0.4 was obtained from the six estimates shown. The inclusion of systematic errors leads to an error of ± 1 keV for the separation energy.

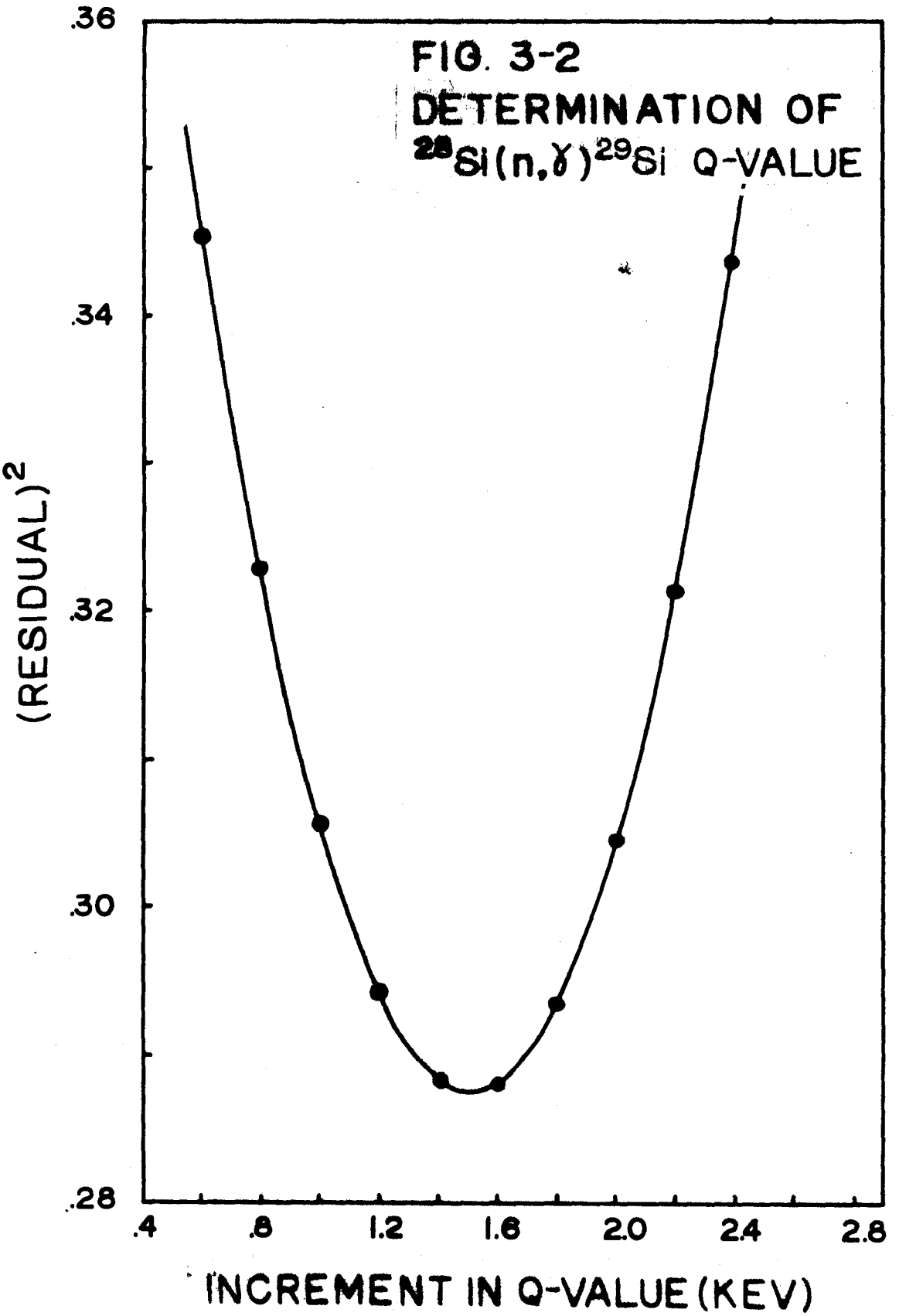
FIG. 3-2
DETERMINATION OF
$^{28}Si(n,\gamma)^{29}Si$ Q-VALUE
.36
.34
.32
.30
.28
(RESIDUAL)^2
.4
.8
1.2
1.6
2.0
2.4
2.8
INCREMENT IN Q-VALUE (KEV)

FIG. 3-3

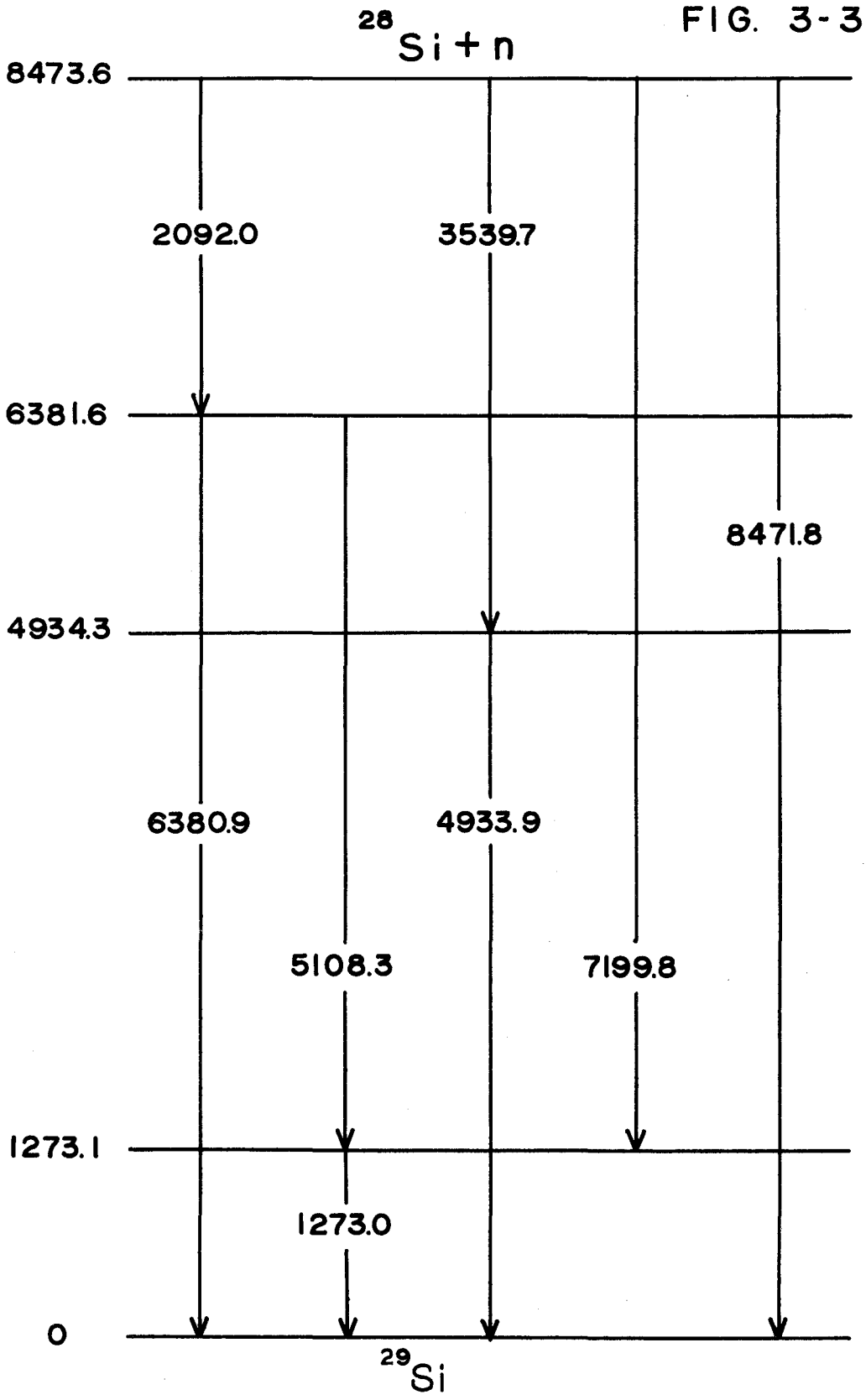
^{28}Si + n
8473.6
2092.0
3539.7
6381.6
8471.8
4934.3
6380.9
4933.9
5108.3
7199.8
1273.1
1273.0
0
^{29}Si

3.3 The $^{35}Cl(n,\gamma)^{36}Cl$ Reaction

The most extensive previous study of the $^{35}Cl(n,\gamma)^{36}Cl$ γ radiations is that of Groshev et al[62] who identified and measured the energies and intensities of some thirty transitions. Segal[63] subsequently established eight cascades using a scintillation pair spectrometer in coincidence with a 3 x 3 in NaI(Tl) detector. These results, along with the $^{35}Cl(d,p)^{36}Cl$ results of Paris et al[64] are summarized in Figure 3-4 which shows the level scheme for A = 36 as presented in the Nuclear Data Sheets. Recently, more accurate γ-ray energies have been obtained with a Compton spectrometer by Rudolph and Gersch[65] and an extensive study of the (d,p) reaction, including the measurement of ℓ_n values, has been reported[66].

The capture cross section of ^{35}Cl is 30 barns compared to 0.6 barns for ^{37}Cl. Since the relative abundance of the former is 75%, 99.5% of the captures in natural Cl occur in ^{35}Cl. Because of this, all strong radiations from naturally occurring Cl are assigned to the $^{35}Cl(n,\gamma)^{36}Cl$ reaction. Figure 3-5 shows the γ-ray spectrum obtained using a target of carbon tetrachloride sealed in a polyethylene container. This spectrum, taken using approximately 3 cc of liquid, required a 48 h counting period.

The prominent low energy peaks were calibrated relative to the peaks produced by the γ rays emitted in the β decay of ^{60}Co and ^{24}Na as well as the annihilation radiation always present in capture γ-ray spectra. These results and the standards used in their calibration are given in Table 3-4. The high energy transitions were originally cal-

Level Scheme for A = 36 S, Cl, A

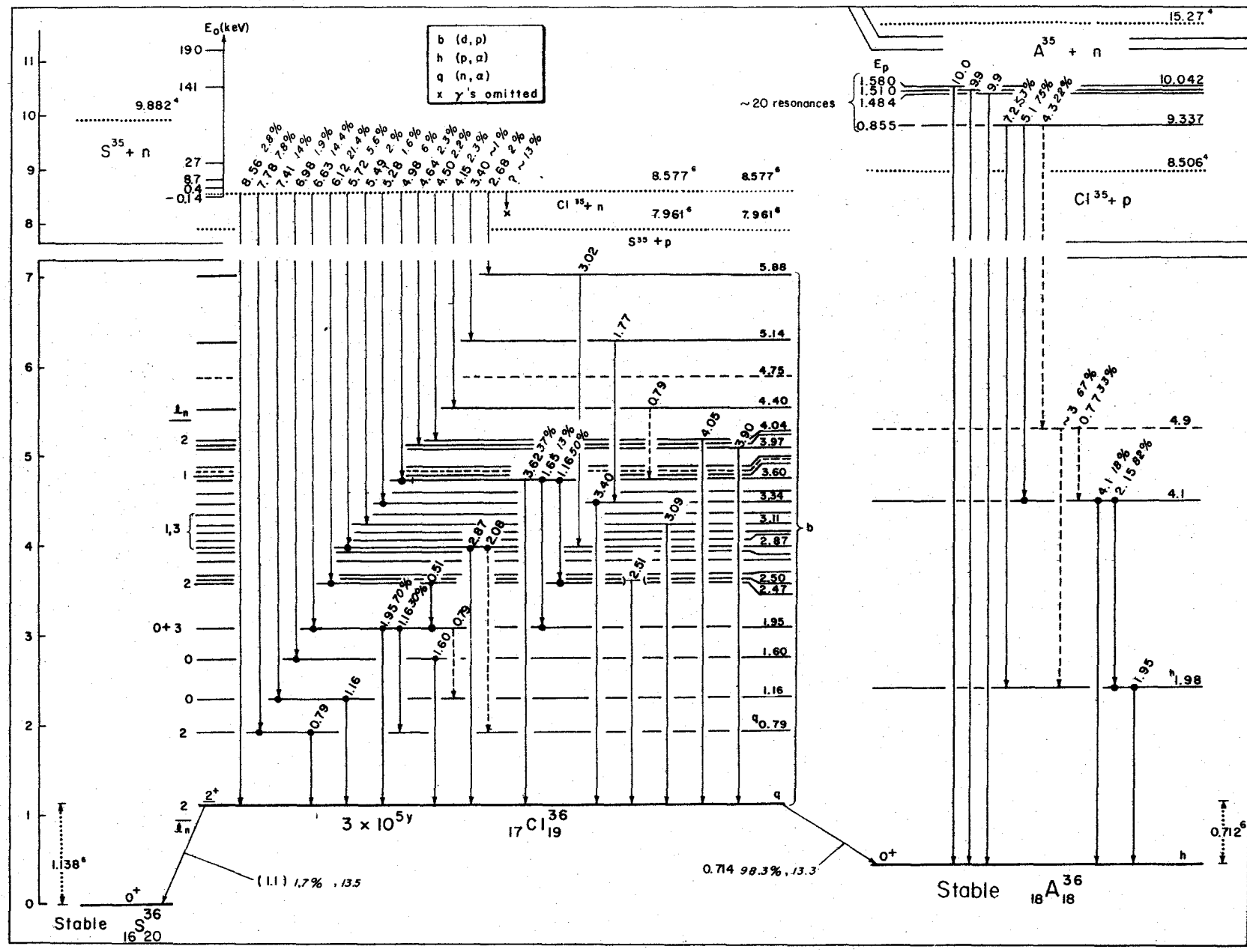

Level Scheme A = 36

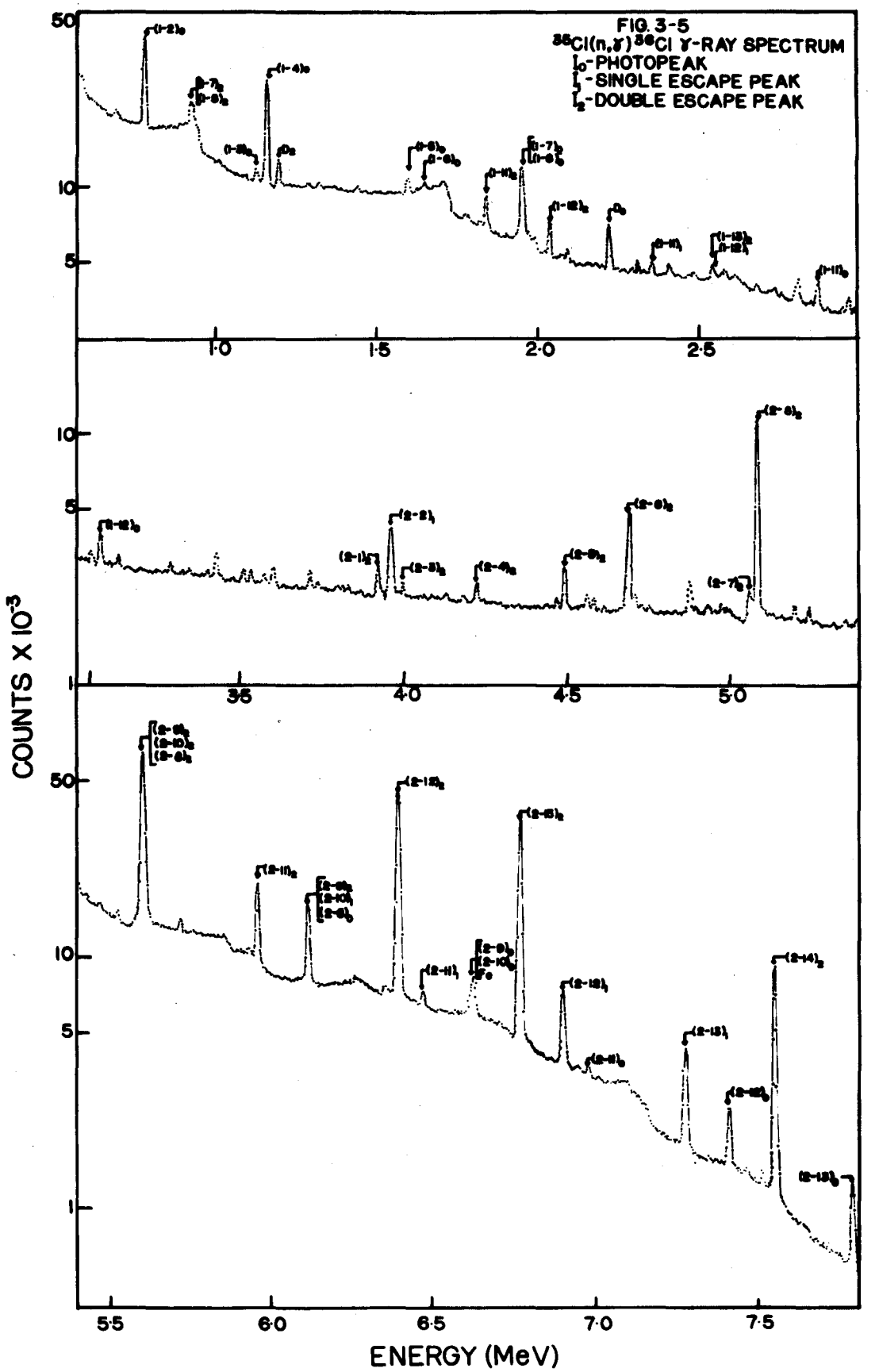
FIG. 3-5
$^{35}Cl(n,\gamma)^{36}Cl$ γ-RAY SPECTRUM
I_0-PHOTOPEAK
I_1-SINGLE ESCAPE PEAK
I_2-DOUBLE ESCAPE PEAK
COUNTS X 10^{-3}
ENERGY (MeV)
50
10
5
1
1·0
1·5
2·0
2·5
3·5
4·0
4·5
5·0
5·5
6·0
6·5
7·0
7·5

TABLE 3-4

$^{35}Cl(n,\gamma)^{36}Cl$ γ-ray Energies

Line No.	Energy (keV)	Calibration Used	Relative Intensity
1-1	517.5 (0.5)	Annihilation γ-ray ,	11
1-2	787.2 (0.5)	β-decay of ^{60}Co,	84
1-3	1130.8 (0.5)	β-decay of ^{24}Na	0.9
1-4	1164.6 (0.5)	and H(n,γ)D	10
1-5	1601.2 (0.5)	reaction	1.7
1-6	1646.4 (1.0)		0.3
1-7	1951.6 (1.0)		6.8
1-8	1958.9 (1.0)		3.4
1-9	2676.4 (1.0)		0.6
1-10	2846.7 (1.0)		0.3
1-11	2864.5 (0.5)		1.7
1-12	3061.5 (0.5)		2.0
1-13	3562.3 (1.0)		0.3
2-1	4944.9 (3)	Calbirated using	0.3
2-2	4980.3 (2)	constraints	1.0
2-3	5017.9 (3)		0.1
2-4	5517.6 (2)		0.3
2-5	5715.8 (2)		1.4
2-6	5903.7 (2)		0.3
2-7	6087.1 (3)		0.1
2-8	6111.5 (2)		4.7
2-9	6620.2 (2)		1.5
2-10	6627.9 (2)		0.9
2-11	6979.1 (2)		0.5
2-12	7414.9 (2)		2.2
2-13	7791.5 (2)		1.3
2-14	8580.0 (2)		0.6

ibrated relative to the energies of the $^{28}Si(n,\gamma)^{29}Si$ standard. The $^{35}Cl(n,\gamma)^{36}Cl$ γ-ray energies found by this procedure were then used to calculate an initial estimate of the Q-value. Using the same techniques employed in the $^{28}Si(n,\gamma)^{29}Si$ energy determinations, the constrained least-squares estimate of the Q-value was determined. A plot of the square of the residuals against Q is shown in Figure 3-6. The high energy data that was obtained using the constrained least-squares estimates of the Q-value, are also presented in Table 3-4. The energies of the intense γ rays, which have been quoted to the nearest 0.1 keV, have an associated error of $\pm$ 1 keV. The energies of the less intense γ rays are reliable to $\pm$ 3 keV. The relative intensities that are quoted were obtained using the techniques that will be discussed at the end of this chapter.

The constrained least-squares analysis was carried out using nine cascades. These nine cascades are presented in Table 3-5 along with their sums, Q. The energies, E_2, are the final estimates of the energies that were constrained to vary with the Q-value, while the energies E_1 were fixed in the analysis. The energies R_1 and R_2 are the recoil energies needed to obtain level energies from γ-ray energies.

The cascades which were used were verified by analysing time-correlated events with a Ge(Li) and a 3 x 3 in NaI(Tl) detector. For this two-parameter measurement, the sample size was limited to approximately one-tenth the size of that used for the one-parameter measurements. This was necessary to keep the true-to-chance ratio below 15%.

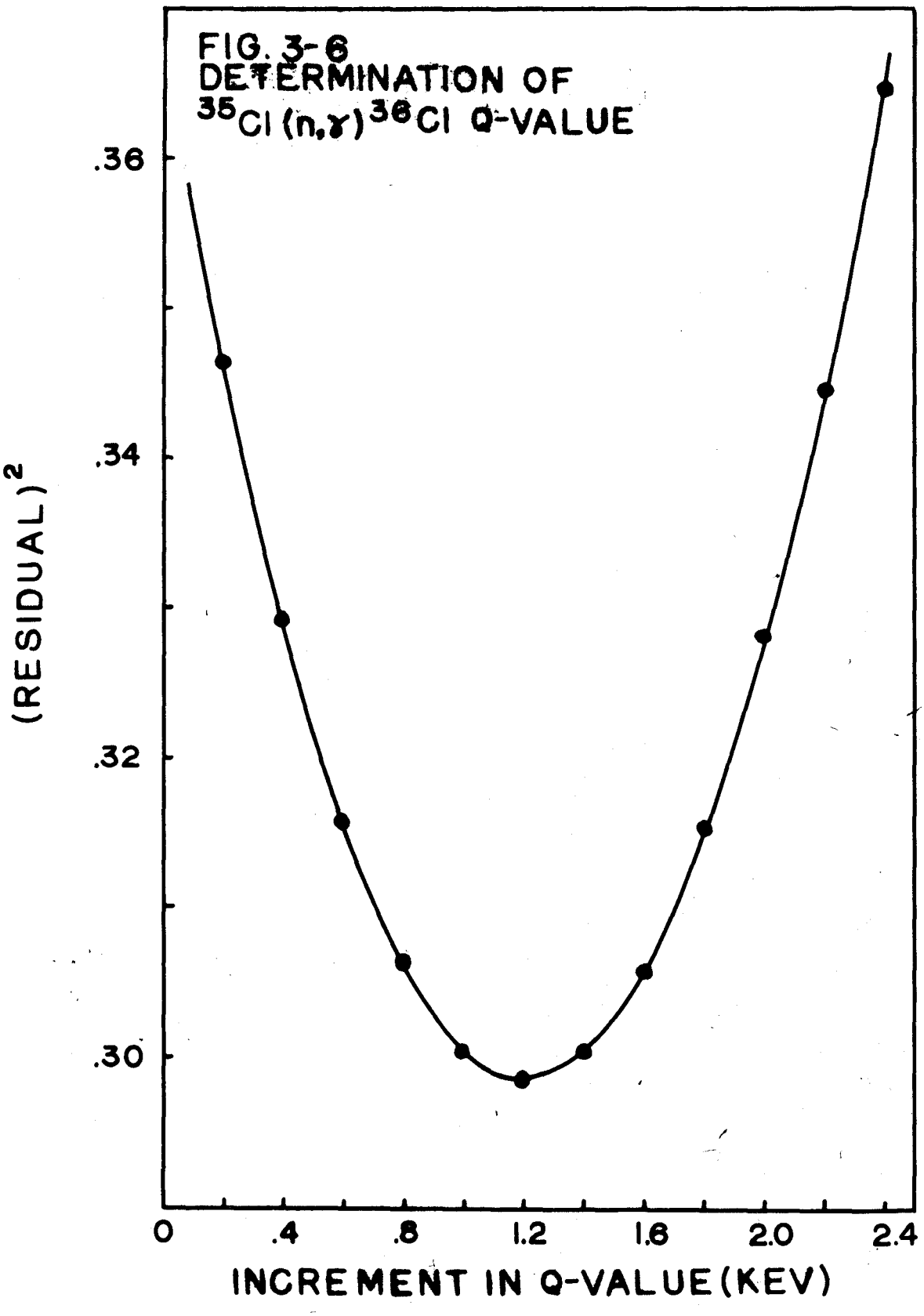
FIG. 3-6
DETERMINATION OF
35Cl (n,γ) 36Cl Q-VALUE
.36
.34
.32
.30
(RESIDUAL)²
0
.4
.8
1.2
1.6
2.0
2.4
INCREMENT IN Q-VALUE (KEV)

TABLE 3-5

Estimates of $^{35}Cl(n,\gamma)^{36}Cl$ Q-value

E_2 (keV)	R_2 (keV)	E_1 (keV)	R_1 (keV)	Q (keV)	Deviations (keV)
8580.0	1.1			8581.1	+ 0.5
7791.5	0.9	787.2	0.0	8579.6	- 1.0
7414.9	0.8	1164.6	0.0	8580.3	- 0.3
6979.1	0.7	1601.2	0.0	8581.0	+ 0.4
6627.9	0.7	1951.6	0.0	8580.2	- 0.4
6620.2	0.7	1958.9	0.0	8579.8	- 0.8
6111.5	0.6	517.4 1951.6	0.0 0.0	8581.1	+ 0.6
5903.7	0.5	2676.4	0.1	8580.1	+ 0.1
5715.8	0.5	2864.5	0.1	8580.9	+ 0.3
5517.6	0.4	3061.5	0.1	8579.6	- 1.0
4980.3	0.4	1130.8 517.4 1951.6	0.0 0.0 0.0	8580.5	- 0.1
			$\bar{Q}$ =	8580.6	± 0.4

Using delayed-time analysis, the resulting coincidence surface was obtained in a 1024 x 256 array; the larger dimension being used for the Ge(Li) detector. The gain in each dimension was chosen to record the entire pulse-height spectrum from its associated detector. The resulting coincidence rate of 40 counts/sec permitted the information obtained in a 12 h period to be stored on one 2,500 ft. reel of tape. In all, twenty-two such tapes were filled over a 10 day period.

The analysis of the coincidence surface to obtain the estimates of the coincidence quotients by the minimization of

$$R^2(\alpha_{ij}) = \sum_{fm} (M_{fm})^{-1} \left[M_{fm} - \sum_{ij} \alpha_{ij} R_{s1}(f,i) R_{s2}(m,j) \right]^2$$

could not be found since this would require the inversion of n x n matrix where n is the total number of γ rays in the spectrum. Fortunately, as has been shown by Slavinskas et al[67], the solutions obtained by first removing the detector response from one dimension and then the other, gives estimates of α_{ij} that are close to those obtained by the direct solution. This latter method requires the introduction of a function $\beta_i(m)$ where

$$\beta_i(m) = \sum_j \alpha_{ij} R_{s2}(m,j) \qquad 3\text{-}1$$

Least-squares estimates of $\beta_i(m)$ are found by minimizing

$$R^2(\beta_i) = \sum_f (M_{fm})^{-1} \left[M_{fm} - \sum_i \beta_i(m) R_{s1}(f,i) \right]^2$$

for each channel in the y-dimension, that is, for each value of m. The least-squares estimates of α_{ij} are then obtained from these estimates by minimizing

$$R^2(\alpha_{ij}) = \sum_m W_i(m) \left[\beta_i(m) - \Sigma\alpha_{ij} R_{s2}(m,j) \right]^2$$

for each γ-ray energy in the x dimension or each i.

These least-squares estimates are only possible when the spectrometer responses associated with both dimensions are known. Since the responses were not known in the present case, another procedure had to be found. The procedure used is based on the fact that the function $\beta_i(m)$ is the spectrum of the γ rays that were in coincidence with a γ ray of energy E_i. This γ-ray spectrum is, of course, that seen by the detector coupled to the m-side and the coincident γ ray, of energy E_i, was detected by the counter associated with the f-side. For the case under discussion, the spectrometer associated with the m-dimension was the NaI(Tl) detector while the spectrometer associated with the f-side was the Ge(Li) detector. As was indicated earlier, the response of the Ge(Li) detector consists, in general, of three peaks and a continuum so that one can write

$$R_{s1}(f,i) = \sum_{k=0}^{2} P_k(f,i) + C(f,i)$$

In this analysis it was assumed that the continuum, C(f,i),is linear over small ranges in f so that

$$C(f,i) = C_{1i} + C_{2i} f$$

Hence, in the region of the double-escape peak associated with a γ ray of energy E_k, we have the model function

$$M_{fm} = \beta_k(m) P_2(f,k) + \sum_i (C_{1i} + C_{2i} f)$$

$$= \beta_k(m) P_2(f,k) + \gamma_k(m) + \delta_k(m) f$$

Using this equation, one can find an estimate of $\beta_k(m)$ from

$$\beta_k(m) = \sum_{f=\ell}^{u} (M_{fm} - \gamma - \delta f)/A_k$$

where ℓ and u are the channel numbers in the f-dimension that bracket the region of the peak. The quantity A_k is the fraction of the total area of the response that is in the peak under consideration. The estimates used for γ and δ were

$$\gamma = M_{\ell m}$$

$$\delta = (M_{um} - M_{\ell m}) / (u - \ell + 1)$$

Hence

$$\beta_k(m) = \frac{1}{A_k} \left(\sum_{f=1}^{u} M_{fm} - 1/2 \, (u - \ell + 1) \, (M_{um} + M_{\ell m}) \right)$$

The normalization factor A_k for the NaI(Tl) spectra is not required if only branching ratios are desired.

A computer program has been developed to calculate these estimates of $A_k\beta_k(m)$ for any peak in the Ge(Li) dimension. It was necessary, when analysing the weaker peaks in the Ge(Li) dimension, to smooth the spectra before subtracting the interference caused by the underlying continuum. In this case the spectra

$$T_i(m) = \sum_{f=\ell}^{u} M_{fm}$$

and

$$B_i(m) = 1/2 \, (u - \ell + 1) \, (M_{um} + M_{\ell m})$$

were plotted, smoothed and subtracted to obtain $A_i \, \beta_i(m)$

The NaI(Tl) spectra obtained by the techniques outlined above contained chance coincidence events. By assuming that the spectrum of these events is like the singles spectrum, the percentage of the chance

contribution can be found and removed. The chance contribution in each of the NaI(Tl) spectra is, of course, not the same. The contribution in each spectrum was obtained in the following way. The coincidence surface was projected onto the f axis by summing over all m; that is

$$P(f) = \sum_{ij} \alpha_{ij} R_{sl}(f,i)$$

was calculated. By separating the ground-state transition out of the sum, we get

$$P(f) = (\sum_{j} \alpha_{1j}) R_{sl}(f,1) + \sum_{i,j}^{i=1} a_{ij} R_{sl}(f,1)$$

Since the ground state transition is not in true coincidence with any γ ray, α_{1j} contains only the chance component, α^{c}_{1j}. Hence

$$P(f) = (\sum_{j} \alpha_{1j}) R_{sl}(f,1) + \sum_{i,j}^{i\neq 1} \alpha_{ij} R_{sl}(f,i)$$

A single-parameter spectrum taken with the f-side spectrometer can then be renormalized so that $a_1 = \sum_j \alpha^{c}_{1j}$, where the renormalized singles spectrum is given by

$$S_1(f) = \sum_i a_i R_{sl}(f,i)$$

This, then, is an estimate of the spectrum of the chance events in the projection P (f). An estimate of the chance contribution in the i^{th} NaI spectrum, $A_i\beta_i(m)$ is given by

$$C_i(m) = A_i a_i S_2(m)$$

where $S_2(m)$ is the singles spectrum associated with the NaI detector. The normalization $A_i a_i$ can be estimated from the area of the appropriate peak in the renormalized singles spectrum associated with the Ge(Li) detector, S (f).

The analysis for the spectrum in coincidence with the 5715-keV γ ray illustrates the method used. Figure 3-7 shows the projection P(f) of the coincidence surface in the region of interest. Only the region $\ell \leq f \leq u$ was considered. The spectrum T(m) shown in Figure 3-8(a), is the total number of coincidence events between channels u and ℓ in the f-dimension, as defined previously. B(m), the estimate of the Compton interference in T(m), is also shown in Figure 3-8(a). The resulting coincidence spectrum, β(m), and its chance component, C(m), are presented in Figure 3-8(b). This latter spectrum is the NaI singles spectrum normalized to the area of the 5715-keV double-escape peak in the renormalized Ge(Li) singles spectrum, $S_1(f)$. This area has been crosshatched in Figure 3-7. From the coincidence spectrum it is clear that the level fed by the 5715-keV γ ray depopulates directly to the ground state by the emission of a 2864-keV γ ray.

This result, along with ten other cascades, is presented in the decay scheme shown in Figure 3-9. The relative intensities shown have the same normalization as those in Table 3-4. For the low-energy transitions the branching ratios obtained from the coincidence data have been used to divide the total intensity coming into the level into the observed decay modes of this level. The intensities of the low-energy γ rays found by this means are all less than those presented in Table 3-4 which is consistent with the assumption that all the components populating the low-energy levels have not been identified.

The decay of the 1952-keV level is not unique. The 787-1164 keV cascade shown could be inverted and still be consistent with the

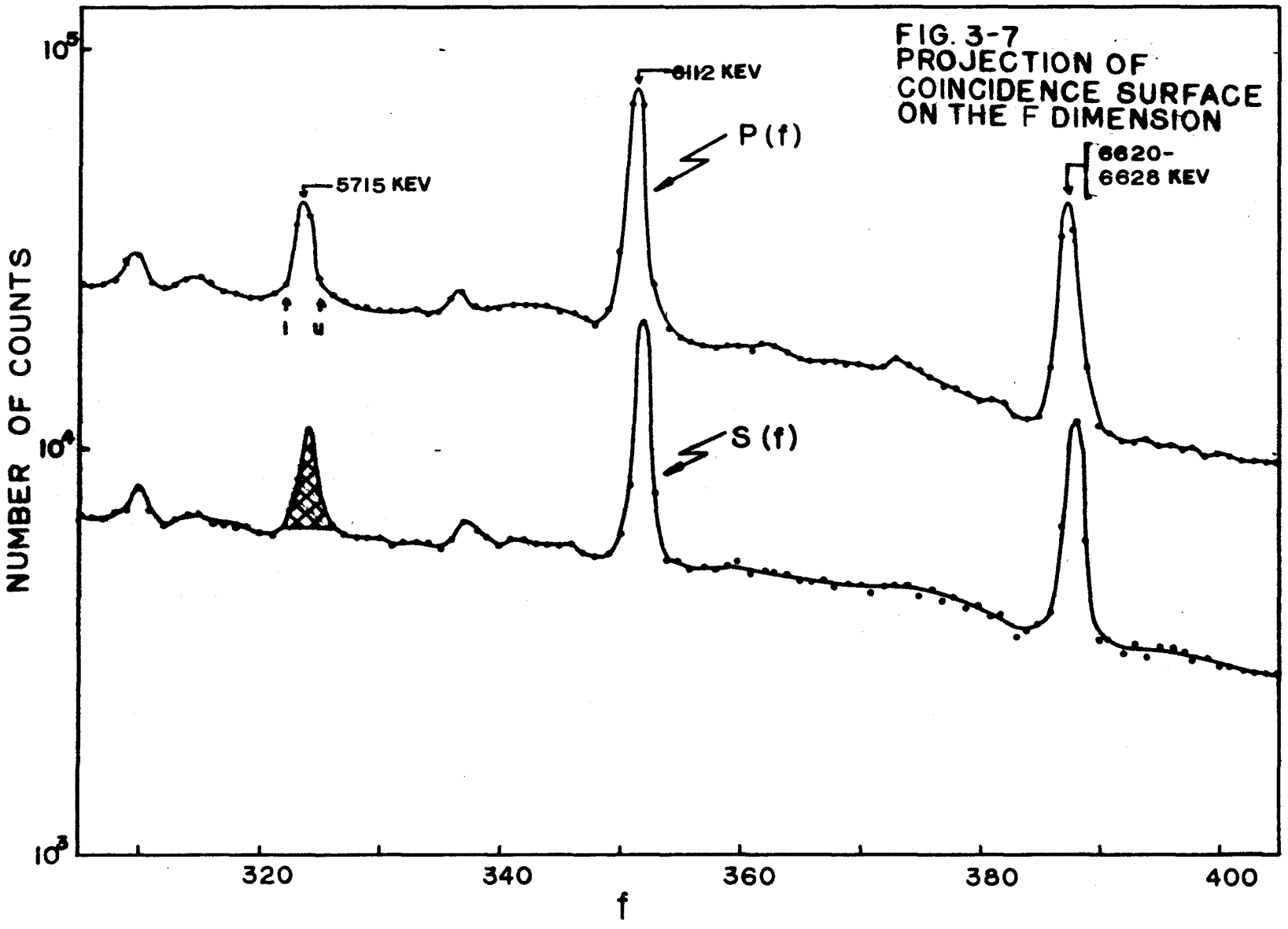
FIG. 3-7
PROJECTION OF
COINCIDENCE SURFACE
ON THE F DIMENSION
6112 KEV
P(f)
5715 KEV
6620-
6628 KEV
l
u
S(f)
NUMBER OF COUNTS
10⁵
10⁴
10³
320
340
360
380
400
f

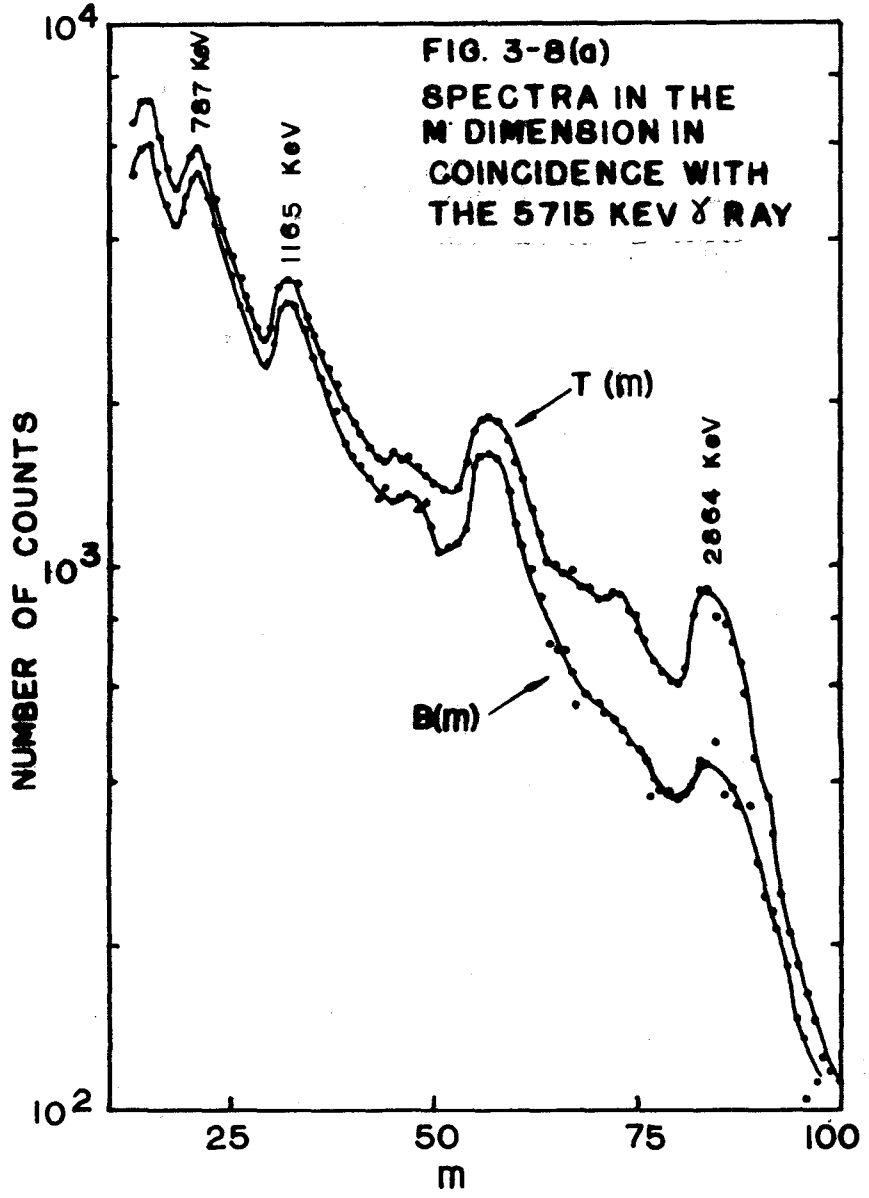
FIG. 3-8(a)
SPECTRA IN THE
M DIMENSION IN
COINCIDENCE WITH
THE 5715 KEV γ RAY
787 KeV
1165 KeV
2864 KeV
T (m)
B(m)
NUMBER OF COUNTS
m

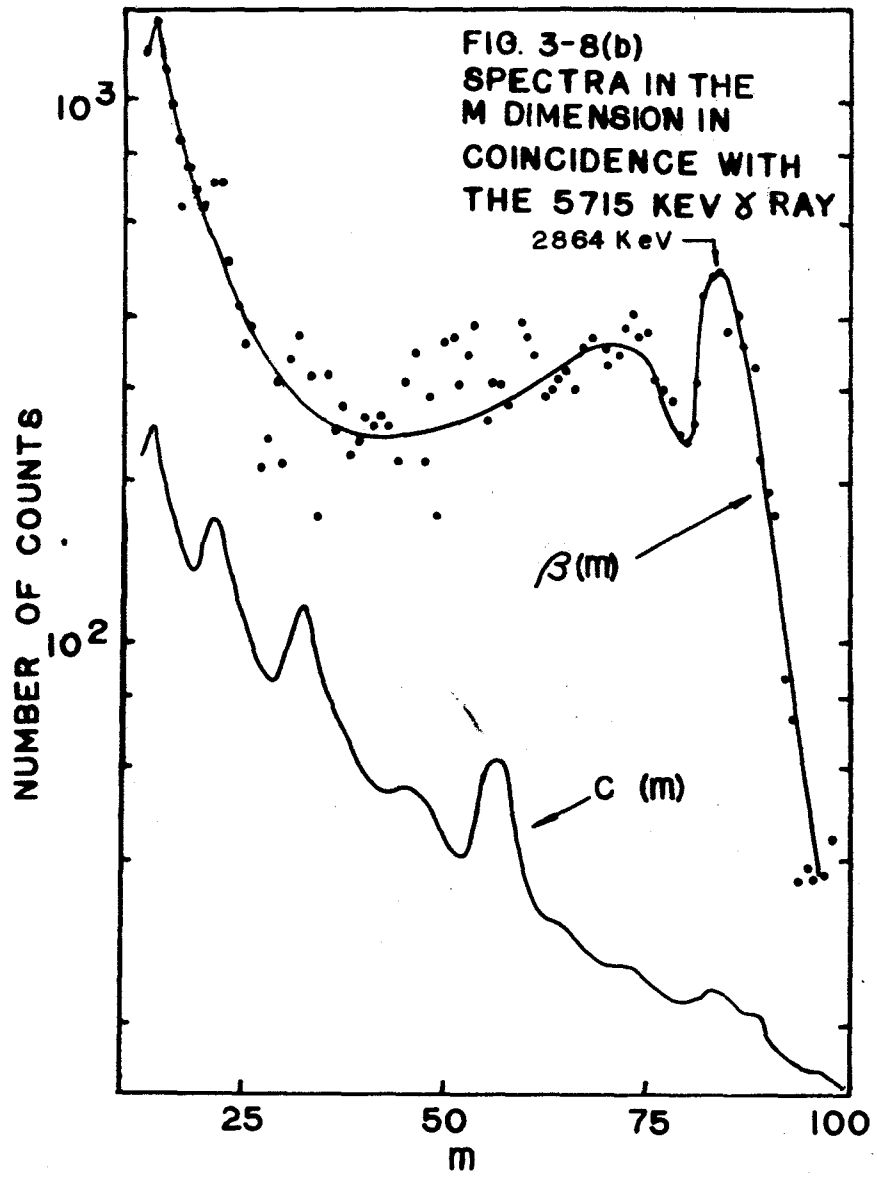
FIG. 3-8(b)
SPECTRA IN THE
M DIMENSION IN
COINCIDENCE WITH
THE 5715 KEV γ RAY
2864 KeV
β(m)
C (m)
NUMBER OF COUNTS
m

$^{35}Cl + n$ FIG. 3-9

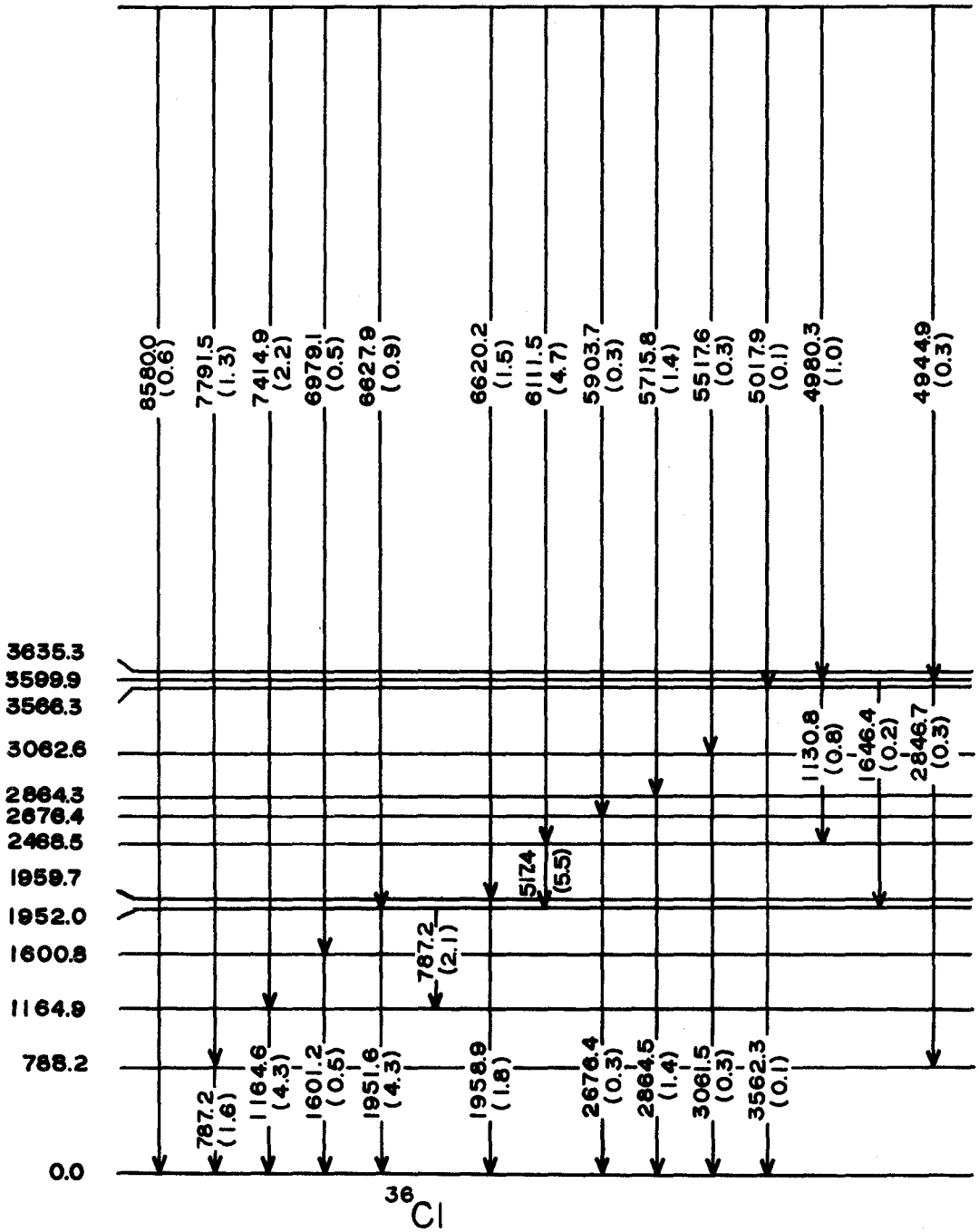
8580.0 (0.8)
7791.5 (1.3)
7414.9 (2.2)
6979.1 (0.5)
6627.9 (0.9)
6620.2 (1.5)
6111.5 (4.7)
5903.7 (0.3)
5715.8 (1.4)
5517.6 (0.3)
5017.9 (0.1)
4980.3 (1.0)
4944.9 (0.3)
3635.3
3599.9
3566.3
3062.6
2864.3
2676.4
2468.5
1959.7
1952.0
1600.8
1164.9
788.2
0.0
1130.8 (0.8)
1646.4 (0.2)
2846.7 (0.3)
5174 (5.5)
787.2 (2.1)
787.2 (1.6)
1164.6 (4.3)
1601.2 (0.5)
1951.6 (4.3)
1958.9 (1.8)
2676.4 (0.3)
2864.5 (1.4)
3061.5 (0.3)
3562.3 (0.1)
^{36}Cl

data. However, the energy of the first excited state observed from the 7792 keV γ-ray and the 4945-2847 keV cascade is consistently 1 keV higher than the observed 787 keV γ-ray. This suggests assigning the 787 keV γ-ray in two places in the decay scheme as has been done. The double escape peaks corresponding to transitions to the 1952 and the 1960 keV levels were not completely resolved in the spectrum. The analysis of this doublet is also complicated by the presence of the 6112 keV first escape peak. The energies and intensities for the transitions to these two levels were obtained by first removing the interfering 6112 first escape peak and stripping the resulting composite peak. The decays of the 3562- and 3635- keV levels have been assigned mainly on the basis of energy considerations although they are consistent with the coincidence data. The coincidence data in this case was of limited value because of the interference from the decays of the other members of this triplet.

The results of the coincidence measurements are in agreement with those of Segel[63]. Clarification of the population and decay of the 1952- and 1959- keV levels, along with the 3635-, 3600- and 3562-keV levels has resulted from these measurements. The decay of the 2864-keV level to the first excited state, as suggested by Segel, is not consistent with these data.

For the energy determinations the 5019-3563 and 4947-2846 keV cascades were not included because of the low intensity and resulting uncertainty in their energies.

3.4 Energy Calibration Using the $^{35}Cl(n,\gamma)^{36}Cl$ Standard

Having found accurate energies for the Cl standard, the spectra of interest were calibrated relative to this standard. For each unknown, two experiments were performed; the mixed spectrum of the unknown and the Cl standard was obtained and, with the same gain, the spectrum of the unknown was obtained. This procedure helped in the identification of the peaks associated with the standard in the mixed spectrum. The energies of the strong lines in the unknown were then calculated and these were then used as internal standards in the spectrum of the unknown.

The majority of the spectrum considered in this work were taken with a biased amplifier and the 1024 channel ADC. Since this system had a relatively large non-linear term, the channel positions of the peaks were transformed to an equivalent input charge. This equivalent input charge, q, is that amount of charge, which, when deposited on the pre-amplifier input terminal, would give rise to a count being stored at channel position x. The transformation depends on the gain of the system, g, the biased-amplifier window setting, w, as well as channel position, so that

$$q = q(g,w,x).$$

The γ-ray energy, E, should be linearly related to the equivalent input charge q, that is

$$E = a + bq$$

Hence, after transforming the channel positions of the peaks to their equivalent input charge, a linear least-squares fit to the standards

was performed and the unknown energies calculated.

For the experiments using the window amplifier, the gains of both amplifiers were adjusted to give approximately 2.5 keV/channel. These gains were then fixed for the entire series of experiments and the region of interest selected by adjusting the window of the biased amplifier. Hence, the transformation from channel number to equivalent input charge can be represented by a two dimensional surface $q(w,x)$.

Using a precise pulser, it was found that the surface could be adequately described by nine parameters. The transformation of channel number to equivalent input charge is then given by

$$q = \sum_{i=1}^{3} \sum_{j=1}^{3} a_{ij} \, w^{j-1} \, x^{i-1}$$

where a_{ij} are the nine parameters describing the surface. These parameters were estimated from the pulser measurements using least-squares techniques. As was done with the two parameter γ-γ coincidence experiment, the functions

$$C_i(w) = \sum_{j} a_{ij} \, w^{j-1}$$

were first estimated using the model equation

$$q = \sum_{i=1}^{3} C_i(w) \, x^{i-1}$$

The values of $C_i(w)$ that were found, are shown in Figure 3-10. The curves shown are those resulting from the least-square estimates of a_{ij} found by minimizing

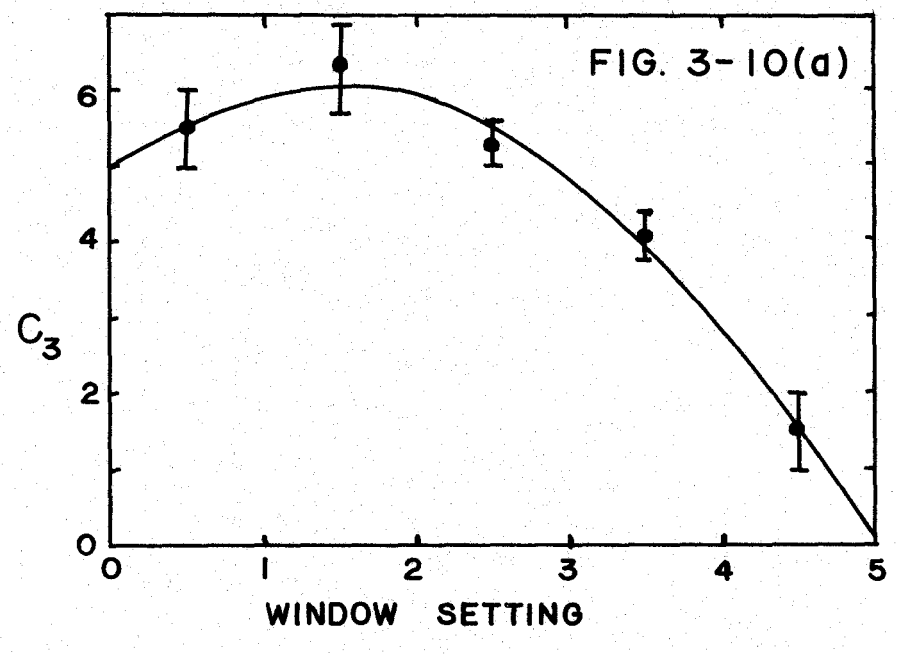
FIG. 3-10(a)
C_3
6
4
2
0
0
1
2
3
4
5
WINDOW SETTING

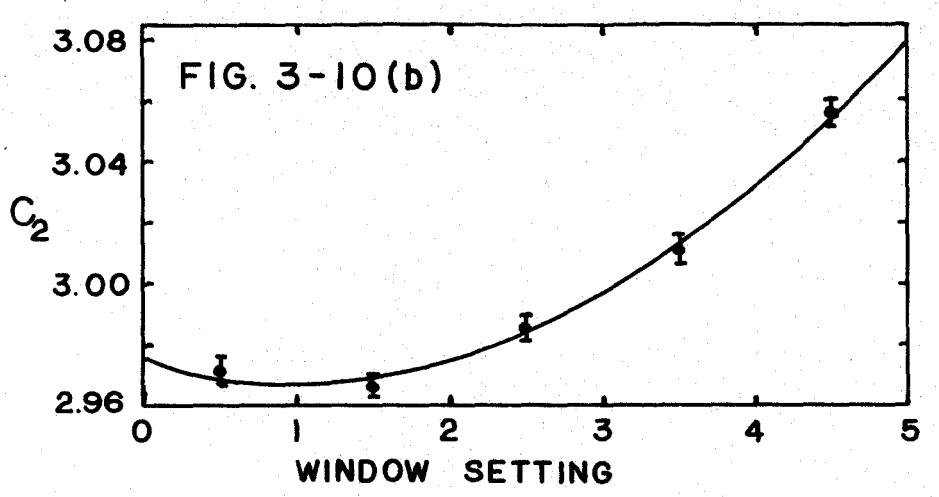
FIG. 3-10(b)
C_2
3.08
3.04
3.00
2.96
0
1
2
3
4
5
WINDOW SETTING

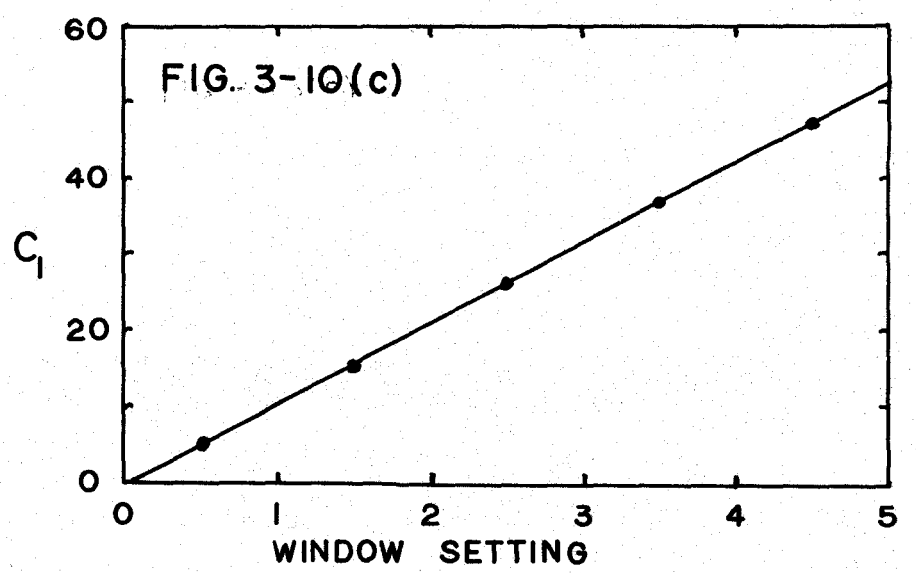
FIG. 3-10(c)
C_1
60
40
20
0
0
1
2
3
4
5
WINDOW SETTING

$$R^2(a_{ij}) = \sum_i W_i \, (C_i(w) - \sum_j a_{ij} \, w^{j-1})^2$$

The weights, W_i, used in this case were one over the variances of the estimates of $C_i(w)$. The estimates of the parameters used are presented in Table 3-6.

3.5 Calibration of the γ-Ray Intensities

Having obtained the energies, E_i, of all the γ-ray components in the single parameter spectrum, the probability that the i^{th} component will be emitted when 100 neutrons have been captured, I_i, is desired. From the spectrum one obtains the probability that the i^{th} component will be detected, a_i, which is related to the desired intensity through the detector efficiency , $\varepsilon(\omega, E)$. This relationship is given by

$$a_i = \varepsilon(\omega, E_i) I_i$$

The detector efficiency is, then, the probability that a γ ray of energy E will interact with the detector.

If the detector response is not known, the intensity can be estimated from the area of a peak in the response provided that A_i^j, the peak-to-total ratio, is known. The index j is used, as before, to distinguish between the three possible peaks, that is j = 0 refers to photoelectric events, j = 1 single escape events and j = 2 double escape events. The area in the peak, a_i^j, is related to the γ-ray intensity by the relation

$$a_i^j = A_i^j \, \varepsilon(\omega, E_i) I_i$$

$$= \varepsilon_j(\omega, E_i) I_i \qquad j = 0 \text{ to } 2$$

TABLE 3-6

Parameters Used to Transform the Channel Number to Equivalent Input Charge

	a_{i1}	a_{i2}	a_{i3}
a_{1j}	- 0.752	10.8	-3.93×10^{-2}
a_{2j}	2.98×10^{-2}	-1.53×10^{-3}	-7.34×10^{-5}
a_{3j}	4.99×10^{-7}	1.37×10^{-7}	4.73×10^{-3}

The relative detector efficiency for the total absorption peak and the second escape peak for the 10 cc counter used for the majority of this work is shown in Figure 3-11. Table 3-7 lists the sources used to determine these efficiencies. In some cases the relative source strengths were obtained using a 3 x 3 inch NaI(Tl) detector in 10 cm geometry and the measured efficiencies of Heath[68]. For the second escape peak efficiency measurements (n,γ) reaction radiations were used. Published results were used for the relative intensities of radiations from the same reaction. The normalization between different reactions was adjusted until the data fell on a smooth curve. The $^{1}H(n,\gamma)^{2}H$ reaction and the γ rays following the β-decay of ^{28}Al and ^{24}Na were used to normalize ε_o to ε_2. The photo electric and pair cross sections are shown in Fig. 3-11 also. They have been adjusted so that the pair cross section coincidences with the detection efficiency of the second escape peak in the region of 2 MeV. In this region one expects the energy dependence to be the same.

The efficiency associated with the photo peak is significantly greater than that expected from the photo electric cross section below 6 MeV. This could be due to multiple interactions in the counter which lead to the total γ-ray energy being absorbed. Above 4 MeV the efficiency begins to decrease rapidly. This decrease is presumably due to a rapid drop in the number of primary electrons that are stopped in the sensitive volume of the detector. Hence for this γ-ray energy, the range of the electrons that are produced, is approaching the dimensions of the active volume. This decrease in efficiency with

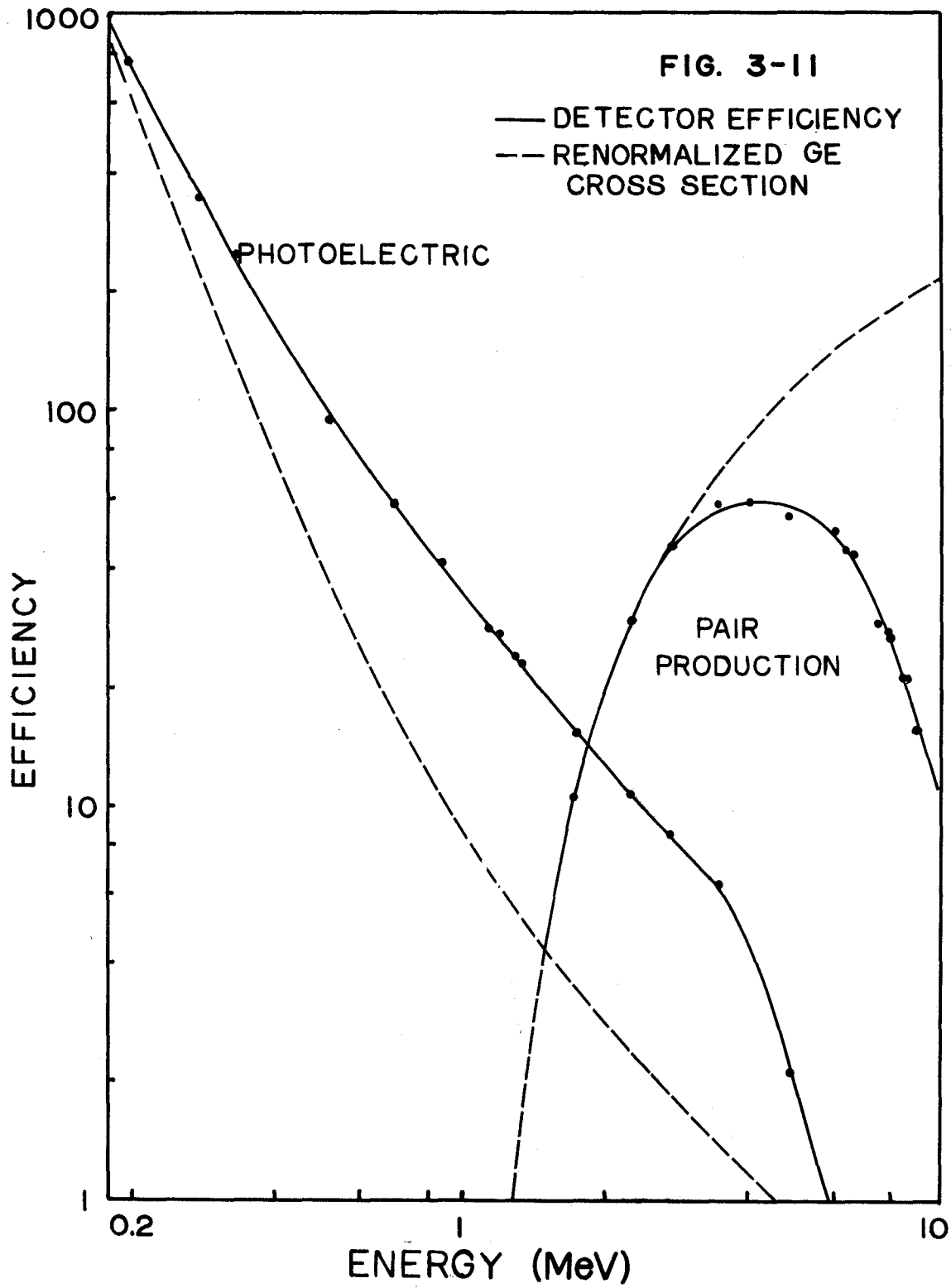
FIG. 3-11
DETECTOR EFFICIENCY
RENORMALIZED GE CROSS SECTION
PHOTOELECTRIC
PAIR PRODUCTION
EFFICIENCY
ENERGY (MeV)
1000
100
10
1
0.2
1
10

TABLE 3-7

Intensity Standards

Reaction	γ Energy (keV)	Relative Intensity	Reference
$^{51}Cr(\beta^-)^{51}V$	320	100	68
$^{22}Na(\beta^+)^{22}Ne$	511	200	69
	1274	100	
$^{46}Sc(\beta^-)^{46}Ti$	887	100	70
	1119	100	
$^{60}Co(\beta^-)^{60}Ni$	1173	100	71
	1322	100	
$^{24}Na(\beta^-)^{24}Mg$	1368	100	72
	2759	100	
$^{1}H(n,\gamma)^{2}H$	2223	100	
$^{28}Si(n,\gamma)^{29}Si$	3540	36.5	73
	4936	37.4	
$^{23}Na(n,\gamma)^{24}Na^*$	3980	17	74
	6400	22	
$^{35}Cl(n,\gamma)^{36}Cl$	6115	21	75
	6627	13	
	7419	9.9	
	7795	8.4	
	8582	2.3	
$^{27}Al(n,\gamma)^{28}Al^*$	7728	14	76
$^{58}Ni(n,\gamma)^{59}Ni$	8532	14	77
	8997	35	

* In these cases the samples were irradiated prior to obtaining the spectrum so that the β-decay had reached saturation. Hence the intensities from the (n,γ) reaction are relative to the appropriate β-decay γ rays.

energy is also seen in the efficiency associated with the second escape peak. At 10 MeV this efficiency, if it were proportional to the cross section, would be a factor of 10 times greater than at 2 MeV but because of this electron escape it is a factor of two smaller.

Analytical expressions of the form

$$\varepsilon_o(E) = a_o E^{n_o}$$

and

$$\varepsilon_2(E) = a_2 \exp (b_2 \ln(E/c_2))^{n_2}$$

have been used with the least-squares estimates of the parameters to calculate relative intensities. The estimates that were used are

$$a_o = 6.33 \times 10^5$$

$$a_o = -1.42$$

and

$$a_2 = 60.0$$

$$b_2 = 2.46$$

$$c_2 = 4130 \text{ MeV}$$

$$n_2 = 2.5$$

CHAPTER IV

DATA ANALYSIS

4.1 Maximum Likelihood Estimates

In this work the data was analysed using the method of Maximum Likelihood (ML). This method of handling statistical data is discussed in detail in standard textbooks on statistical analysis[69,70]. Very briefly, it consists of forming the joint frequency function, $L(x_1,x_2,\ldots x_n|\theta)$, for obtaining the sampling $(x_1,x_2,\ldots x_n)$. The parameter θ is assumed to completely determine the parent distribution. The joint frequency function is called the Likelihood Function (LF). The ML estimates of θ are that value which maximizes the LF. For example, let us assume we sample n times from a distribution

$$P(x)dx = \exp(-x/\bar{x})\ dx/\bar{x} \qquad (4\text{-}1)$$

and obtain the vector $(x_1,x_1,\ldots x_n)$. If we also assume that each sampling is statistically independent from all the others then the LF is given by

$$L(x_1,x_1\ldots x_n|\bar{x}) = \prod_i (1/\bar{x})\exp(-x_i/\bar{x})$$

The ML estimate of $\bar{x}$ is

$$\bar{x}^* = (1/n)\ \Sigma\ x_i \qquad (4\text{-}2)$$

which is intuitively what one would expect.

Any estimate obtained from data that are distributed will also be distributed. For example, the ML estimate $\bar{x}^*$ in the example above has a distribution which is determined from its defining

equation(4-2) and the distributions of the x_i's. Two important parameters of the distribution of an estimate are the mean value and the variance. If the mean value equals the true value, the estimate is said to be unbiased, that is if

$$\theta = \int \theta \, P(\theta^*) \, d\theta^*$$

then θ^* is an unbiased estimate of θ. The variance of θ^* is usually quoted as the error in the estimate, θ^*. It also determines whether an estimate is efficient, for if an estimate is efficient, the inverse of its variance is given by

$$1/\mathrm{var}(\theta^*) = - \int \cdots \int \frac{\partial^2}{\partial\theta^2} \ell n \, L(x_1 \cdots x_n \, \theta) \;\; L(x_1 \cdots x_n \, \theta) dx_1 \cdots dx_n$$

$$= - E\left[\frac{\partial^2}{\partial\theta^2} \ell n \, L(x_1 \cdots x_n \, \theta)\right]$$

It can be shown that (see for example p 10 of ref.69) for any unbiased estimate of θ, θ^* say,

$$\mathrm{var}\,(\theta^*) \quad - 1/E\left[\frac{\partial^2 \ell nL}{\partial\theta^2}\right]$$

Hence $-1/E\left[\frac{\partial^2 \ell nL}{\partial\theta^2}\right]$ is the smallest variance that can be obtained for all unbiased estimates and an efficient estimate is one which has this variance.

To further clarify these definitions let us return to our simple example. For ease of notation we will write $\bar{x} = \theta$ and $\bar{x}^* = \theta^*$ so that equations 4-1 and 4-2 become

$$P(x)dx = \exp(-x/\theta)dx/\theta$$

and

$$\theta^* = \frac{1}{n} \Sigma \, x_i$$

The frequency function of θ^* can be calculated explicitly from

$$P(\theta^*) = \prod_i \exp(-x_i/\theta)\ \delta(\frac{1}{n}\Sigma x_i - \theta^*)dx_i/\theta$$

This has been done by Klump[71] to give

$$P(\theta^*) = \frac{n}{\theta}\ \frac{1}{(n-1)!}\ (\frac{n\theta^*}{\theta})^{n-1}\ \exp\ (-n\theta^*/\theta)$$

Again simple integration shows that

$$E\ \left[\theta^*\right] = \theta$$

$$E\left[(\theta^* - \theta)^2\right] = \theta^2/n$$

The first result shows that this ML estimate is unbiased and the second, when compared to

$$-E\left[\frac{\partial^2\ \ell nL}{\partial\theta^2}\right] = \frac{-n}{\theta^2} + \frac{2}{\theta^2}\ \Sigma\ (x_i/\theta)\exp(-x_i/\theta)dx_i/\theta$$

$$= n/\theta^2$$

shows that it is also efficient.

In this general case, the ML estimates do not have these desirable properties. It can be shown, however, (see for example p.43 of ref. 69) that provided

$$E\ \left[\frac{\partial\ \ell nL}{\partial\theta}\right] = 0$$

and

$$R^2(\theta) = -E\left[\frac{\partial^2\ \ell nL}{\partial\theta^2}\right]$$

exists and is nonzero, the ML estimator is asymptotically normally distributed with mean θ and variance $1/R^2(\theta)$. Hence provided the sample size is sufficiently large the ML estimates are unbiased and efficient.

For simplicity we have assumed that the distributions depend on only one parameter. The generalization to the multiparameter case, where the LF is given by $L(x_1 \ldots x_n \mid \theta_1 \ldots \theta_n)$, is obvious. The ML

estimates of the θ_i's are those values which simultaneously maximize the LF function. Again, provided

$$E\left[\frac{\partial \ell nL}{\partial \theta_i}\right] = 0$$

for all i and

$$R^2_{ij} = - E\left[\frac{\partial^2 \ell nL}{\partial \theta_i \, \partial \theta_j}\right] \qquad (4\text{-}3)$$

exists and is nonzero for all i and j, the ML estimates are asymptotically normal with means θ_i and with a variance-covariance matrix given by the inverse of the matrix

$$R^2 = (R^2_{ij}) \qquad (4\text{-}4)$$

As we shall see, it is very difficult to obtain the distributions of the ML estimates used in this work. In order to calculate an error for the estimates it will be assumed that the sample size is sufficiently large and the asymptotic values are realized. The inverse of R^2 can then be used to estimate the errors. It should be kept in mind that the estimates of the errors will be too small if the sample size isn't large enough.

4.2 Analysis of Transition Probabilities

In Chapter I, we have seen that there are two predictions for the energy dependence of the average transition probability from initial states at 8 MeV excitation energy. The first, the single particle estimates, predict that the average partial width for E1 radiation is given by

$$\Gamma_W(E1) = \gamma_1 E^3$$

These estimates predict, furthermore, that γ-ray emission from states

with excitation energies below 10 MeV will be predominantly El in character provided that appropriate final states exist. The second prediction suggests that γ-ray emission from states with high excitation energies should reflect the existance of the El giant resonance by having enhanced El transition rates. Explicitly, for initial states in the region of 7 MeV, Axel predicts average partial widths for El radiation of the form

$$\Gamma_A(El) = \gamma_2 E^5$$

Provided there is no enhancement of the transition probabilities for other multipolarities, transitions from such states will be again predominantly of El character.

In the analysis of the transition probabilities it will be assumed that only El radiations have been observed. This assumption is consistent with the previous discussion and with the measured transition rates for cases where the multipolarity is known. The possible existance of enhanced Ml transitions reported by Lundberg and Starfelt[72] does not seem to be consistent with other experiments[73,74,75] and hence will be neglected.

With this assumption the average partial radiative width as a function of the γ-ray energy is of the form

$$\bar{\Gamma} = \Gamma_\gamma (aE)^n$$

where Γ_γ is the total radiative width. For $n = 3$, $\bar{\Gamma} = \Gamma_W$ and for $n = 5$, $\bar{\Gamma} = \Gamma_A$. ML estimates have been obtained for the parameters a and n for ten odd-odd nucleidesin the mass range $56 \leq A \leq 204$. The choice of odd-even target nuclei was made since many of these are

monoisotopic and hence separated isotopes are not required. These systems also have relatively dense and quite complex low energy excitations which suggests that a statistical description, such as is used here, might be applicable at low energies.

In order to find these ML estimates, the probability density function for the distribution in the partial radiative widths must be known. The density function for the partial radiative widths to a given final state from different initial states is a χ^2 function with $\nu = 1$, that is one degree of freedom. For this analysis it has been assumed that the same probability density function applies to the widths from a given initial state to different final states. This assumption has recently been supported by the analysis of Cote and Prestwich[76] on the partial radiative widths obtained from resonance capture in platinum.

Since we are dealing with thermal neutron capture a further complexity arises. If the thermal neutron cross section can be thought of as resulting from contributions from more than one resonance, the measured partial radiative widths for thermal neutron capture are average values. The averaging is, in general, very complicated. The contribution from each resonance is proportional to its Γ_n, its Γ_γ and E_o^{-2}, where E_o is the resonance energy. Furthermore, the contributions from each resonance with the same total angular momentum quantum number are coherent, which results in interference effects. This is not true for the contributions from resonances with different angular momenta, which add incoherently.

The probability density function associated with the partial

widths must reflect this averaging. If, for example, two resonances incoherently contribute an equal amount to a given partial width, the density function for that partial width will be a χ^2 function with $\nu = 2$. We have assumed, in this analysis, that the true probability density function can be approximated, to a sufficiently high degree of accuracy, by a χ^2 function with $\nu = 2$, that is

$$P_T(\Gamma)d\Gamma = (1/\bar{\Gamma}) \exp(-\Gamma/\bar{\Gamma})d\Gamma$$

The distribution from which the measured partial widths have been sampled is different from $P_T(\Gamma)d\Gamma$ because of imperfections in the spectrometer. One such imperfection is the finite signal-to-noise ratio that is present when one tries to measure γ-ray intensities. This is due to the presence of a continuum on which the peaks are superimposed and results in the loss of low intensity γ rays because of the statistical fluctuations in this continuum. Hence there is a minimum partial width, Γ_{min}, which can be observed. If we assume that the sensitivity for measuring partial widths is given by a step function

$$S(\Gamma) = 0 \qquad \Gamma < \Gamma_{min}$$
$$= 1 \qquad \Gamma \geq \Gamma_{min}$$

the observed probability density function for the partial widths will be given by

$$P(\Gamma) = (1/N)\, P_T(\Gamma) \qquad \Gamma < \Gamma_{min}$$
$$= 0 \qquad \Gamma \geq \Gamma_{min}$$

where

$$N = \int_{\Gamma_{min}}^{\infty} P_T(\Gamma)d\Gamma$$

$$= \exp(-\Gamma_{min}/\bar{\Gamma})$$

By defining $\Gamma' = \Gamma - \Gamma_{min}$ the observed probability density function becomes

$$P(\Gamma) = (1/\bar{\Gamma}) \exp(-\Gamma'/\bar{\Gamma}) \qquad \Gamma' \geq 0$$

$$= 0 \qquad \Gamma' < 0$$

Figure 4-1 shows the modified χ^2 function for ν = 1, 2 and 3. The effect of the nonzero threshold in the measurement of the partial widths has been corrected for in all three cases, using the techniques discussed above for the ν = 2 case. Since the major difference between the χ^2 functions with ν = 1, 2 and 3 occurs when the independent variable is small, the threshold correction significantly reduces the difference between the functions with ν = 1, 2 and 3 and makes the results of the analysis less sensitive to the explicit value of ν that has been chosen.

The natural logarithm of the LF can be written explicitly for M samples as

$$\ell nL(a,n) = -Mn\ell n(a) - n\Sigma\ell n(E_i) - a^{-n}\Sigma\, \Gamma_i'/E_i^n$$

The ML estimators of a and n can be obtained from

$$\frac{\partial \ell nL}{\partial a} = 0 = -\frac{Mn}{a} + \frac{n}{a^{n+1}}\, \Sigma\, \Gamma_i'/E_i^n$$

and

$$\frac{\partial \ell nL}{\partial n} = 0 = -M\ell n(a) - \Sigma\ell n(E_i) + a^{-n}\, \ell n(a)\Sigma\, \Gamma_i'/E_i^n + \Sigma_i \ell n(E_i)\, \Gamma_i'/E_i^n$$

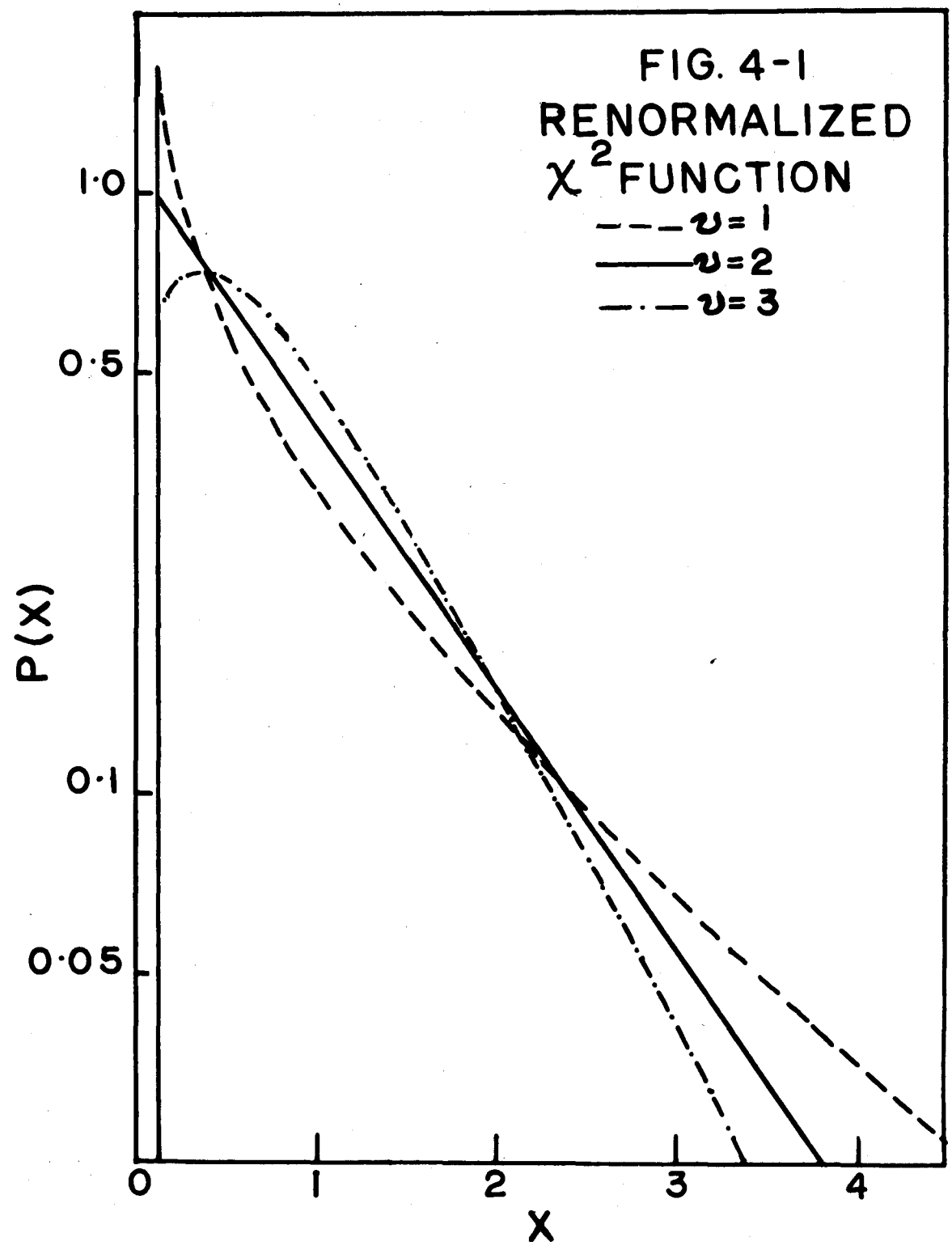
FIG. 4-1
RENORMALIZED
χ^2 FUNCTION
$\upsilon = 1$
$\upsilon = 2$
$\upsilon = 3$
1·0
0·5
0·1
0·05
P(X)
0
1
2
3
4
X

which can be written as

$$a = \left[\frac{1}{M} \Sigma \Gamma_i' / E_i^n \right]^{1/n} \qquad (4\text{-}5)$$

and

$$\sum_{ij} (1 - \delta_{ij}) \ln(aE_i) \Gamma_j' / E_j^n = 0 \qquad (4\text{-}6)$$

The ML estimates are those values which simultaneously satisfy 4-5 and 4-6. For ease of notation the asterisk used previously to distinguish the ML estimates, has not been included here.

As can be appreciated from the forms of equations 4-5 and 4-6, the two-dimensional probability density function for the ML estimate (a,n) will be extremely hard to find. This means that one can not estimate errors in the usual way. As has been suggested earlier, the problem can be avoided by assuming that the sample is of sufficient size so that the ML estimates are unbiased and normally distributed. Since

$$E\left[\frac{\partial \ln L}{\partial a}\right] = -\frac{Mn}{a} + \frac{Mn}{a}$$

$$= 0$$

$$E\left[\frac{\partial \ln L}{\partial n}\right] = -M\ln(a) - \Sigma\ln(E_i) + M\ln(a) + \Sigma\ln(E_i)$$

$$= 0$$

the inverse of

$$R^2 = \begin{pmatrix} \frac{Mn}{a^2} & \frac{n}{a} \Sigma \ln(aE_i) \\ \frac{n}{a} \Sigma \ln(aE_i) & \Sigma \left[\ln(a E_i)\right]^2 \end{pmatrix}$$

can be used as an estimate of the variance-covariance matrix.

4.3 Level Density Analysis

The analysis of the level spacings used in this work is quite similar to the analysis of the level widths that was discussed in the previous section. In this case a model function of the form

$$\bar{S} = A \exp\left(-(BE)^N\right)$$

was used and ML estimates found for A, B and N. A value of N of 0.5 corresponds to a Fermi gas approximation and an N of 1.0 to the constant temperature model.

In order to find the ML estimates the spacing distribution must be known. As we have seen in Chapter 1, the theoretical distribution suggested by Wigner has been experimentally confirmed for levels above the neutron binding energy. Wigner suggested that the spacing between levels having the same angular momentum and parity is distributed according to the frequency function

$$P_1(S/\bar{S}) = \frac{1}{2}\pi\,(S/\bar{S}) \exp\left[-\frac{1}{4}\pi\,(S/\bar{S})^2\right]$$

The frequency function for levels with a range of angular momenta can be derived from the above distribution with the assumption that levels of different angular momenta are not correlated in position. Rosensweig and Porter[33] have performed such a calculation. The resulting frequency function is

$$P_1(X) = \left\{ \sum_J q_J^2 \frac{P_1(q_J X)}{D(q_J X)} + \left[\sum_J \frac{R(q_J X)}{D(q_J X)}\right]^2 - \sum_J \left[q_J \frac{R(q_J X)}{D(q_J X)}\right]^2 \right\} \prod_k D(q_k X) \qquad (4\text{-}7)$$

where

$$X = S/\bar{S}$$

$$q_j = N\,(2J + 1)\exp(-J(J+1)/2\sigma^2)$$

$$N = 1/\sum_J q_j$$

$$R(X) = \exp\left(-\frac{1}{4}\pi X^2\right)$$

$$D(X) = 1 - \sqrt{2/\pi}\int_0^{X\sqrt{\pi/2}} \exp(-y^2/2)\,dy$$

In the limit of an infinite number of different angular momenta the frequency function becomes

$$P_T(X) = \exp(-X)$$

As with analysis of the partial radiative widths discussed in the previous section, the detector has a nonzero threshold associated, in this case, with the measurement of level spacings. This arises from the finite energy resolution of the spectrometer. Again, this can be approximately corrected for by using the frequency function

$$P(X) = 0 \qquad X < R/\bar{S}$$

$$= P_T(X) \qquad X \geq R/\bar{S}$$

This assumes that doublets in the spectrum separated by any energy less than R are observed as single peaks while those with a separation energy greater than or equal to R are recognized. The effect of the relative intensity of the two peaks and the counting statistics obtained for the doublet has been ignored in this approximation.

Equation 4-7 has been evaluated using typical value for the parameter σ and the range of angular momenta that are populated in the (n,γ) reactions studied in this work. The results are presented in Fig. 4-2. The curve with $\sigma = 3$ corresponds to the frequency function of the level spacings expected for the $^{55}Mn(n,\gamma)^{56}Mn$ reaction †

† The value of the spin-dependence parameter used here corresponds to those calculated by Gilbert and Cameron [29].

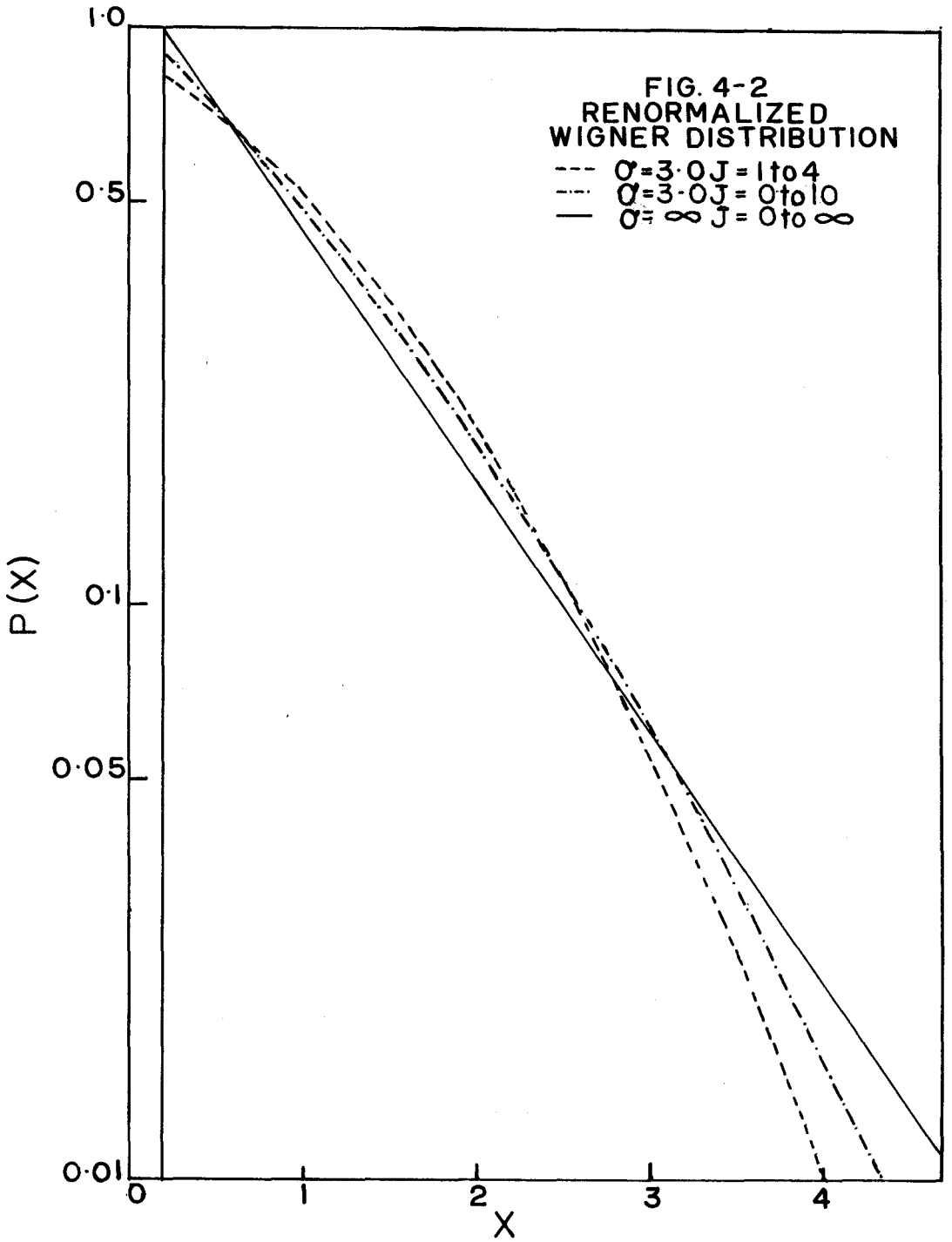
FIG. 4-2
RENORMALIZED
WIGNER DISTRIBUTION
--- σ=3·0 J = 1 to 4
-·-·- σ=3·0 J = 0 to 10
— σ= ∞ J = 0 to ∞
1·0
0·5
0·1
0·05
0·01
P(X)
0
1
2
3
4
X

The resolution correction used corresponds to R = 7 keV and an excitation energy in ^{56}MN of 2 MeV. The effect of varying σ and the allowed values of J are also presented along with the limiting case

$$P_T(X) = \exp(-X)$$

Because of the uncertainty in the value of σ and the range in J to be used, it was felt that the frequency function could be approximated by the limiting case to a sufficiently high degree of accuracy. This approximation permits fairly simple analytical expressions to be derived for the ML estimators and also allows corrections to be made for missed levels due to γ-ray intensity fluctuations.

The effect of nonzero intensity threshold of the spectrometer can be seen by defining $P_>$ as the probability of observing a γ ray with an intensity greater than or equal to the threshold, T. Using the results of section 4-2 $P_>$ can be written explicitly as

$$P_> = \int_0^{T/(aE)^n} \exp(-Y)dY \qquad (4\text{-}8)$$

The probability of observing a spacing, S, is given by

$$P_o(X)dX = \sum_{i=1} P_>(1-P_>)^{i-1} P_i(X)dX \qquad (4\text{-}9)$$

where $X = S/\bar{S}$ and S is the probability of finding i spacings in an energy interval S. The physical interpretation of each term in the above sum is shown in Figure 4-3. Since $P_1(X) = \exp(-X)$ it follows that $P_i(X)$ is a Poisson distribution of order (i-1), that is

$$P_i(X) = \frac{(X)^{i-1}}{(i-1)!} \exp(-X)$$

FIG. 4-3
PHYSICAL INTERPRETATION
OF EQUATION 4-9

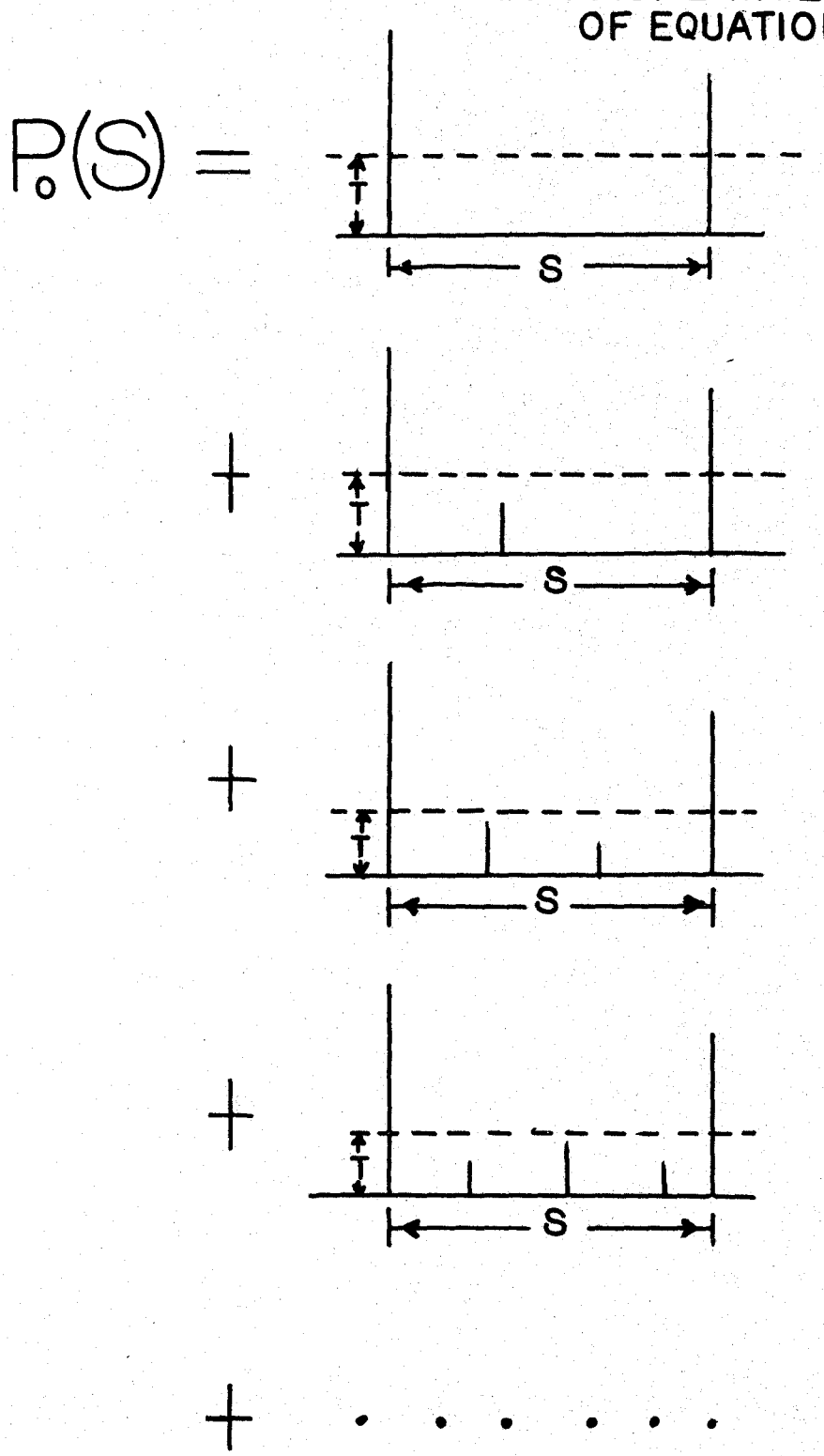

Equation 4-9 can then be written

$$P_o(X)dX = P_> \exp(-X)dX \sum_i \left[(1-P_>) X\right]^{i-1}/(i-1)!$$

$$= P_> \exp(-X)dX \exp\left[(1-P_>)X\right]$$

$$= P_> \exp(-P_> X)dX$$

We see then, that the effect of the loss of peaks in the spectrum because of the statistical uncertainty in the underlying continuum is to increase the observed average spacing by the factor $1/P_>$ where $P_>$ is given by equation 4-8. Values of the parameters a and n can be obtained by the method of analysing the γ-ray intensities discussed in section 4-2.

If the approximate corrections for the nonzero counter resolution is also included, the observed frequency function for the nearest neighbour spacings is given by

$$P_o(X') = \exp(-X')$$

where

$$X' = (S - R)P_> / \bar{S}$$

The LF can be written as

$$L(A,B,N) = \prod(1/\bar{S}_i) \exp(-S_i'/\bar{S}_i) \qquad (4\text{-}10)$$

where

$$S_i' = (S_i - R)P_{>i}$$

and

$$\bar{S} = A \exp(-(BE_i)^N)$$

Hence

$$\ell nL(A,B,N) = - M\ell n(A) \sum_{i=1}^{M} (BE_i)^N$$

$$- \sum_{i=1}^{M} (S_i'/A) \exp (BE_i)^N \qquad (4\text{-}11)$$

Maximization of the natural logarithm of the LF with respect to A, B and N leads to the following

$$E\left[\frac{\partial \ell nL}{\partial A}\right] = 0$$

Similarly it can be shown that

$$E\left[\frac{\partial \ell nL}{\partial B}\right] = 0$$

and

$$E\left[\frac{\partial \ell nL}{\partial N}\right] = 0$$

Hence in the limit of an infinite sample size the inverse of the dispersion matrix is given by equations 4-3 and 4-4. Analytical expressions for the matrix elements can be easily evaluated. For example

$$R_{11}^2 = - E\left[\frac{\partial^2 \ell nL}{\partial A^2}\right]$$

$$= - \prod_i \int_0^\infty \left[\frac{M}{A^2} - \frac{2}{A^2} \Sigma X_i\right] \exp(-X_i')dX_i'$$

$$= M/A^2$$

Similarly it can be shown that

$$R_{12}^2 = - \frac{N}{AB} \Sigma(BE_i)^N$$

$$R_{13}^2 = - \frac{1}{A} \Sigma(BE_i)^N \ell n(BE_i)$$

$$R_{22}^2 = \frac{N^2}{B^2} \Sigma (BE_i)^{2N} \ell n (BE_i)$$

$$R_{23}^2 = \frac{N}{B} \Sigma (BE_i)^{2N} \ell n (BE_i)$$

$$R_{33}^2 = \Sigma \left[(BE_i)^N \ell n (BE_i)\right]^2$$

For all the nucleides studied in this work, information about the level densities at the neutron binding energy exists. This information is obtained from the measurements of the total neutron cross section in the resonance region. Since, in this region, the energy of the incident neutrons is low, only s-wave resonances are normally observed. As a result, the observed average spacing, S_R, obtained from these experiments, is that associated with levels of the same parity as the ground state of the target nucleus, π_T, and with angular momenta in the range $J_1 \leq J_R \leq J_2$ where

$$J_1 = |J_T - 1/2| \qquad (4\text{-}12)$$

$$J_2 = J_T + 1/2 \qquad (4\text{-}13)$$

and J_T is the angular momentum of the ground state of the target nucleus.

Under the assumption that only E1 radiation is emitted from the capture state , the levels that are populated, in this case, have parity $-\pi_T$ and angular momenta in the range J_3 to J_4 where

$$J_3 = J_T - 3/2 \quad \text{for } J_T \geq 3/2 \qquad (4\text{-}14a)$$

$$= 0 \quad \text{otherwise} \qquad (4\text{-}14b)$$

and

$$J_4 = J_T + 3/2 \qquad (4\text{-}15)$$

Using the statistical model, the average spacing between levels at the neutron binding energy with this parity and range of angular momenta can be calculated from S_R, the observed average spacing. Since both parities are assumed to be equally probable, the desired spacing, S_R', is given by

$$S_R' = S_R \sum_{J_1}^{J_2} P(J) \Big/ \sum_{J_3}^{J_4} P(J)$$

where J_1, J_2, J_3 and J_4 are given by equations 4-12 through 4-15 and P(J) is given by equation 1-1. Using the spacing so obtained and the neutron binding energy, E_R, the values of the parameters A, B and N should be constrained so that

$$A \exp(-(BE_R)^N) = S_R' \qquad (4\text{-}16)$$

Since the level spacings are distributed quantities, S_R' has an associated uncertainty. Because of this, equation 4-16 is only true on the average and the constraint is better included in the LF. To do this we note that if

$$P(X) = \exp(-X)$$

then

$$P(X_R) = \frac{(X_R)^{M_R-1}}{(M_R-1)!} \exp(-X_R)$$

where

$$X_R = M_R S_R'/\bar{S}_R$$

and M_R is the number of observed spacings in the resonance region. The average spacing in the resonance region $\bar{S}_R$ is given by

$$\bar{S}_R = A \exp(-(BE_R)^N)$$

The resulting LF, which includes estimates of the level spacings from the radiative capture experiment and the total cross section measurements, is then

$$L_c(A,B,N) = L(A,B,N)\, P(X_R)\, M_R/\bar{S}_R$$

where L(A,B,N) is the unconstrained LF as given by equation 4-10. Neglecting terms that are not functions of A,B or N we can write

$$\ell nL_c(A,B,N) = -(M+M_R)\ell n(A) + \sum_{i=1}^{M} (BE_i)^N + M_R(BE_R)^N -$$

$$\sum_{i=1}^{M} (S_i'/A)\exp(BE_i)^N + M_R(S_R'/A_R)\exp(BE_R)^N$$

$$= M_T\ \ell n(A) + \Sigma\ (BE_i)^N + \Sigma(S_i'/A)\exp(BE_i)^N \qquad (4\text{-}17)$$

where M_T is the total number of observed spacings in both experiments and the sums in equation 4-17 run from 1 to M_T with $E_i = E_R$ and $S_i' = S_R'$ for $i > M$, where M is, as before, the number of spacings observed in the thermal neutron capture work. Comparison of equation 4-17 with 4-11 shows that the equations that give the ML estimates which were derived from equation 4-11 still apply, provided M is replaced by M_T and we define $E_i = E_R$ and $S_i' = S_R'$ for $i > M$.

It should be noted in passing that no corrections have been made for missed levels in the resonance data. In practice the energy range used was limited to the region where the number of missed levels due to resolution effects is negligible. The procedure used is that suggested by Gilbert and Cameron[29]. It consists of plotting the number of resonances below an energy E against E. Since the average spacing is constant in this region, a straight line plot results up to the region where levels are missed. The average spacing obtained in the linear region was then used for S_R.

4.4 Results

In discussing the results of the analysis of the data, one particular case, the $^{55}Mn(n,\gamma)^{56}Mn$ reaction, will be considered in detail. Since the analysis of the data for the other nucleides is

essentially the same, only a brief discussion for these cases will be presented. The energies and intensities of the radiations that were observed for all the nucleides are presented in the Appendix. The errors associated with the γ-ray energies are approximately ± 3 keV while the relative intensities have an associated error of about 20%.

The data for the $^{55}Mn(n,\gamma)^{56}Mn$ reaction were obtained as part of an extensive study of thermal neutron capture γ-ray spectra. Detailed results have been published by Hughes, Kennett and Prestwich[77]. The pertinent part of the high-energy spectrum for this reaction is shown in Figure 4-4. This spectrum was accumulated over a 16 hr period using two window settings of the biased amplifier. The sample consisted of approximately 2 gms of 99.9% pure manganese metal sealed in a polyethylene capsule. Using the methods described in Chapter 3, this spectrum was analysed to obtain the energies and relative intensities of some sixty-three γ rays.

Since the spin and parity of the ground state of ^{55}Mn is $5/2^-$, s-wave neutron capture will populate states with spins and parity 2^- and 3^-. The polarization measurements of Bernstein et al[78] suggest that the contribution to the thermal neutron cross section from both spin states is nearly equal. Hence, assuming that E1 radiation predominates in the γ decay of the capture state, levels with spins and parity 1^+, 2^+, 3^+ and 4^+ will be populated.

Since the spin and parity of the ground state of ^{56}Mn is 3^+ the ground state transition should be observed. The levels at 30 keV and 110 keV have also been assigned spins and parity 2^+ and 1^+ respectively, so that E1 transitions are also allowed from the

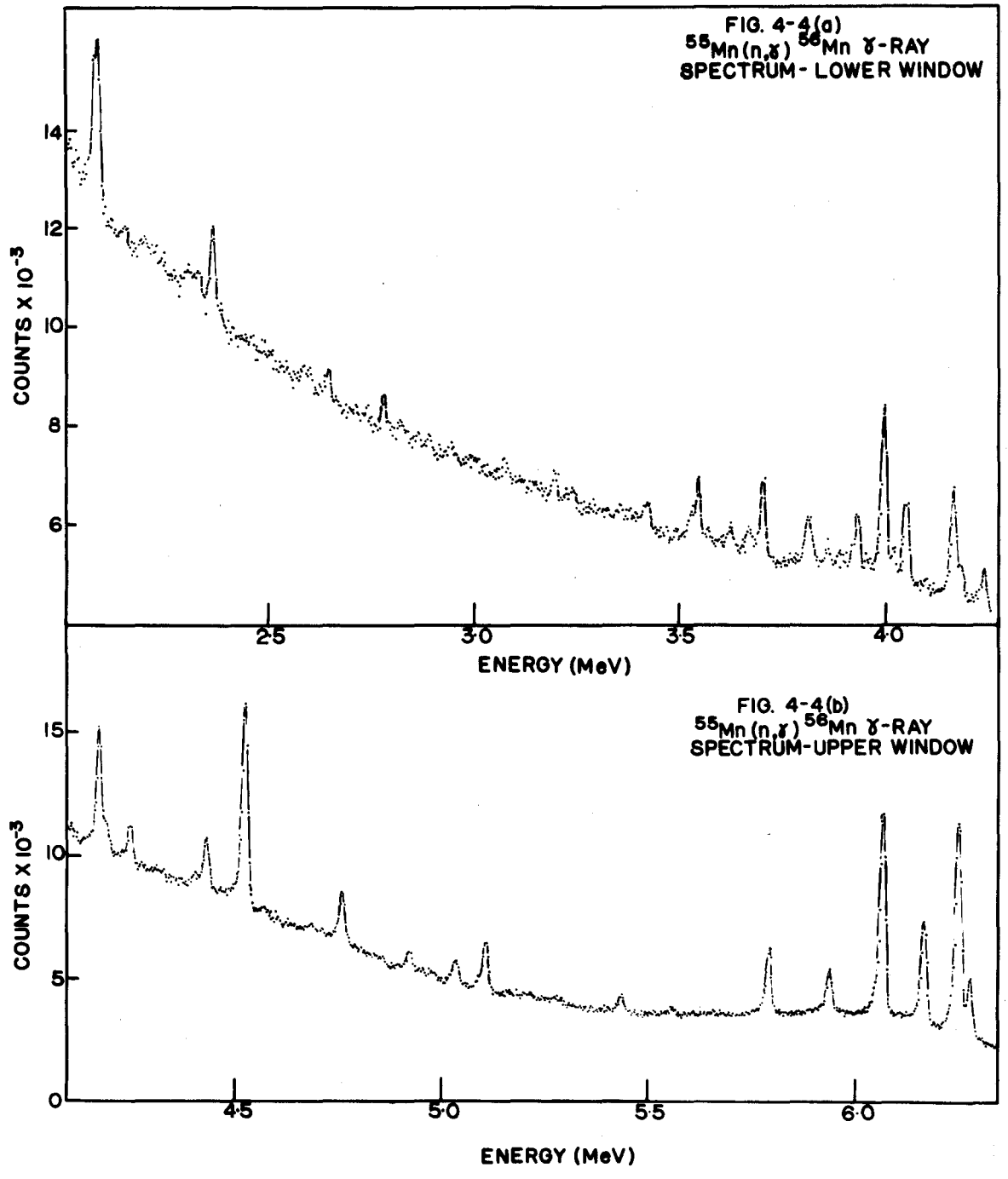
FIG. 4-4(a)
55Mn(n,γ) 56Mn γ-RAY
SPECTRUM - LOWER WINDOW
COUNTS X 10-3
14
12
10
8
6
2·5
3·0
3·5
4·0
ENERGY (MeV)
FIG. 4-4(b)
55Mn(n,γ) 56Mn γ-RAY
SPECTRUM-UPPER WINDOW
COUNTS X 10-3
15
10
5
0
4·5
5·0
5·5
6·0
ENERGY (MeV)

capture state to these levels. The separation between the three highest energy γ rays are consistent with the assumption that they correspond to transitions from the capture state to the three levels in question. On this basis, the highest energy γ ray seen is the ground state transition, which leads to a neutron separation energy of 7272 ± 3 keV for ^{56}Mn. This assignment has been confirmed by NaI(Tl)-NaI(Tl) and NaI(Tl)-Ge(Li) coincidence studies, and is also consistent with the value of 7277 ± 5 keV† obtained by Green et al[79] from the ^{55}Mn(d,p)^{56}Mn reaction.

Unfortunately, the angular distribution studies for the ^{55}Mn(d,p)^{56}Mn reaction reported by Dalton et al[81], were performed with poorer resolution than that obtained by Green et al[79]. Hence, while the decays to some forty-five levels seen by the latter authors can be found, only seven of these levels can be identified as states with $\ell_n = 1$. Since these states can be populated from the capture state by E1 radiation, the γ-ray intensities to these states can be unambiguously interpreted.

The energies of the seven transitions to the states with ℓ_n are given in Table 4-1, along with their relative intensities. Also shown are the reduced intensities calculated for the two cases where the transition probability is assumed to be proportional to E^3 and to E^5. The values of the parameter a were chosen so that the first moments are unity. In both cases, the reduced intensities have

---

† This energy has been adjusted to account for the more recent ^{210}Po α-ray as has been suggested by Sperduto and Buechner[80].

TABLE 4-1

Transitions to levels with $\ell_n = 1$

Energy (keV)	Relative Intensity	$\frac{I_{REL}}{(aE)^3}$	$\frac{I_{REL}}{(aE)^5}$
7161	1162	1.58	1.43
7059	2297	3.27	3.06
6932	456	0.69	0.67
6430	154	0.29	0.31
6105	389	0.86	1.07
6019	83	0.19	0.25
5631	48	0.13	0.20

rather large fluctuations. The sample variances are 1.20 for an assumed E^3 dependence and 1.03 for an assumed E^5 dependence. Since the variance of a χ^2 distribution is given by $2/\nu$, where ν is the number of degrees of freedom, the data are consistent, in both cases, with an exponential distribution for the intensities. When such large fluctuations are observed for E1 transitions, M1 or higher order transitions are clearly impossible to distinguish by their transition probabilities.

For the analysis of the intensities, only transitions observed in the upper one third of the spectrum were used. In this region it was felt that all the transitions that were observed were from the capture state. Figure 4-5 shows the γ-ray intensities as as a function of energy. Each point was obtained by averaging the intensity observed in a 500 keV interval. The errors shown were calculated by assuming that the intensities have an exponential distribution. The results of the threshold correction are also shown. The ML analysis of these data gave a value of $n = 3.37 \pm 0.40$ and a value of $a = 1.01 \pm 0.67$ MeV^{-1}, where $\bar{I} = (aE)^n$. The curve in Figure 4-5 was calculated using these estimates.

ML estimates for n and a were also obtained using all sixty-three γ rays, in order to observe the effect of selecting intensities from only the upper one third of the spectrum. The values of $n = 3.98 \pm 0.80$ and $a = 0.76 \pm 0.21$ MeV^{-1} so obtained, indicate that the results are relatively insensitive to the range that is used. This suggests that the majority of the γ rays that are observed in the upper one half of the spectrum are direct transitions from the capture state.

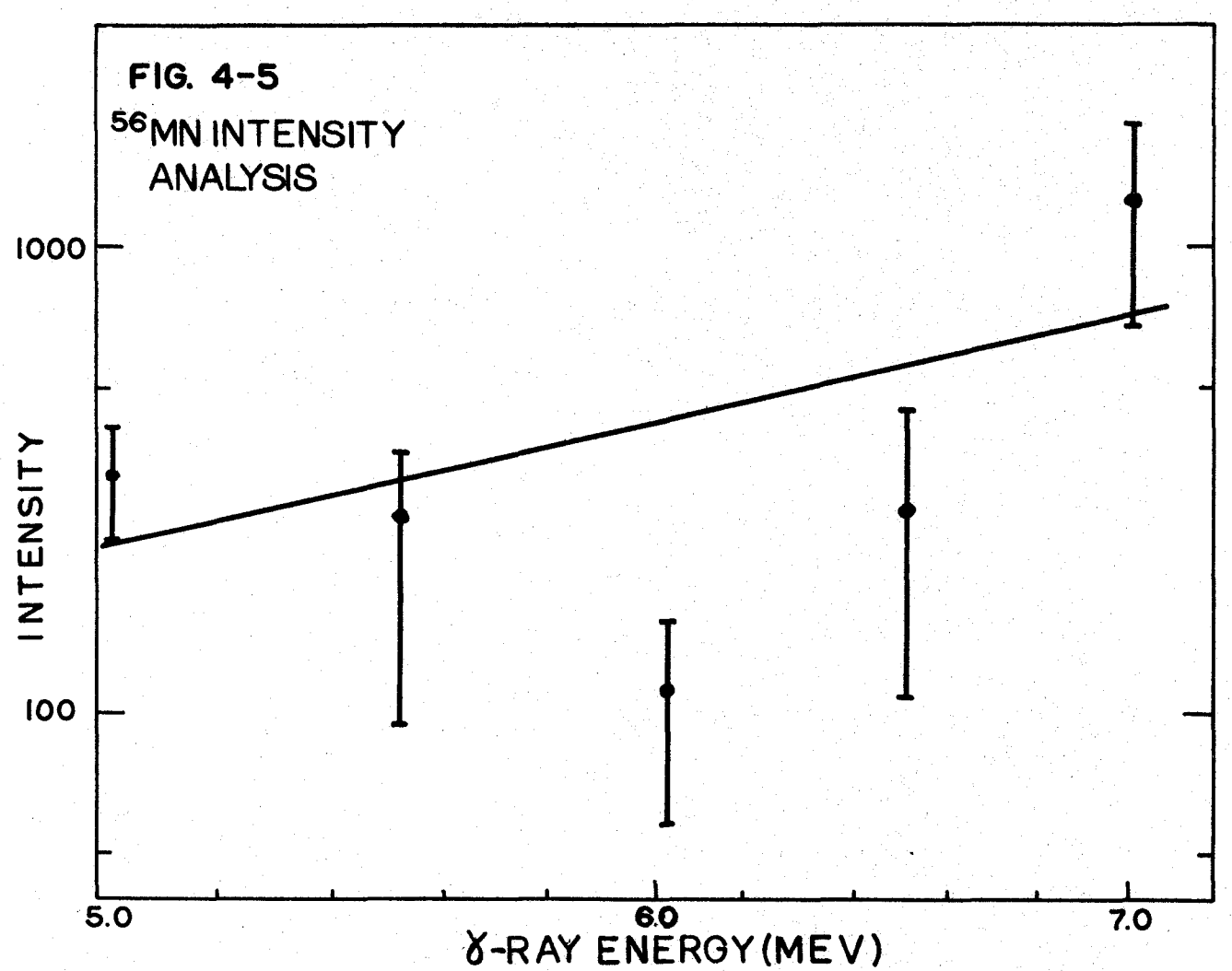
FIG. 4-5
56MN INTENSITY
ANALYSIS
1000
100
INTENSITY
5.0
6.0
7.0
γ-RAY ENERGY (MEV)

For the spacing analysis, the value of 2630 eV was used for the average spacing of 2^- and 3^- levels at the neutron binding energy. This value was obtained using the first 30 resonances reported by Garg et al[82]. The correction to the appropriate spin range was made using a spin-dependence parameter of 3.1, the value calculated by Gilbert and Cameron[29] for ^{56}Mn. Again only the upper one third of the spectrum was considered in the ML analysis. Using the model function $\bar{S} = A \exp(-(BE)^N)$, the estimates that were obtained are $A = 0.15 \pm 0.08$ MeV, $B = 0.76 \pm 0.42$ MeV^{-1} and $N = 0.93 \pm 0.24$. These data along with the fitted function are shown in Figure 4-6. Again, the sensitivity of the estimates to the region of the spectrum that was used, was observed by estimating the parameters using all sixty-three observed transitions. The results are $A = 0.16 \pm 0.08$ MeV, $B = 0.83 \pm 0.41$ MeV^{-1} and $N = 0.89 \pm 0.20$. As with the analysis of the intensities, the changes are much less than the statistical errors of the estimates.

The results for the ^{59}Co(n,γ)^{60}Co reaction have been published by Prestwich, Kennett and Hughes[83]. Since the ground state of ^{59}Co is $7/2^-$ and that of ^{60}Co is 5^+, the states with $J = 4^-$ that result from the capture of s-wave neutrons can decay to the ground state by the emission of E1 radiation. By assuming that the 7494 keV γ ray is the ground state transition, the excitation energies given in the Appendix were calculated. This assignment agrees with the ^{59}Co(d,p)^{60}Co results of Enge et al[84]. The fitting of the intensities to the function $\bar{I} = (aE)^n$ for gamma rays populating

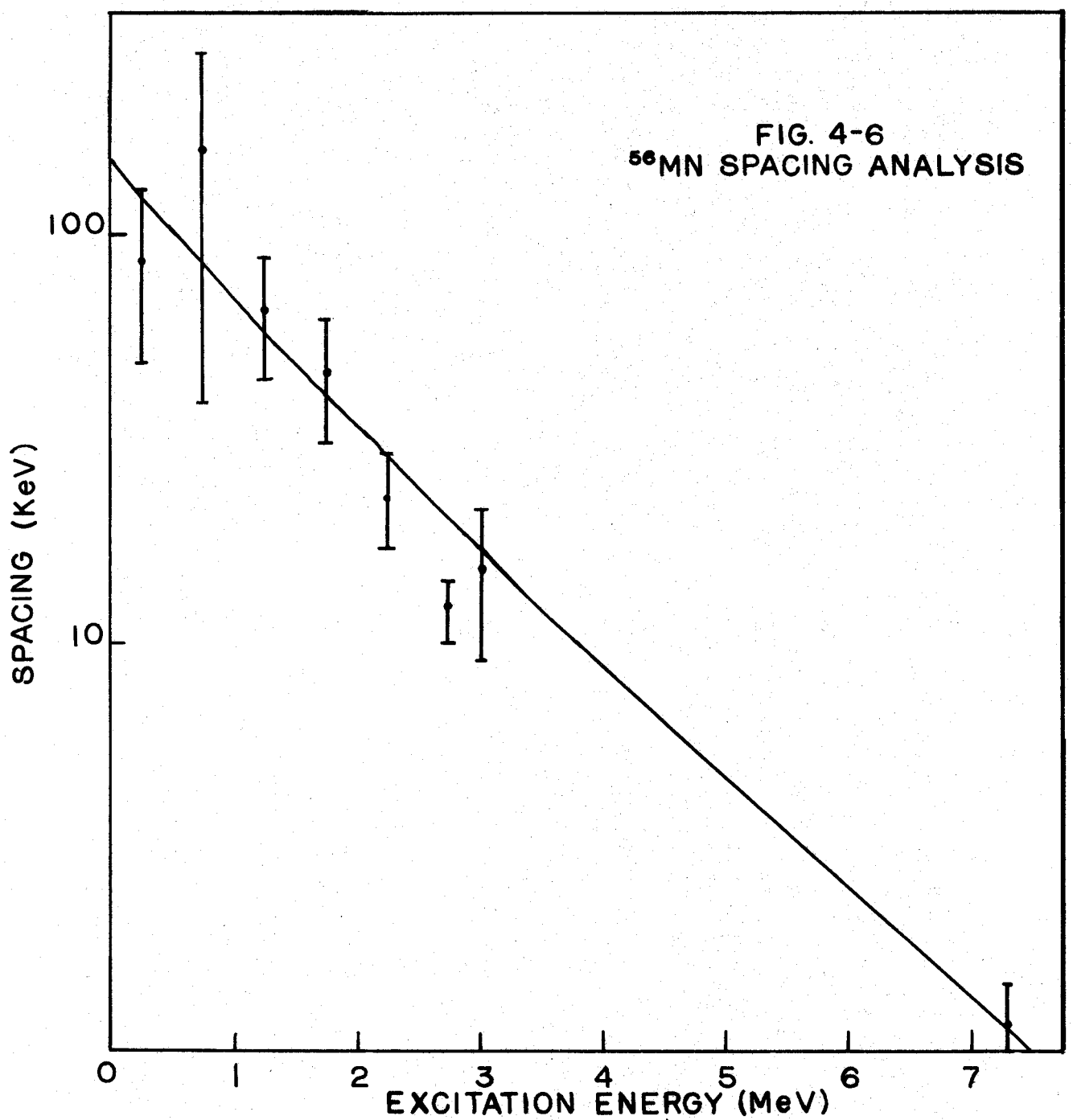
FIG. 4-6
56MN SPACING ANALYSIS
100
10
SPACING (KeV)
0
1
2
3
4
5
6
7
EXCITATION ENERGY (MeV)

levels in the region 0 to 5 MeV above the ground state, resulted in the values 0.56 ± 0.13 MeV^{-1} and 5.7 ± 1.3 for a and n respectively. For the level density analysis, the spacing for s-wave neutron resonance of 1280 eV was used. This value was obtained from the first twenty resonances observed by Garg et al[82]. The value of the spin-dependence parameter that was used was 3.2[29]. The result of fitting the data in the region of 0 to 5 MeV to the model function $\bar{S} = A \exp(-(BE)^N)$ leads to the estimates $A = 0.21 \pm 0.13$ MeV, $B = 0.98 \pm 0.64$ MeV^{-1} and $N = 0.87 \pm 0.23$.

The analysis of the $^{75}As(n,\gamma)^{76}As$ data resulted in the determination of the energies and intensities for seventy-one γ rays. Since the ground state of ^{75}As is $3/2^-$, the capture states are 1^- or 2^-. Hence, since the ground state of ^{76}As is 2^-, the multipolarity of the ground state transition must be M1 or higher. A detailed analysis of these data along with NaI(Tl)-Ge(Li) and Ge(Li)-Ge(Li) coincidence measurements performed by Johnson and Kennett[85], indicates that the highest energy γ ray observed populates a level at 43 keV. This assignment leads to a neutron separation energy of 7329 ± 3 keV which was used in this analysis. The analysis of the transition probabilities using all seventy-one γ rays resulted in the values $a = 0.97 \pm 0.69$ MeV^{-1} and $n = 2.5 \pm 1.0$ where, as before, $\bar{I} = (aE)^n$. For the spacing analysis, the average spacing that was used for s-wave neutron resonances was 76.5 eV, obtained from the first forty resonances observed by Garg et al[86]. The value for the spin-dependence parameter that was used was 3.9[29]. The ML estimates for A, B and N are 0.032 ± 0.008 MeV, 0.38 ± 0.09 MeV^{-1} and 1.8 ± 0.4 respectively, where $\bar{S} = A \exp(-(BE)^N)$.

The data that were obtained from the $^{103}Rh(n,\gamma)^{104}Rh$ reaction revealed the presence of sixty-nine γ rays with energies between 4.4 and 7.0 MeV. The results of this analysis have been published by Hughes, Kennett and Prestwich[87]. Since the ground state spin and parity of ^{103}Rh is $1/2^-$ while that of ^{104}Rh is 1^+, the ground state transition should be observed. The assignment of the 6999 keV transition as the ground state transition leads to the excitation energies shown in the Appendix. The analysis of intensities using the model function $\bar{I} = (aE)^n$ resulted in ML estimates of a and n equal to 0.036 ± 0.035 MeV^{-1} and 0.7 ± 1.2. The value used in the level density analysis for the s-wave neutron spacing was 32.1 eV obtained from the fifteen lowest energy s-wave resonances observed by Ribon and Michaudon[88]. Since the resonance parameters for the 1.257 eV resonance[89] indicate that the thermal neutron cross section is almost entirely due to this resonance, the capture state was assumed to have J = 1, the value reported by Brockhouse[90] for the resonance in question. The value of the spin-dependence parameter used was 4.5[29]. The analysis using the model function $\bar{S} = A \exp(-(BE)^N)$ resulted in the estimates $A = 0.065 \pm 0.024$ MeV, $B = 0.63 \pm 0.17$ MeV^{-1} and $N = 1.4 \pm 0.2$.

The study of the $^{127}I(n,\gamma)^{128}I$ reaction lead to the observation of fifty-three γ rays in the region of 5 to 7 MeV. In this case the capture of s-wave neutrons leads to states with positive parity and a spin of either 2 or 3. Since the ground state of ^{128}I is 1^+, the lowest order multipole for the ground state transition is M1. A detailed examination of these data, along with the analysis of the

of the spectrum in the low energy region and coincidence studies using NaI(Tl) and Ge(Li) detectors has been published by Archer et al[75]. These studies indicate that the 6694 keV γ ray populates a level at 132 keV. The resulting separation energy is 6826 ± 3 keV. The analysis of the intensities in the region of 5 to 7 MeV, assuming that the average intensity is of the form $\bar{I} = (aE)^n$, gave ML estimates for a and n of 0.056 ± 0.025 MeV^{-1} and - 3.5 ± 1.4, respectively. For the analysis of the level density, an average s-wave resonance spacing of 13.4 eV was used which was obtained using the first twenty resonances observed by Desjardins et al[91]. A spin-dependence parameter of 4.85[29] was used for these calculations. The results of the ML analysis of the spacings using an average spacing of the form $\bar{S} = A \exp(-(BE)^N)$ are A = 0.028 ± 0.006 MeV, B = 0.38 ± 0.01 and N = 2.2 ± 0.7.

The capture of s-wave neutrons in ^{133}Cs leads to states in ^{134}Cs with spin and parity 3^+ and 4^+. Since the ground state of ^{134}Cs is 4^+, the lowest multipole radiation required for the direct population of the ground state from the capture state is M1. The coincidence studies reported by Archer et al[75] indicate that the highest energy γ ray seen, that at 6714 keV, populates a level at 116 keV which leads to a neutron separation energy of 6830 ± 3 keV. When the usual form for the average intensity was used, that is $\bar{I} = (aE)^n$, the value of n that was obtained was - 0.06 ± 1.00. Assuming that the average intensity is independent of energy leads to the ML estimate of a = 144 ± 19 where a = $\bar{I}$. For the level density analysis, an average spacing for s-wave neutron resonances of 21.7 eV was obtained using the first eleven resonances reported by Harvey

et al[92] The value of the spin dependence parameter used was 4.9[78]. Fitting the spacings to the form $\bar{S} = A \exp(-(BE)^N)$ leads to the ML estimates A = 0.037 ± 0.008 MeV, B = 0.39 ± 0.08 MeV^{-1} and N = 2.1 ± 0.1.

The analysis of the spectrum for the $^{139}La(n,\gamma)^{140}La$ reaction resulted in fifty-three γ rays being observed in the region 3 to 5.2 MeV. These results have been published by Hughes, Kennett and Prestwich[93]. In this case, the ground state can be directly populated from the capture state by the emission of El radiation, since the ground state of ^{139}La is $7/2^+$ while that of ^{140}La is 3^-. Assuming that the highest energy transition that was observed is the ground state transition, a neutron separation energy of 5165 ± 3 keV is obtained for ^{140}La. Analysis of the γ-ray intensities observed in the upper one third of the spectrum resulted in the estimate a = 0.19 ± 0.03 MeV and n = 1.7 ± 0.4 where $\bar{I} = (aE)^n$. The analysis of the level spacings using the model function $\bar{S} = A \exp(-(BE)^N)$ resulted in ML estimates for A, B and N of 0.031 ± 0.007 MeV, 0.37 ± 0.14 and 2.7 ± 1.5. For these estimates, an average spacing for s-wave neutron resonances of 236 eV was used. This value was calculated using the resonances 2 through 9 reported by Bianchi et al[94]. The value of the spin-dependence parameter used was 4.75, the value calculated by Gilbert and Cameron[29] from the resonance data of ^{141}Pr. Because of the relatively poor nature of the resonance data for this nucleide, the analysis was performed as if the resonance data were obtained from only two resonances.

The results of the study of the $^{141}Pr(n,\gamma)^{142}Pr$ reaction have been published along with the $^{139}La(n,\gamma)^{140}La$ study[93]. For this reaction, thirty-eight γ rays between 4 and 6 MeV have been observed. The analysis of the intensities in this region, again using the model function $\bar{I} = (aE)^n$ resulted in the estimates $a = 3.4 \pm 0.5$ MeV^{-1} and $n = 3.4 \pm 1.5$. As with the $^{139}La(n,\gamma)^{140}La$ reaction, the spins and parities of the ground states of ^{141}Pr ($5/2^+$) and ^{142}Pr (2^-) allow the ground state and the states formed by s-wave neutron capture to be connected by E1 radiation. The deduced value for the neutron separation energy of ^{142}Pr, assuming that the highest energy γ ray seen is the ground state transition, is 5844 ± 3 keV. The average spacing for s-wave resonances that was used was 65.3 eV which was obtained using the first twenty-one resonances reported by Willard[95]. The spin range was corrected using a spin-dependence parameter of 4.75[29]. The results of the level density analysis are $A = 0.057 \pm 0.019$ MeV, $B = 0.62 \pm 0.19$ MeV^{-1} and $N = 2.0 \pm 0.3$.

For the $^{197}Au(n,\gamma)^{198}Au$ reaction, eighty γ rays in the region 4 to 6.5 MeV have been observed. These data have been published by Johnson et al[74]. The average γ-ray intensity in this region, when fitted to the function $I = (aE)^n$ resulted in the estimates $a = 0.65 \pm 0.18$ MeV^{-1} and $n = 3.8 \pm 0.9$. For the spacing analysis, the value for the neutron separation energy that was used was 6513 ± 3 keV, which was obtained by assuming that the highest energy γ ray that was observed corresponds to the ground state transition. This assignment is supported by the study of the low energy cascades[74]

and the fact that the ground state of ^{198}Au ($J = 2^-$) can be reached by the emission of E1 radiation from both spin states that are possible for the capture state ($J = 1^+$ and 2^+). The value for the spacing of $J = 1^+$ and 2^+ levels at the neutron binding energy that was used was 16.9 eV which was obtained using the first thirty resonances reported by Desjardins et al[96]. This was corrected to the range of spins that would be observed for E1 radiation if the capture state was entirely due to the $J = 2$ resonance of 4.9 eV. The values of the parameters that were obtained are $A = 0.035 \pm 0.008$ MeV, $B = 0.45 \pm 0.08$ MeV^{-1} and $N = 1.99 \pm 0.3$ where the average spacing $\bar{S} = A \exp(-(BE)^N)$.

The study of the γ-ray spectrum of $^{203}Tl(n,\gamma)^{204}Tl$ in the region 4.2 to 6.5 MeV resulted in the observation of forty-five γ rays. The results have been published by Prestwich et al[73]. The analysis of the intensities in this region gave ML estimates for the parameters a and n of 2.5 ± 0.7 and 2.3 ± 1.2 respectively. The results of NaI(Tl)-Ge(Li) coincidence studies indicate that the highest energy transition that was observed populates a level at 138 keV[73]. This leads to a neutron separation energy of 6654 ± 4 keV which was used to calculate the excitation energy used for the level density analysis. It is interesting to note that the ground state of ^{204}Tl ($J=2^-$) should be populated by the emission of E1 radiation from the 1^+ capture state according to the selection rules. This again indicates that the distribution of gamma intensities is rather broad. A value of 390 eV was used for the

average spacing of s-wave neutrons. This was obtained using the first six resonances observed by Harvey[97]. The spin correction was made assuming that the $J = 1^+$ resonance dominates the thermal neutron capture as is suggested by the resonance parameters[98]. The spin-dependence parameter that was used was 5.5[29]. The result of fitting these data to an average spacing given by $\bar{S} = A \exp(-(BE)^N)$ are $A = 0.066 \pm 0.021$ MeV, $B = 0.41 \pm 0.11$ MeV^{-1} and $N = 2.0 \pm 0.5$.

CHAPTER V

DISCUSSION OF THE RESULTS

The results of the analysis for the ten isotopes that were given in Chapter IV are summarized in Table 5-1. In column one the product nucleus is designated and in column two the assumed spins and parity for the capture state are given. Column three gives the neutron separation energy for the product nucleus while column four shows the region of excitation in the product nucleus that was used in the analysis. In the next two columns the ML estimates for n, the power of the energy dependence of the average transition probability, and for N, the power of the energy dependence for the average level spacing, are given.

In Figure 5-1, the values of n, obtained for the different mass numbers, are shown. The two horizontal lines are the values of n predicted by the single particle estimate[10] and by the enhanced electric dipole estimate of Axel[11]. The trends in the data are quite similar to the trends in the s-wave neutron strength function[99] which peaks in the region of A~60, A~140 and A~180 and has a pronounced minimum for A~100. Since the value of n indicates the strength of the transitions to the region of the ground state relative to the strength of the transitions to the states at about 2.5 MeV, the data suggests that

TABLE 5-1

Summary of the Analysis of the γ-ray Intensities and the Level Spacings

Isotope	Jπ	E_R (keV)	ΔE (keV)	n	N
^{56}Mn	$2^-,3^-$	7272 ± 3	0-2500	3.4 ± 0.4	0.9 ± 0.2
^{60}Co	$3^-,4^-$	7494 ± 3	0-2500	5.7 ± 1.3	0.9 ± 0.2
^{76}As	$1^-,2^-$	7329 ± 3	0-2400	2.6 ± 1.0	1.5 ± 0.4
^{104}Rh	1^-	6999 ± 3	0-2400	0.7 ± 1.2	1.4 ± 0.2
^{128}I	$2^+,3^+$	6826 ± 3	0-1875	-3.5 ± 0.4	2.2 ± 0.7
^{134}Cs	$3^+,4^+$	6830 ± 3	0-2300	-0.06 ± 1.0	2.1 ± 0.4
^{140}La	$3^+,4^+$	5165 ± 3	0-1700	1.7 ± 1.3	2.7 ± 1.5
^{142}Pr	$2^+,3^+$	5844 ± 3	0-1685	3.4 ± 1.5	1.6 ± 0.4
^{198}Au	2^+	6513 ± 3	0-2460	3.8 ± 0.9	2.0 ± 0.3
^{204}Tl	1^+	6516 ± 3	0-2425	2.3 ± 1.2	2.0 ± 0.5

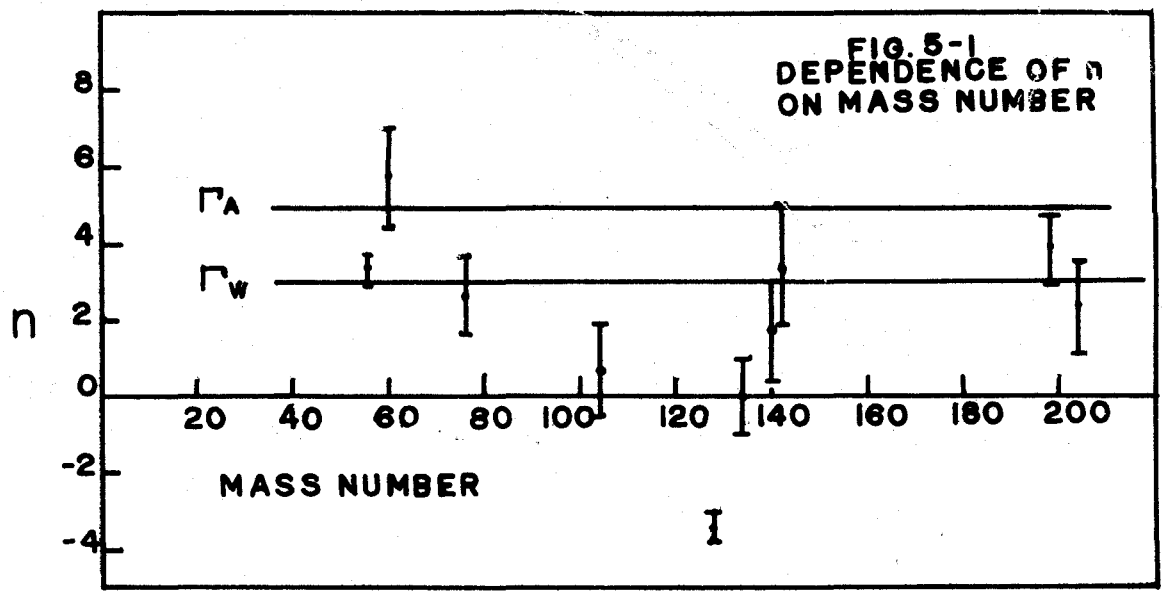
FIG. 5-1
DEPENDENCE OF n
ON MASS NUMBER
n
8
6
4
2
0
-2
-4
Γ_A
Γ_W
20
40
60
80
100
120
140
160
180
200
MASS NUMBER

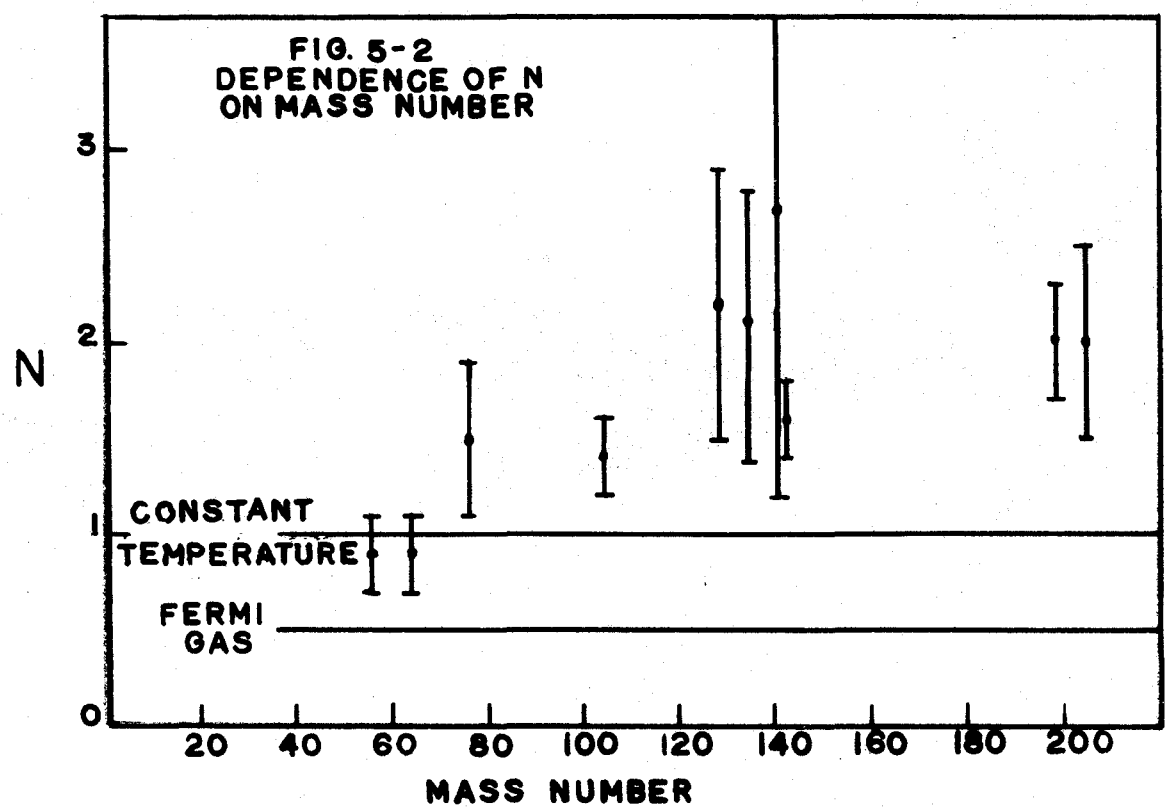
FIG. 5-2
DEPENDENCE OF N
ON MASS NUMBER
N
3
2
1
0
CONSTANT
TEMPERATURE
FERMI
GAS
20
40
60
80
100
120
140
160
180
200
MASS NUMBER

a positive correlation exists between the s-wave neutron strength function and the transition probability to the low lying states.

In the case of Co and Mn the transitions to the low lying levels are quite strong as indicated by the relatively high value of n. Since the shell model 2p neutron states are in the region of the ground state and the 3s neutron state is near the neutron binding energy, as is indicated by the peak in the s-wave neutron strength function in this region, a fairly large direct capture cross section can be expected. For the $^{59}Co(n,\gamma)^{60}Co$ reaction such a process has been invoked to explain the correlation between (d,p) stripping strengths and (n,γ) reduced partial widths to states with a large $\ell_n = 1$ component[83]. Wasson et al[100] have also observed interference between direct capture and resonance capture in the 132-eV resonance, for the ground state transition in the $^{59}Co(n,\gamma)^{60}Co$ reaction. The (n,γ) partial radiative reduced widths for ^{56}Mn also show a positive correlation with the (d,p) stripping strengths[77], although the result is not very precise because of small sample size that was used.

The values of the parameter n for transitions to levels in the region 0 to 2 MeV for ^{104}Rh, ^{128}I and ^{134}Cs are all below the value obtained from the single particle estimate for E1 radiation. The data for these nucleides are shown in Figure 5-3. The data points that are shown, were obtained by averaging the intensities over a 500 keV range. All these data show an increase in the intensity to states that are about 1 MeV above the ground state relative to the intensity to states near the ground state. The intensity to states above the region where the break

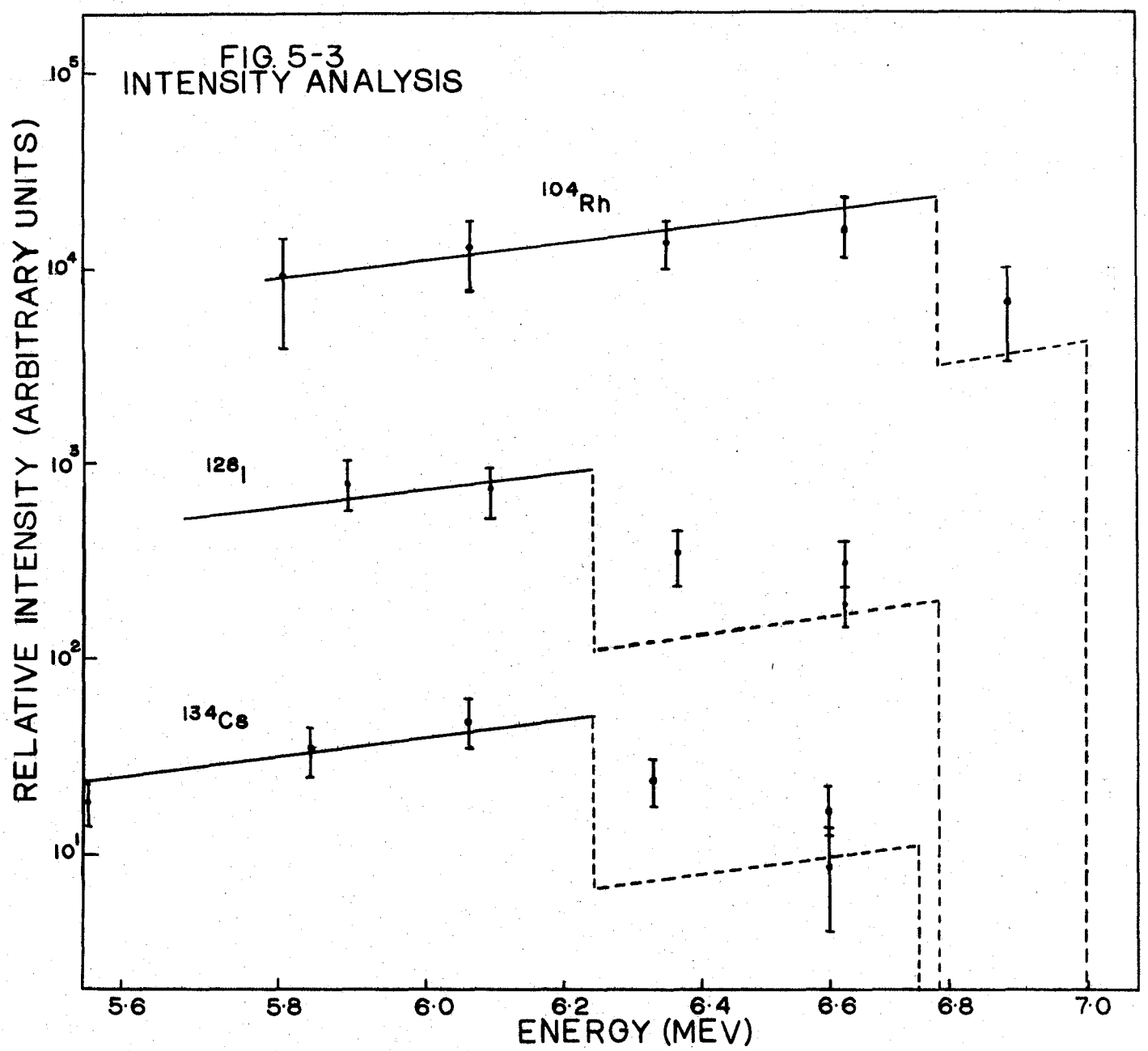
FIG. 5-3
INTENSITY ANALYSIS
RELATIVE INTENSITY (ARBITRARY UNITS)
10^5
10^4
10^3
10^2
10^1
^{104}Rh
^{126}I
^{134}Cs
5·6
5·8
6·0
6·2
6·4
6·6
6·8
7·0
ENERGY (MEV)

occurs are consistent with an E^3 dependence as is shown by the solid line. The dotted curve, which extends past the break, is lower than the solid line by the ratio of the M1 to E1 single particle estimates. In the case of ^{128}I and ^{139}Cs, two values are shown for the intensity to levels in the 0 to 500 keV range. The lower of the data points was obtained by excluding the two largest transitions to this region. These lower values, and the high energy transitions in ^{104}Rh are consistent with the assumption that the transitions to states in this region are mainly M1 in nature, while those above the break are E1 in nature. With this assumption, the low lying states in ^{104}Rh must be negative parity states and those in ^{128}I and ^{134}Cs must have positive parity. In the case of I and Cs, one can easily find shell model configurations which could give rise to these states. In the case of Rh the proton single particle p states that are in the region of the ground state, could give rise to the required negative parity states.

Ikegami and Emery[101] have postulated the existence of "doorway states" for the (n,γ) reaction in the $A\sim60$ mass region. Explicitly for the Fe isotopes, they suggest that these "doorway states" are the seniority-three, two-particle one-hole states that are obtained by coupling the extra nucleon to the seniority-two, particle-hole states of the even-even core. Ignoring the first 2^+ state, the lowest seniority-two configuration for the even-even system occurs in the region above about twice the energy of the first 2^+ state. This should correspond to the region where the lowest lying seniority-three states are found in the even-odd system.

Hence, according to these authors, the transition probabilities to states above about twice the energy of the 2^+ state in the even-even system, should be enhanced.

One could speculate that the increase in the partial radiative widths to levels above 1 MeV in Rh, I and Cs are the result of the reaction proceeding through "doorway states" similar to those postulated for the A~60 mass region. In these cases, the product nuclei are odd-odd configurations so that the states through which the reaction would be proceeding would be seniority-four, three-particle one-hole configurations. The energies of the first 2^+ states for the appropriate even-even systems are 475 keV, 665 keV and 673 keV, which should be correlated with the excitation energy at which the partial radiative width increases for Rh, I and Cs respectively. These latter energies are 750 keV, 1100 keV and 600 keV so that this interpretation is questionable. If the levels strongly populated in the (n,γ) reaction are weakly populated in the (d,p) reaction the postulation of such "doorway states" would be on much better grounds. Unfortunately good (d,p) data for these isotopes does not exist at present.

The results of the spacing analysis for the ten nucleides that were considered are shown in Figure 5-2. Again, the two predictions for the value of N are indicated by the two horizontal lines. There seems to be a general increase in the value of N with A. This, it is felt, is due to the inability of this analysis to fully correct for missed levels. The high values for N in the region of I and Cs result from the high density of levels near the ground state that are populated by M1 radiations, as has been discussed previously. In all ten cases the data favours an energy

dependence for the average spacing of the form

$$\bar{S}(E) = A \exp(-BE) \qquad (5\text{-}1)$$

over the $\sqrt{E}$ dependence of the Fermi gas model.

Assuming that the average spacing as a function of energy is given by equation 5-1 for levels above an excitation energy of 1 MeV, ML estimates have been obtained for the nuclear temperature $T = 1/B$. The values for the ten nucleides considered here are presented in Table 5-2. The values obtained for the nuclear temperature, for the different mass numbers are shown in Figure 5-4. The upper and lower limits of the empirically determined nuclear temperatures published by Gilbert and Cameron[29] are indicated by the two curves shown in this figure. The data obtained in this work follows the upper limit of this region quite well. The data show a general decrease in temperature with mass number.

The increase in the nuclear temperature near A=55 and A=200 is due to the closing of major shells for both neutrons and protons in these regions as was indicated by Gilbert and Cameron[29]. In the region A = 140 these data also show a slight increase due to the closing of the 82 neutron shell.

In conclusion we may state that the energy dependence of the partial radiative widths from states populated in thermal neutron capture, are consistent with the energy dependence of the single particle estimates for El radiation. There would seem to be little indication of an E^5 energy dependence that has been suggested by Axel[11]. The energy

TABLE 5-2

Estimates of the Nuclear Temperature

Isotope	Temperature
^{56}Mn	1.6 ± 0.2
^{60}Co	1.4 ± 0.1
^{76}As	0.93 ± 0.03
^{104}Rh	0.74 ± 0.03
^{128}I	0.66 ± 0.02
^{134}Cs	0.68 ± 0.03
^{140}La	0.90 ± 0.19
^{141}Pr	0.69 ± 0.03
^{198}Au	0.62 ± 0.02
^{204}Tl	0.78 ± 0.06

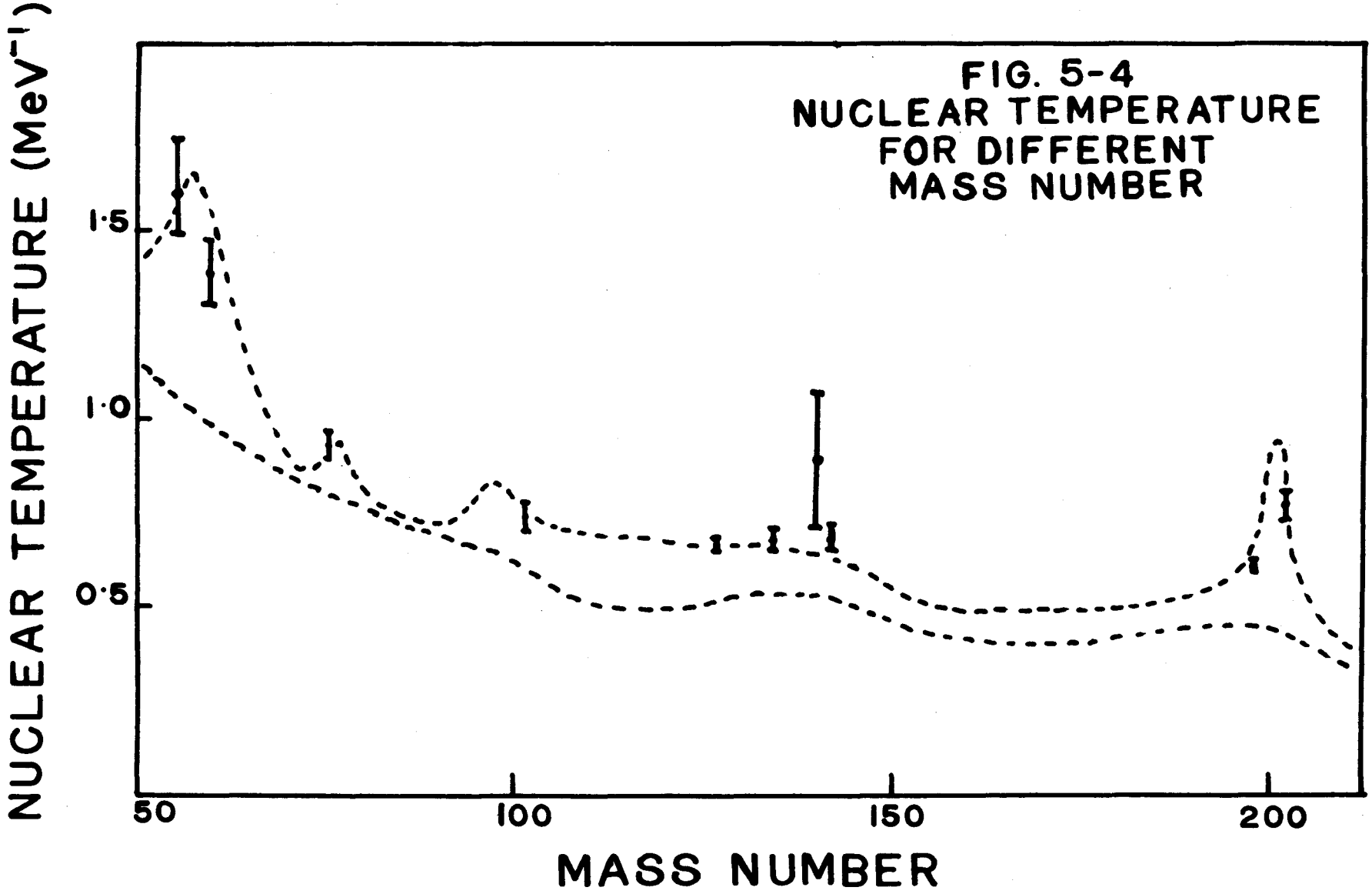
FIG. 5-4
NUCLEAR TEMPERATURE
FOR DIFFERENT
MASS NUMBER
NUCLEAR TEMPERATURE (MeV⁻¹)
1·5
1·0
0·5
50
100
150
200
MASS NUMBER

dependence of the level density obtained from the (n,γ) reaction is not consistent with the Fermi gas approximation, which predicts an $\exp(\sqrt{E})$ energy dependence. The data also suggest that above about 1 MeV to the neutron binding energy the level density is given by an $\exp(E/T)$ energy dependence.

REFERENCES

1. H. H. Landon and V. L. Sailor, Phys. Rev. 98, 1267 (1955)

2. R. T. Carpenter, AEC Report ANL-6589 (1962)

3. L. M. Bollinger, D. A. Dahlberg, R. R. Palmer and G. E. Thomas, Phys. Rev. 100 , 126 (1955)

4. L. M. Bollinger, R. E. Cote, Argonne National Laboratory Phys. Div. Summary Report ANL 6146, 1 (1959)

5. G. A. Bartholomew, Ann. Rev. Nucl. Sci. 11, 259 (1961)

6. A. M. Lane, Nucl. Phys. 11, 625 (1959)

7. A. M. Lane and J. E. Lynn, Nucl. Phys. 11, 646 (1959)

8. A. M. Lane and J. E. Lynn, Nucl. Phys. 17, 563 (1960)

9. A. M. Lane and J. E. Lynn, Nucl. Phys. 17, 586 (1960)

10. J. M. Blatt and V. F. Weisskopf, Theoretical Nuclear Physics, Chpt. XII (John Wiley and Sons, New York, 1952)

11. P. Axel, Phys. Rev. 126, 671 (1962)

12. R. G. Sachs and N. Austern, Phys. Rev. 81, 705 (1951)

13. M. A. Preston, Physics of the Nucleus, Chpt. 13 (Addison-Wesley Publishing Co., Reading, 1962)

14. A. de-Shalit and I. Talmi, Nuclear Shell Theory, Chpt. 17 (Academic Press, New York, 1963)

15. P. P. Singh, R. E. Segel, L. Meyer-Schiitzmeister, S. S. Hanna and R. G. Allas, Nucl. Phys. 65, 577 (1965)

16. C. E. Porter and R. G. Thomas, Phys. Rev. 104, 482 (1956)

17. H. Bethe, Phys. Rev. 50, 332 (1936)

18. H. Bethe, Rev. Mod. Phys. 9, 69 (1937)

19. J. M. Lang and K. J. Le Couteur, Proc. Phys. Soc. A67, 585 (1954)

20. C. Block, Phys. Rev. 93, 1094 (1954)

21. A. G. W. Cameron, Proc. of the 2nd U. N. Int. Conf. on the Peaceful Uses of Atomic Energy, Vol. 15, p 425 (United Nations, Geneva, 1958)

22. T. D. Newton, Can. J. Phys. 34, 804 (1956)

23. T. Ericson, Nucl. Phys. 8, 265 (1958)

24. D. W. Lang and K. T. Le Couteur, Nucl. Phys. 14, 21 (1959)

25. A. Bohr, B. R. Mottelson and D. Pines, Phys. Rev. 110, 936 (1958)

26. S. T. Belyaev, Kgl. Danske Videnskab. Selskab, Mat.-fys. Medd. 31, No. 11 (1959)

27 D. W. Lang, Nucl. Phys. 42, 353 (1963)

28. H. K. Vonach, R. Vandenbosch and J.R. Huizenga, Nucl. Phys. 60, 70 (1964)

29. A. Gilbert and A. G.W.Cameron, Can. J. Phys. 43, 1446 (1965)

30 E. P. Wigner, Conference on Neutron Physics by Time-of-Flight, Gatlinburg, Tennessee, 1956. ORNL-2309, 59 (1957)

31. E. P. Wigner, Can. Math. Congr. Proc., p.174 (University of Toronto Press, Toronto, 1957)

32. F. J. Dyson, J. Math. Phys. 3, 140 (1962)

33. C. E. Porter and N. Rosenzweig, Suomalaisen Tiedeakatemian Toimituksia (Ann. Acad. Sci. Fennicae) AVI, No. 44 (1960)

34. M. L. Mehta, Nucl. Phys. 18, 395 (1960)

35. D. Kurath, Phys. Rev. 101, 216 (1956)

36. L. M. Bollinger, T. J. Kennett and R. E. Cote, Phys. Rev. Letters 3, 376 (1959)

37. H. E. Jackson, J. Julien, C. Samour, A. Bloch, C. Lopata, J. Morgenstein, H. Mann and G. E. Thomas, Phys. Rev. Letters 17, 656 (1966)

38. S. Blumberg and C. E. Porter, Phys. Rev. 110, 786 (1958)

39. N. Rosenzwieg, Phys. Rev. Letters 1, 24 (1958)

40. C. E. Porter, J. Math. Phys. 4, 1039 (1963)

41. V. Fano, Phys. Rev. 72, 26 (1947)

42. H. M. Mann, Bull. Am. Phys. Soc. 11, 127 (1966)

43. E. M. Pell, J. Applied Phys. 31, 291 (1960)

44. G. L. Miller, B. D. Pate and S. Wagner, IEEE Proc. NS-10, No. 1 220 (1963)

45. A. J. Tavendale, IEE Trans. Nucl. Sci. NS-12, No. 1, 255 (1965)

46. H. J. Fiedler, L. B. Hughes, T. J. Kennett, W. V. Prestwich and B. J. Wall, Nucl. Instr. and Meth. 40, 229 (1966)

47. H. Reiss, C. S. Fuller and F. J. Morin, Bell System Tech. J. 35, 535 (1956)

48. G. Armantrout, IEEE Trans. Nucl. Sci. NS-13, 84 (1966)

49. W. L. Hansen and B. V. Jarrett, Nucl. Instr. and Meth. 31, 301 (1964)

50. H. DenHartog and F. A. Muller, Physica 13, 571 (1947)

51. E. T. Arecchi, G. Cavalleri, E. Gatti and V. Svelto, Semiconductor Nuclear Particle Detectors, NAS-NRC 871, p. 226 (1961)

52. E. Fairstein and J. Hahm, Nucleonics 23-11, 50 (1960)

53. A.B. Gillespie, Noise and Resolution in Nuclear Counter Amplifiers, Chpt. 4 (Pergamon Press, London, 1953)

54. E. Fairstein, T. A. Love and R. W. Peele, Proc. Sixth Tripartite Inst. Conf., Chalk River, 1959 - AECL-804, 117 (1959)

55. R. L. Chase, Rev. Sci. Instr. 31, 945 (1960)

56. G. Murray, R. L. Graham and J. S. Geiger, Nucl. Phys. 63, 353 (1965)

57. J. W. Knowles, Int. Conf. on Nucl. Phys. with Reactor Neutrons, Argonne, 1963 - ANL-6797, 179 (1963)

58. R. E. Carter and H. J. Motz, Int. Conf. on Nucl. Phys. with Reactor Neutrons, Argonne, 1963 - ANL-6797, 179 (1963)

59. B. P. Adyasevich, L. V. Groshev and A. M. Demidov-Atomnaya Energ. 1, No. 2, 40 (1956) and J. Nuclear Energy 3, 258 (1956)

60. G. Manning and G. A. Bartholomew, Phys. Rev. 115, 401 (1959)

61. W. V. Prestwich, T. J. Kennett, L. B. Hughes and H. J. Fiedler, Can. J. Phys. 43, 2086 (1965)

62. L. V. Groshev, B. P. Adyasevich, A. M. Demidov, Proc. U. N. Int. Conf. on the Peaceful Uses of At. Energy, Vol. 2, p. 39 (United Nations, New York, 1958)

63. R. E.Segel, Phys. Rev. 113, 844 (1959)

64. C. H. Paris, W. W. Buechner and P. M. Endt, Phys. Rev. 100, 1317 (1955)

65. W.Rudolph and H. V. Gersch, Nucl. Phys. 71, 221 (1965)

66. A. M. Hoogenboom, E. Kashy and W. W. Buechner, Phys. Rev. 128, 305 (1962)

67. D. D. Slavinskas, T. J. Kennett, W. V. Prestwich and G. L. Keech, Nucl. Instr. and Methods 41, 341 (1966)

68. R. L. Heath, A.E.C. Report IDO-16408 (1957)

69. M. G. Kendall and A. Stuart, The Advanced Theory of Statistics, Chpt. 18 (Hafner Publishing Co., New York, 1961)

70. N. P. Klepikow and S. N. Sokolov, Analysis and Planning of Experiments by the Method of Maximum Likelihood, Chpt. 1, (The MacMillan Co., New York, 1961)

71. R. A. Klump, Thesis, McMaster University (1966)

72. B. Lundberg and N. Starfelt, Nucl. Phys. 67, 321 (1965)

73. W. V. Prestwich, L. B. Hughes, T. J. Kennett and H. J. Fiedler, Phys. Rev. 140, B1562 (1965)

74. L. V. Johnson, L. B. Hughes, T. J. Kennett and W. V. Prestwich, Nucl. Phys. 84, 113 (1966)

75. N. P. Archer, L. B. Hughes, T. J. Kennett and W. V. Prestwich, Nucl. Phys. 83, 241 (1966)

76. R. E.Cote and W. V. Prestwich, Proc. of the Slow Neutron Capture Gamma-Ray Conf., Argonne, 1966, - to be published.

77. L. B. Hughes, T. J. Kennett and W. V. Prestwich, Nucl. Phys. 80,131 (1966)

78. S. Bernstein, L. D.Roberts, C. P. Stanford, J. W. T. Dabbs and T. E. Stephenson, Phys. Rev. 94, 1243 (1954)

79. J. W. Green, A. J. Smith, W. W. Buechner and M. Mazari, Phys. Rev. 108, 841 (1957)

80. A. Sperduto and W. W. Buechner, Proc. of the Vienna Conf. on Nuclidic Masses, Vienna, 1966 - in press

81. A. W. Dalton, G. Dairy, H. D. Scott and S. Swierszcewski, Proc. Phys. Soc. 78, 404 (1961)

82. J. B. Garg, J. Rainwater and W. W. Havens, Jr., AEC Report TID-21144 (1964)

83. W. V. Prestwich, T.J. Kennett and L. B. Hughes, Nucl. Phys. 88, 548 (1966)

84. H. A.Enge, D. L. Jarrell and C. C. Angleman, Phys. Rev. 119, 735 (1960)

85. L. V. Johnson and T. J. Kennett (to be published)

86. J. B. Garg, W.W. Havens Jr., and J. Rainwater, Phys. Rev. 136, B177 (1964)

87. L. B. Hughes, T. J. Kennett and W. V. Prestwich, Can. J. Phys. 44, 2041 (1966)

88. P. Ribon and A. Michandon, J. Phys. (Paris) 24, 987 (1963)

89. D. J. Hughes and R. B.Schwartz, Brookhaven Natl. Lab Report. BNL 325 (1958)

90. B. N. Brockhouse, Can. J. Phys. 31, 432 (1953)

91. S. Desjardins, W. W. Havens Jr., J. Rainwater and J. L. Rosen, Bull. Am. Phys. Soc. 5, No. 4, 295z7 (1960)

92. J. A. Harvey, D. J. Hughes, R. S. Carter and V. E. Pilcher, Phys. Rev. 99, 10 (1955)

93. L. B. Hughes, T. J. Kennett and W. V. Prestwich, Nucl. Phys. 89 241 (1966)

94. G. Bianchi, J. Colmin, C. Corge, V.-D. Huynh, J. Julien, J. Morgenstein, F. Netter and M. Vastel, J. Phys. (Paris) 24, 997 (1963)

95. H. B.Willard, Oak Ridge Nat'l. Lab. Rept. ORNL-TM-874

96. J. S. Desjardins, J. L. Rosen, W. W. Havens Jr., and J. Rainwater, Phys. Rev. 120, 2214 (1960)

97. J. A. Harvey, private communication

98. A. Stolovy and J. A. Harvey, Phys. Rev. 108, 353 (1957)

99. J. A. Harvey, Proc. of the Int. Conf. on Nuclear Structure, p.670 (University of Toronto Press, Toronto, 1960)

100. O. A. Wasson, M. R. Bhat, R. E. Chrien, M. A. Love and M. Beer, Phys. Rev. Letters 17, 1220 (1960)

101. H. Ikegami and G. I. Emery, Phys. Rev. Letters 13, 26 (1964)

APPENDIX

The data obtained from the thermal neutron capture spectra of the ten odd-odd nucleides studied in this work, are presented in Tables A-1 through A-10. The energies that are quoted, were determined relative to the prominent γ rays of the $^{35}Cl(n,\gamma)^{36}Cl$ reaction using the procedure discussed in Section 3.4. The errors associated with these energies are $\pm$ 3 keV.

The relative intensities and the energy of the final states are also given in these tables. The relative intensities were obtained by dividing the observed peak height by the empirically determined efficiency. The determination of the counter efficiency is discussed in Section 3.5. The quoted intensities have an error of $\pm$ 20%. Since we are concerned only with the energy variation of the transition probabilities, no attempt has been made to determine absolute intensities.

The excitation energies that are shown were calculated by subtracting the γ-ray energy from the reaction Q-value. These excitation energies are based, then, on the assumption that the observed radiation was emitted from the capture state. This assumption is substantiated in the cases where good (d,p) reaction data is available.

TABLE A-1

Energies and Intensities from the $^{55}Mn(n,\gamma)^{56}Mn$ Reaction

NO.	ENERGY (KEV)	RELATIVE INTENSITY	EXCITATION ENERGY (KEV)	NO.	ENERGY (KEV)	RELATIVE INTENSITY	EXCITATION ENERGY (KEV)
1	7272	694	0	33	4969	95	2303
2	7245	2676	27	34	4949	361	2323
3	7161	1161	111	35	4941	160	2331
4	7059	2297	213	36	4906	86	2366
5	6932	456	340	37	4877	183	2395
6	6786	666	486	38	4838	219	2434
7	6550	52	722	39	4829	284	2443
8	6430	154	842	40	4797	49	2475
9	6105	389	1167	41	4729	637	2543
10	6091	114	1181	42	4714	141	2558
11	6034	199	1238	43	4690	197	2582
12	6019	83	1253	44	4646	193	2626
13	5979	53	1293	45	4621	44	2651
14	5921	133	1351	46	4592	100	2680
15	5894	20	1378	47	4569	500	2703
16	5836	16	1436	48	4555	248	2717
17	5760	371	1512	49	4516	96	2756
18	5714	35	1558	50	4491	96	2781
19	5688	27	1584	51	4452	191	2820
20	5631	48	1641	52	4438	147	2834
21	5603	68	1669	53	4403	72	2869
22	5575	53	1697	54	4382	91	2890
23	5528	1495	1744	55	4351	44	2921
24	5435	368	1837	56	4319	95	2953
25	5403	99	1869	57	4269	131	3003
26	5257	289	2015	58	4253	107	3019
27	5197	245	2075	59	4225	230	3047
28	5182	927	2090	60	4193	79	3079
29	5113	58	2159	61	4174	75	3098
30	5068	623	2204	62	4144	40	3128
31	5037	186	2235	63	4105	167	3167
32	5016	1364	2256				

TABLE A-2

Energies and Intensities from the $^{59}Co(n,\gamma)^{60}$ Reaction

NO.	ENERGY (KEV)	RELATIVE INTENSITY	EXCITATION ENERGY (KEV)	NO.	ENERGY (KEV)	RELATIVE INTENSITY	EXCITATION ENERGY (KEV)
1	7494	1638	0	39	5041	190	2453
2	7217	2427	277	40	5005	508	2489
3	7180	254	314	41	4958	118	2536
4	7058	980	436	42	4924	610	2570
5	6989	1641	505	43	4908	1124	2586
6	6953	351	541	44	4887	701	2607
7	6942	1292	552	45	4837	93	2657
8	6880	4592	614	46	4778	162	2716
9	6709	4048	785	47	4722	231	2772
10	6488	3649	1006	48	4704	300	2790
11	6277	596	1217	49	4648	149	2846
12	6175	172	1319	50	4624	195	2870
13	6150	320	1344	51	4607	573	2887
14	6111	275	1383	52	4592	286	2902
15	6043	270	1451	53	4548	194	2946
16	5979	3893	1515	54	4533	137	2961
17	5926	1113	1568	55	4472	137	3022
18	5850	179	1644	56	4445	114	3049
19	5743	1129	1751	57	4398	205	3096
20	5703	232	1791	58	4375	330	3119
21	5661	4099	1833	59	4350	239	3144
22	5639	734	1855	60	4328	239	3166
23	5607	948	1887	61	4307	114	3187
24	5510	354	1984	62	4275	102	3219
25	5442	184	2052	63	4249	57	3245
26	5410	293	2084	64	4210	590	3284
27	5395	366	2099	65	4155	341	3339
28	5357	273	2137	66	4124	136	3370
29	5272	732	2222	67	4073	114	3421
30	5248	122	2246	68	4029	704	3465
31	5216	242	2278	69	3968	375	3526
32	5183	1677	2311	70	3930	455	3564
33	5168	289	2326	71	3901	250	3593
34	5146	120	2348	72	3860	46	3634
35	5130	276	2364	73	3816	125	3678
36	5103	84	2391	74	3799	34	3695
37	5070	190	2424	75	3749	892	3745
38	5053	59	2441				

TABLE A-3

Energies and Intensities from the $^{75}As(n,\gamma)^{76}As$ Reaction

NO.	ENERGY (KEV)	RELATIVE INTENSITY	EXCITATION ENERGY (KEV)	NO.	ENERGY (KEV)	RELATIVE INTENSITY	EXCITATION ENERGY (KEV)
1	7286	153	43	37	5932	29	1397
2	7244	86	85	38	5883	97	1446
3	7217	11	112	39	5870	136	1459
4	7206	13	123	40	5856	63	1473
5	7167	35	162	41	5815	31	1514
6	7126	23	203	42	5784	130	1545
7	7065	205	264	43	5759	72	1570
8	7023	618	306	44	5688	157	1641
9	6978	67	351	45	5668	153	1661
10	6929	276	400	46	5649	21	1680
11	6884	23	445	47	5621	40	1708
12	6862	29	467	48	5579	111	1750
13	6813	845	516	49	5544	29	1785
14	6789	111	540	50	5508	33	1821
15	6698	30	631	51	5496	51	1833
16	6586	105	743	52	5470	75	1859
17	6544	70	785	53	5458	32	1871
18	6532	63	797	54	5446	38	1883
19	6466	53	863	55	5418	176	1911
20	6419	106	910	56	5399	31	1930
21	6396	223	933	57	5374	127	1955
22	6369	82	960	58	5298	102	2031
23	6345	72	984	59	5277	24	2052
24	6314	68	1015	60	5208	57	2121
25	6297	342	1032	61	5180	28	2149
26	6226	95	1103	62	5156	109	2173
27	6202	111	1127	63	5123	55	2206
28	6179	55	1150	64	5086	201	2243
29	6145	68	1184	65	5072	111	2257
30	6103	62	1226	66	5017	36	2312
31	6091	31	1238	67	4999	136	2330
32	6060	120	1269	68	4987	72	2342
33	6028	114	1301	69	4962	103	2367
34	6013	43	1316	70	4943	64	2386
35	5984	70	1345	71	4921	56	2408
36	5970	34	1359				

TABLE A-4

Energies and Intensities from the $^{103}Rh(n,\gamma)^{104}Rh$ Reaction

NO.	ENERGY (KEV)	RELATIVE INTENSITY	EXCITATION ENERGY (KEV)	NO.	ENERGY (KEV)	RELATIVE INTENSITY	EXCITATION ENERGY (KEV)
1	6999	39	0	36	5378	33	1621
2	6783	89	216	37	5350	343	1649
3	6730	15	269	38	5328	47	1671
4	6535	9	464	39	5296	36	1703
5	6512	13	487	40	5269	226	1730
6	6485	11	514	41	5207	93	1792
7	6356	92	643	42	5159	131	1840
8	6306	48	693	43	5141	42	1858
9	6288	29	711	44	5110	74	1889
10	6266	22	733	45	5024	80	1975
11	6212	187	787	46	5010	63	1989
12	6173	163	826	47	4981	54	2018
13	6141	17	858	48	4965	47	2034
14	6113	144	886	49	4924	102	2075
15	6085	147	914	50	4904	52	2095
16	6049	169	950	51	4868	39	2131
17	5994	29	1005	52	4858	48	2141
18	5918	261	1081	53	4840	111	2159
19	5814	53	1185	54	4814	20	2185
20	5801	116	1198	55	4788	24	2211
21	5772	27	1227	56	4777	51	2222
22	5716	74	1283	57	4756	41	2243
23	5702	56	1297	58	4735	51	2264
24	5675	54	1324	59	4698	56	2301
25	5640	21	1359	60	4674	58	2325
26	5620	67	1379	61	4639	103	2360
27	5608	80	1391	62	4605	57	2394
28	5594	62	1405	63	4587	19	2412
29	5551	56	1448	64	4553	61	2446
30	5525	149	1474	65	4516	40	2483
31	5500	41	1499	66	4493	181	2506
32	5467	70	1532	67	4480	27	2519
33	5433	59	1566	68	4453	67	2546
34	5419	53	1580	69	4433	30	2566
35	5398	37	1601	70	4943	64	2386

TABLE A-5

Energies and Intensities from the $^{127}I(n,\gamma)^{128}I$ Reaction

NO.	ENERGY (KEV)	RELATIVE INTENSITY	EXCITATION ENERGY (KEV)	NO.	ENERGY (KEV)	RELATIVE INTENSITY	EXCITATION ENERGY (KEV)
1	6742	21	84	28	5727	139	1099
2	6694	162	132	29	5632	21	1194
3	6682	40	144	30	5576	172	1250
4	6664	20	162	31	5561	244	1265
5	6646	47	180	32	5526	56	1300
6	6598	11	228	33	5484	102	1342
7	6577	14	249	34	5461	129	1365
8	6548	9	278	35	5449	46	1377
9	6533	11	293	36	5410	18	1416
10	6479	19	347	37	5384	46	1442
11	6455	41	371	38	5363	27	1463
12	6446	42	380	39	5337	38	1489
13	6431	15	395	40	5298	130	1528
14	6392	61	434	41	5289	90	1537
15	6309	156	517	42	5275	36	1551
16	6294	38	532	43	5198	249	1628
17	6273	56	553	44	5113	26	1713
18	6217	25	609	45	5092	158	1734
19	6166	16	660	46	5078	26	1748
20	6148	14	678	47	5060	35	1766
21	5994	40	832	48	5042	52	1784
22	5985	37	841	49	5031	52	1795
23	5970	24	856	50	5016	122	1810
24	5945	21	881	51	4998	87	1828
25	5887	32	939	52	4981	52	1845
26	5792	44	1034	53	4951	207	1875
27	5741	60	1085				

TABLE A-6

Energies and Intensities from the $^{133}Cs(n,\gamma)^{134}Cs$ Reaction

NO.	ENERGY (KEV)	RELATIVE INTENSITY	EXCITATION ENERGY (KEV)	NO.	ENERGY (KEV)	RELATIVE INTENSITY	EXCITATION ENERGY (KEV)
1	6714	145	116	31	5437	145	1393
2	6699	366	131	32	5393	53	1437
3	6657	44	173	33	5375	390	1455
4	6625	39	205	34	5310	123	1520
5	6565	19	265	35	5266	233	1564
6	6523	28	307	36	5255	612	1575
7	6511	68	319	37	5225	196	1605
8	6443	99	387	38	5205	96	1625
9	6387	64	443	39	5155	64	1675
10	6318	80	512	40	5134	71	1696
11	6309	67	521	41	5023	372	1807
12	6268	31	562	42	4970	173	1860
13	6247	53	583	43	4923	157	1907
14	6188	194	642	44	4894	117	1936
15	6179	409	651	45	4853	82	1977
16	6140	107	690	46	4829	103	2001
17	6108	42	722	47	4812	72	2018
18	6054	323	776	48	4771	85	2059
19	5977	133	853	49	4753	190	2077
20	5951	104	879	50	4706	146	2124
21	5912	77	918	51	4686	81	2144
22	5900	105	930	52	4671	81	2159
23	5856	42	974	53	4663	152	2167
24	5794	250	1036	54	4654	144	2176
25	5750	133	1080	55	4625	105	2205
26	5729	163	1101	56	4598	59	2232
27	5637	398	1193	57	4587	168	2243
28	5570	345	1260	58	4566	121	2264
29	5505	521	1325	59	4546	141	2284
30	5493	416	1337				

TABLE A-7

Energies and Intensities from the $^{139}La(n,\gamma)^{140}La$ Reaction

NO.	ENERGY (KEV)	RELATIVE INTENSITY	EXCITATION ENERGY (KEV)	NO.	ENERGY (KEV)	RELATIVE INTENSITY	EXCITATION ENERGY (KEV)
1	5165	101	0	28	4043	42	1122
2	5130	153	35	29	3967	17	1198
3	5101	737	64	30	3945	28	1220
4	5066	17	99	31	3922	10	1243
5	5049	14	116	32	3899	67	1266
6	4988	17	177	33	3851	17	1314
7	4957	31	208	34	3819	40	1346
8	4930	10	235	35	3775	18	1390
9	4890	168	275	36	3740	81	1425
10	4846	78	319	37	3728	114	1437
11	4771	12	394	38	3717	71	1448
12	4733	25	432	39	3679	181	1486
13	4706	22	459	40	3664	186	1501
14	4688	24	477	41	3609	153	1556
15	4624	20	541	42	3580	60	1585
16	4585	13	580	43	3477	55	1688
17	4559	64	606	44	3461	34	1704
18	4503	195	662	45	3440	74	1725
19	4441	17	724	46	3424	118	1741
20	4415	276	750	47	3382	52	1783
21	4390	284	775	48	3284	71	1881
22	4362	22	803	49	3266	119	1899
23	4292	23	873	50	3245	878	1920
24	4271	25	894	51	3189	54	1976
25	4122	23	1043	52	3109	46	2056
26	4104	32	1061	53	3080	140	2085
27	4061	30	1104	54	4654	144	2176

TABLE A-8

Energies and Intensities from the $^{141}Pr(n,\gamma)^{142}Pr$ Reaction

NO.	ENERGY (KEV)	RELATIVE INTENSITY	EXCITATION ENERGY (KEV)	NO.	ENERGY (KEV)	RELATIVE INTENSITY	EXCITATION ENERGY (KEV)
1	5844	280	0	20	4721	187	1123
2	5825	99	19	21	4690	603	1154
3	5770	67	74	22	4589	52	1255
4	5739	10	105	23	4574	34	1270
5	5715	93	129	24	4554	35	1290
6	5666	671	178	25	4496	213	1348
7	5517	24	327	26	4456	47	1388
8	5476	15	368	27	4439	85	1405
9	5456	15	388	28	4416	45	1428
10	5394	15	450	29	4387	33	1457
11	5202	85	642	30	4370	100	1474
12	5138	688	706	31	4347	60	1497
13	5092	398	752	32	4324	45	1520
14	5051	66	793	33	4298	53	1546
15	5020	49	824	34	4278	80	1566
16	4976	61	868	35	4249	75	1595
17	4941	35	903	36	4174	68	1670
18	4840	43	1004	37	4160	58	1684
19	4799	283	1045				

TABLE A-9

Energies and Intensities from the $^{197}Au(n,\gamma)^{198}Au$ Reaction

NO.	ENERGY (KEV)	RELATIVE INTENSITY	EXCITATION ENERGY (KEV)	NO.	ENERGY (KEV)	RELATIVE INTENSITY	EXCITATION ENERGY (KEV)
1	6513	256	0	41	4997	90	1516
2	6458	342	55	42	4953	183	1560
3	6320	538	193	43	4929	52	1584
4	6276	179	237	44	4900	146	1613
5	6253	884	260	45	4888	117	1625
6	6165	47	348	46	4865	93	1648
7	6148	217	365	47	4853	118	1660
8	6109	197	404	48	4827	29	1686
9	5982	243	531	49	4794	213	1719
10	5940	110	573	50	4780	68	1733
11	5904	17	609	51	4765	94	1748
12	5878	83	635	52	4733	59	1780
13	5839	44	674	53	4727	51	1786
14	5810	63	703	54	4681	34	1832
15	5785	29	728	55	4658	34	1855
16	5764	30	749	56	4636	68	1877
17	5711	300	802	57	4599	51	1914
18	5676	55	837	58	4586	202	1927
19	5652	32	861	59	4571	151	1942
20	5618	75	895	60	4539	153	1974
21	5592	115	921	61	4526	50	1987
22	5522	197	991	62	4504	109	2009
23	5492	111	1021	63	4454	92	2059
24	5467	88	1046	64	4440	117	2073
25	5419	31	1094	65	4419	75	2094
26	5401	37	1112	66	4390	59	2123
27	5386	37	1127	67	4367	84	2146
28	5351	85	1162	68	4358	84	2155
29	5306	117	1207	69	4336	33	2177
30	5277	102	1236	70	4314	17	2199
31	5221	125	1292	71	4275	67	2238
32	5200	44	1313	72	4241	50	2272
33	5174	62	1339	73	4221	33	2292
34	5147	150	1366	74	4186	67	2327
35	5100	255	1413	75	4173	33	2340
36	5082	177	1431	76	4122	33	2391
37	5056	28	1457	77	4111	17	2402
38	5044	73	1469	78	4086	33	2427
39	5035	91	1478	79	4055	50	2458
40	5023	84	1490				

TABLE A-10

Energies and Intensities from the $^{203}Tl(n,\gamma)^{204}Tl$ Reaction

NO.	ENERGY (KEV)	RELATIVE INTENSITY	EXCITATION ENERGY (KEV)	NO.	ENERGY (KEV)	RELATIVE INTENSITY	EXCITATION ENERGY (KEV)
1	6516	564	138	23	5048	38	1606
2	6337	94	317	24	5015	304	1639
3	6223	283	431	25	4982	153	1672
4	6183	280	471	26	4943	85	1711
5	6167	761	487	27	4916	747	1738
6	6120	144	534	28	4866	65	1788
7	6036	52	618	29	4843	265	1811
8	6024	133	630	30	4808	73	1846
9	5918	434	736	31	4754	697	1900
10	5895	58	759	32	4708	373	1946
11	5859	54	795	33	4691	540	1963
12	5642	1527	1012	34	4664	54	1990
13	5604	1345	1050	35	4605	192	2049
14	5534	599	1120	36	4571	123	2083
15	5452	400	1202	37	4544	219	2110
16	5405	604	1249	38	4499	232	2155
17	5281	988	1373	39	4443	74	2211
18	5263	466	1391	40	4405	49	2249
19	5242	71	1412	41	4345	202	2309
20	5181	674	1473	42	4312	132	2342
21	5128	257	1526	43	4229	277	2425
22	5081	32	1573				